

**WP4 & WP5 – EXPERIMENTAL AND NUMERICAL
INVESTIGATION OF CLASS 4 COLUMNS, SIMPLE
DESIGN RULES AND APPLICATION EXAMPLES**

Table of contents

1	Fire tests.....	3
1.1	General parameters of tested columns.....	3
1.1.1	Set-up of experimental tests.....	11
1.1.2	Progress and results of the experiments.....	20
1.1.3	Development of numerical models and correlation with experimental results.....	59
2	Description of the parametric studies and comparisons with simple design rules.....	85
2.1	Numerical parametric study for class 4 columns subjected to axial compression.....	85
2.1.1	Presentation of chosen parameters.....	85
2.1.2	Detailed list of results of the parametric study and comparisons with simple design rules of EN 1993-1-2.....	89
2.1.3	Detailed list of results of the parametric study and comparisons with new proposed simple design rules	92
2.2	Numerical parametric study for class 4 columns subjected to axial compression and bending	95
2.2.1	Presentation of chosen parameters.....	95
2.2.2	Detailed list of results of the parametric study and comparisons with simple design rules of current EN 1993-1-2.....	97
2.2.3	Calibration of in-plane interaction factor and update of reduction factors.....	101
3	Application examples.....	107
3.1	Evaluation of the compression resistance of a class 4 axially loaded column.....	107
3.1.1	Classification of the cross-section.....	107
3.1.2	Evaluation of the effective area in compression.....	108
3.1.3	Calculation of the compression resistance.....	110
3.2	Resistance of a beam-column subjected to combined axial compression and bending....	112
3.2.1	Formulae used.....	112
3.2.2	Classification of the cross-section.....	113
3.2.3	Evaluation of the effective area and effective section modulus.....	114
3.2.4	Evaluation of the critical temperature.....	119
3.2.5	Fire resistance.....	122
4	List of references.....	124

1 Fire tests

The fire tests concern I-columns with slender cross-sections. Four columns subjected to axial compression and four columns subjected to combined axial compression and bending are tested at elevated temperature. Six columns with welded constant cross-sections and tapered cross-sections are studied. Two columns with hot-rolled tapered cross-sections are also investigated. The fire tests consist in applying a mechanical load until reaching the load ratio (percentage of the cold failure load) for the steel members and then heating the latter at least until mechanical failure. The column is heated along its whole length. This procedure is the same for the eight tests. These tests are designed so that the failure is induced by a global buckling along weak or strong axis eventually combined with local buckling of sections walls. There is no lateral restraint installed along the weak axis.

1.1 General parameters of tested columns

The four tested columns which are axially loaded and the different tested cross-sections are given hereafter. One cross-section is a hot-rolled IPE240A. The three other columns are made of welded cross-sections. The following table describes the main parameters to take into account for these tests:

Test number	Cross-section	Strong axis λ_p	Weak axis λ_p
Test 1	Constant - IPE240A	0.245	1.255
Test 2 & test 3	Constant - 440x4+150x5	0.164	0.995
Test 4	Tapered - 490-290x4.5+150x5	0.267	1.029

Table 1: List of axially loaded columns tested

The four tested columns which are subjected to combined compression and bending and the different tested cross-sections are given hereafter. One cross-section is a hot-rolled HE340AA. The three other columns are made of welded cross-sections. The following table describes the main parameters to take into account for these tests:

Test number	Cross-section	Strong axis λ_p	Weak axis λ_p
Test 5 & 6	Constant – 350x4+150x5	0.212	0.991
Test 7	Constant – HE340AA	0.256	0.478
Test 8	Tapered – 440-340x4+150x5	0.164	0.995

Table 2: List of columns subjected to combined compression and bending

The tested columns and corresponding cross-sections are illustrated in the following figures.

An eccentricity of 5 mm is provided to the applied load in the direction of the weak axis in order to control the failure mode. For this test, the eccentricity of the load and of the support is arranged in such a way as to produce a small uniform bending moment distribution ($\psi = 1$):

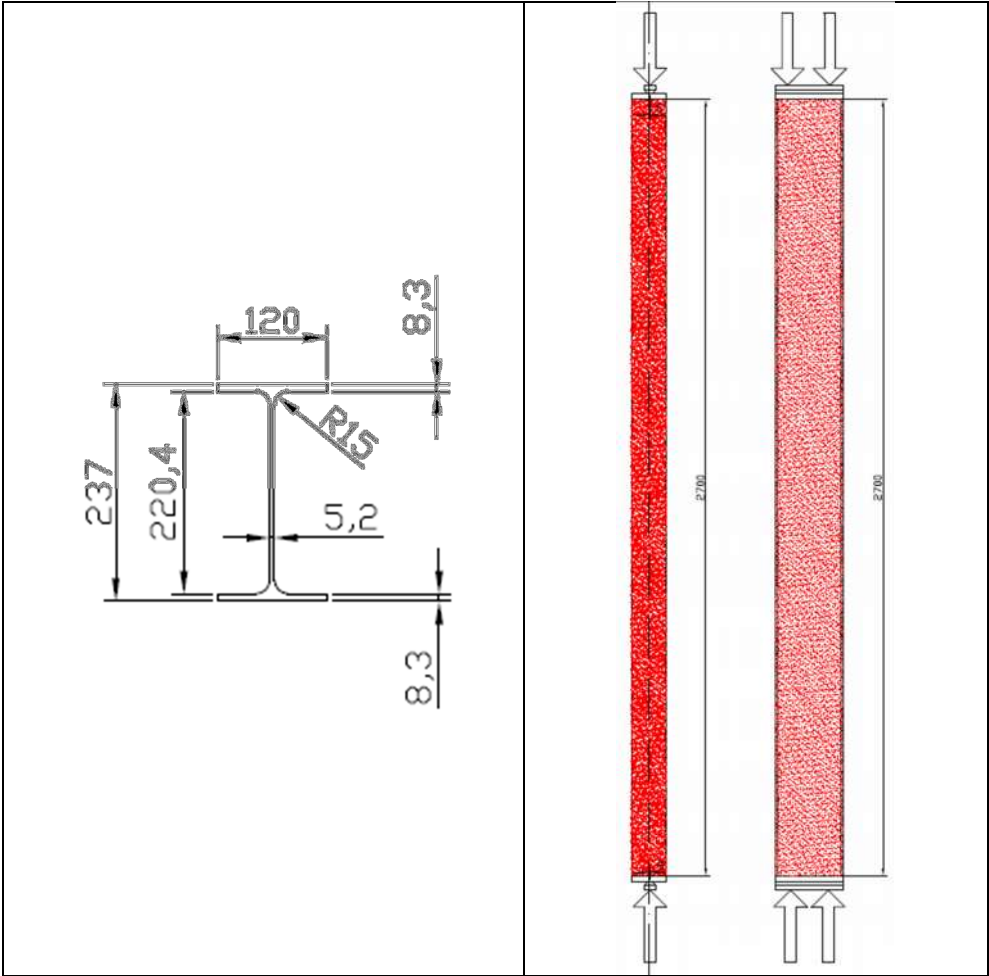


Figure 1: Cross-section design and global design of the test 1

An eccentricity of 5 mm is provided to the applied load in the direction of the weak axis in order to control the failure mode. For this test the eccentricity of the load and of the support are arranged in such a way as to produce a small uniform bending moment distribution ($\psi = 1$):

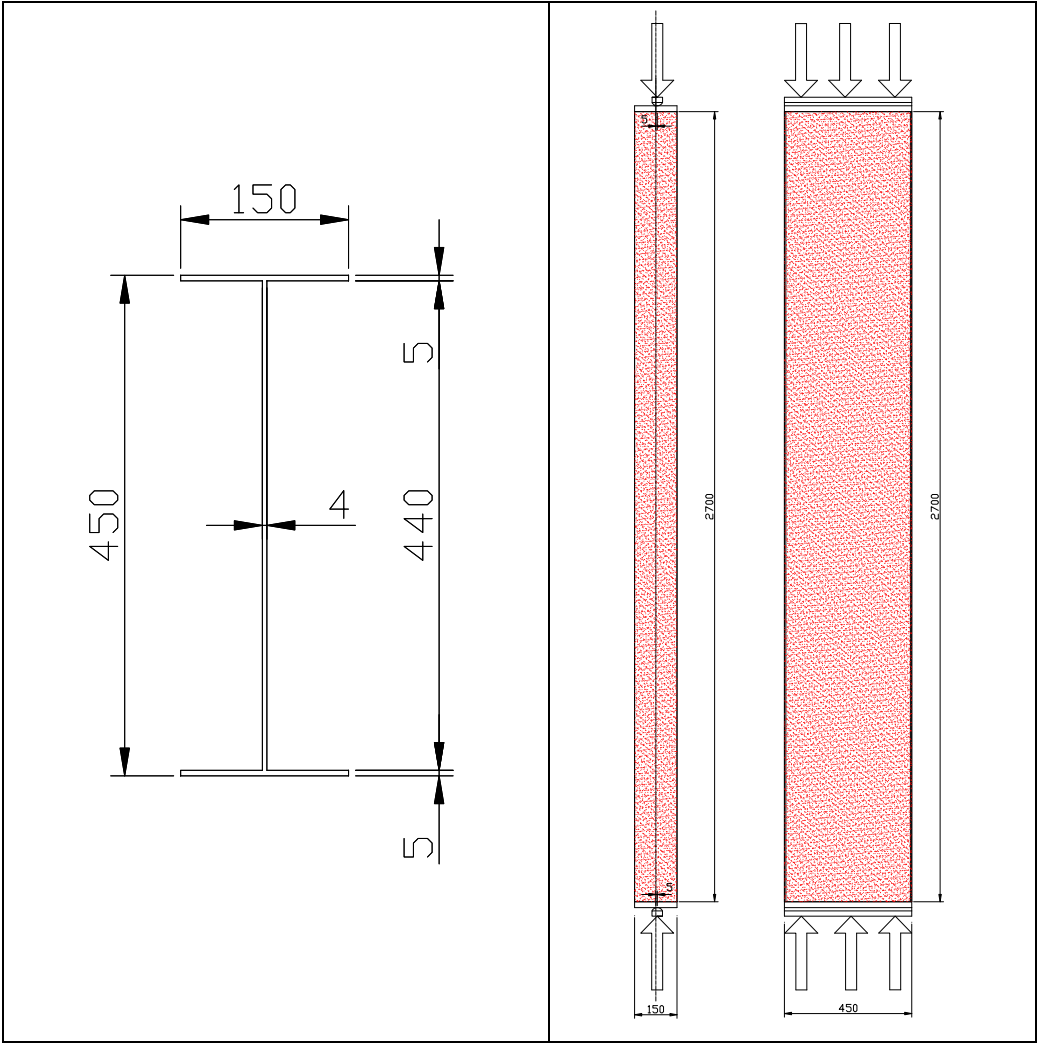


Figure 2: Cross-section design and global design of the tests 2 & 3

The load is applied with an eccentricity of 6 mm. in the direction of the strong axis. For this test the eccentricity of the load and of the support are arranged in such a way as to produce a uniform bending moment distribution ($\psi = 1$):

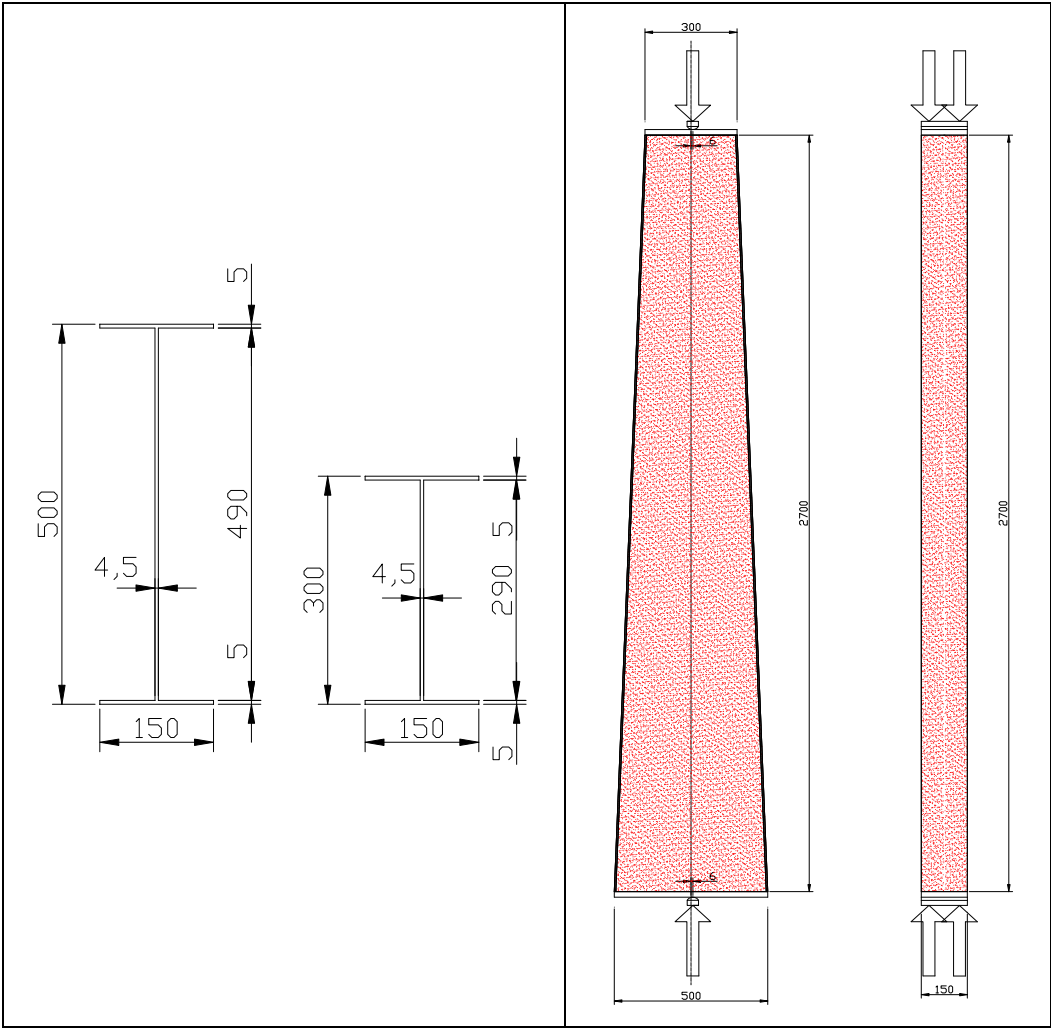


Figure 3: Cross-section design and global design of the test 4

The load is applied with an eccentricity of 71 mm. in the direction of the strong axis. For this test the eccentricity of the load and of the support are arranged in such a way as to produce a uniform bending moment distribution ($\psi = 1$):

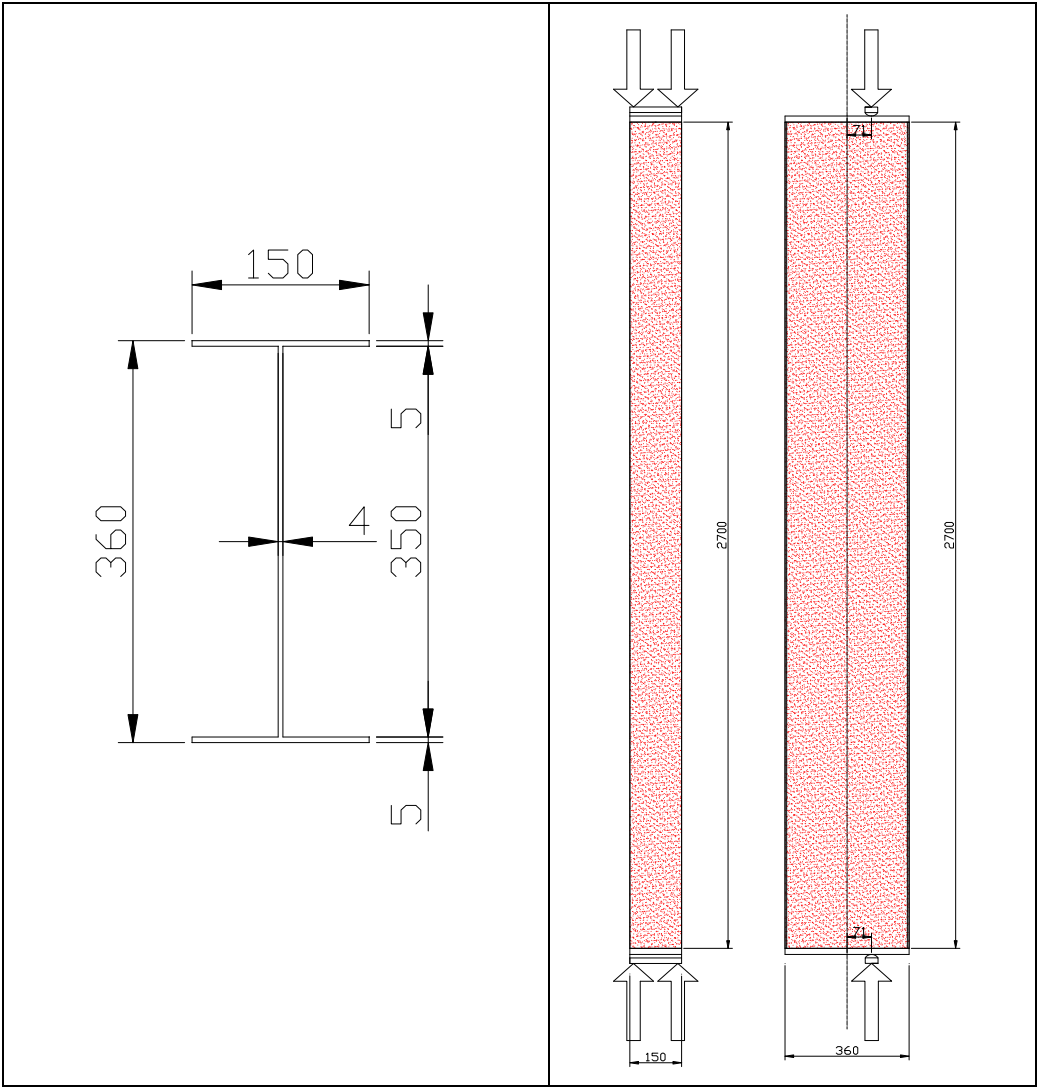


Figure 4: Cross-section design and global design of the tests 5

The same column geometry and test set-up as for the test No 5 is used. The eccentricity of the applied load is larger. Indeed, the load is applied with an eccentricity of 177.5 mm in the direction of the strong axis:

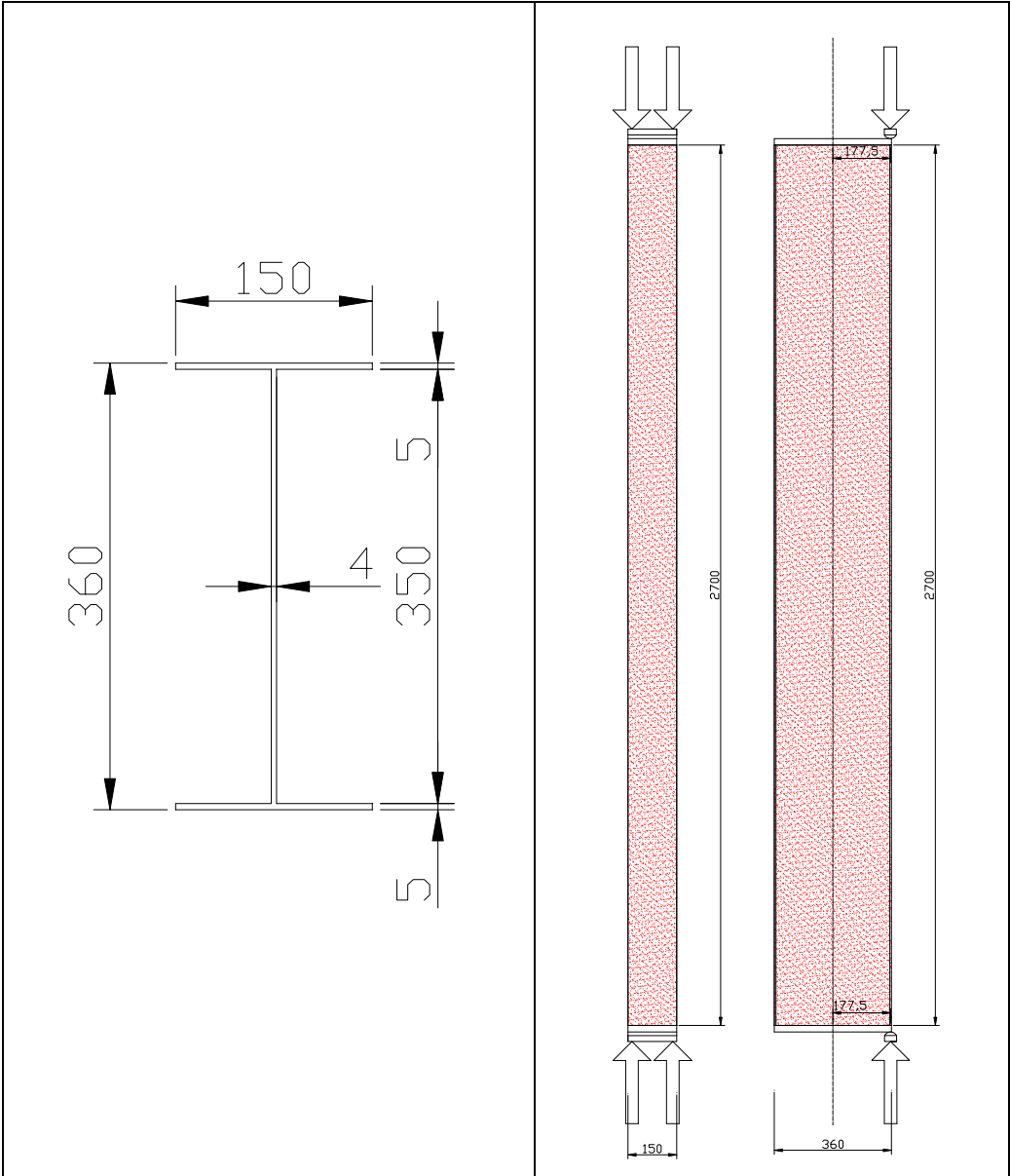


Figure 5: Cross-section design and global design of the test 6

The load is applied with an eccentricity of 100 mm. in the direction of the strong axis at the top of the column and without eccentricity at the other extremity. For this test the eccentricity of the load and of the support are arranged in such a way as to produce a triangular bending moment distribution ($\psi = 0$):

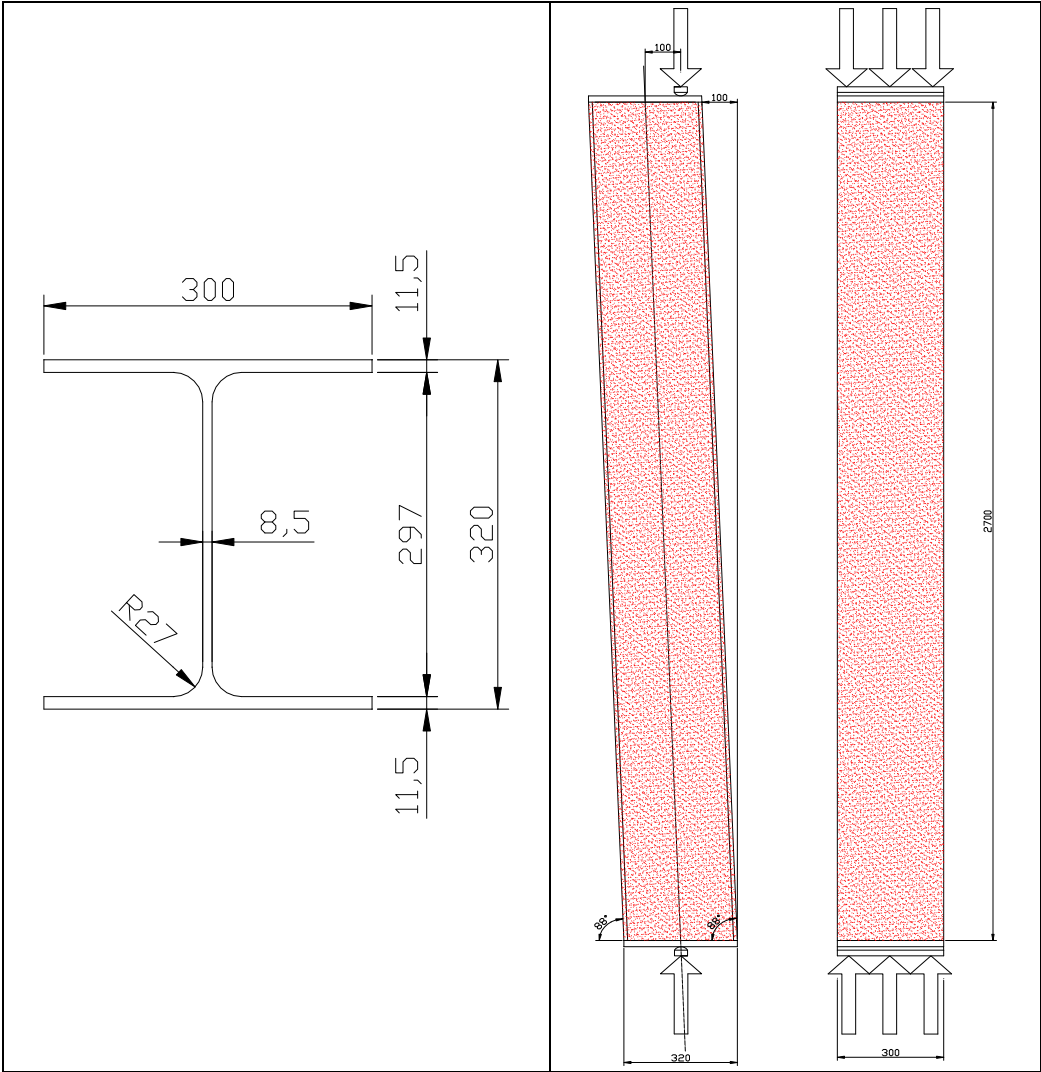


Figure 6: Cross-section design and global design of the test 7

The load is applied with an eccentricity of 150 mm in the direction of the strong axis at the larger base of the steel member and without eccentricity at the other base. For this test the eccentricity of the load and of the support are arranged in such a way as to produce a triangular bending moment distribution ($\psi = 0$).

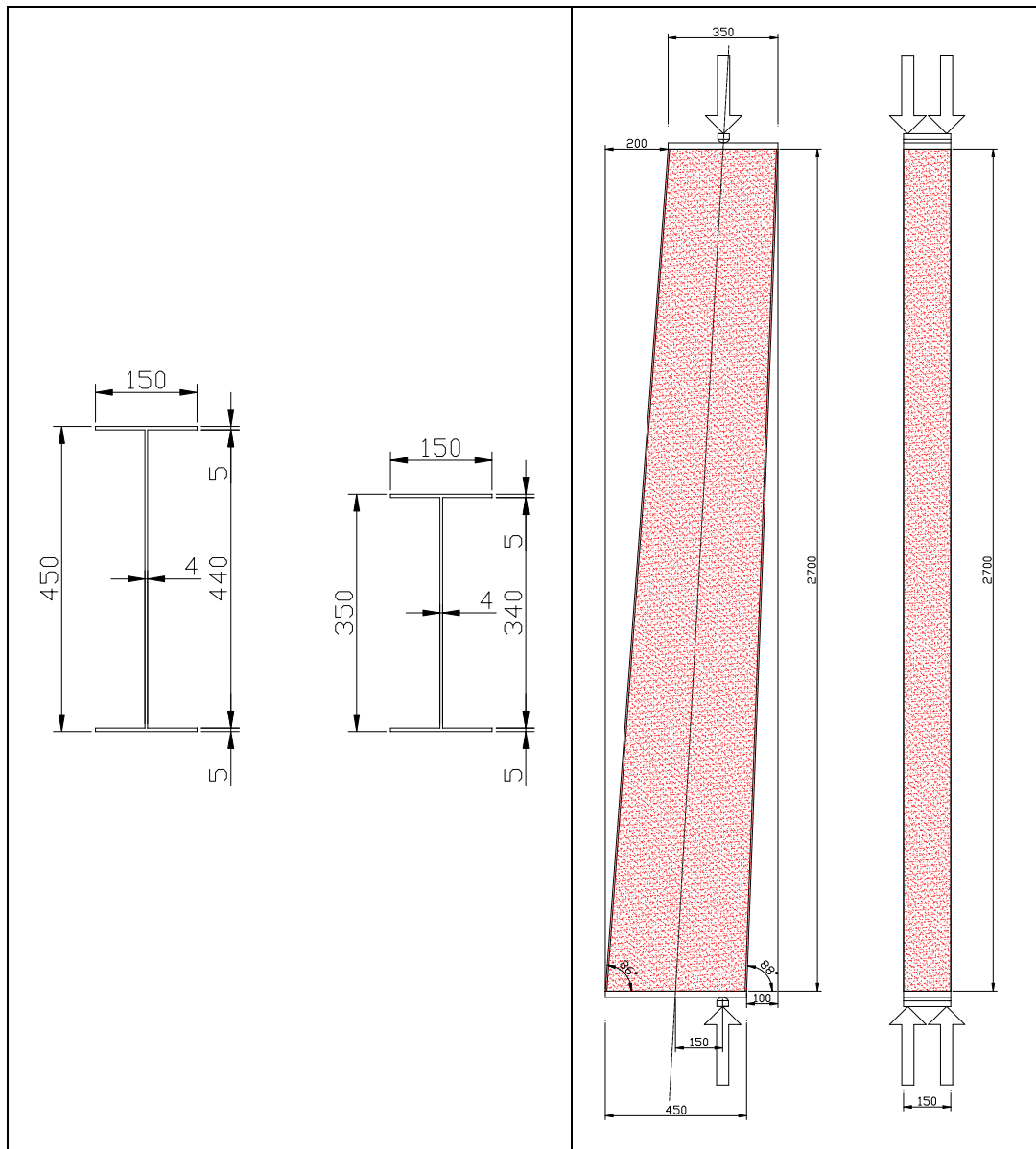


Figure 7: section design and global design of the test 8

1.1.1 Set-up of experimental tests

The measurements of the global and local imperfections of the eight specimens are performed manually. The methodology is to put a straight aluminium bar (with the same length than the specimen) along the web and along both flanges of each column. Once the rule placed, the distance between the bottom of the ruler and the web (or the flange) of the column is measured each ten centimetres length. Finally, a profile with the imperfections along the web and the flanges of each column is obtained.

The reference for these profiles is the bottom of the ruler; so by deducing the distance between the ruler and the web (or flange) measured at the two extremities of the specimen from all the other measured distances, the profiles presented in the schemes here below for each column with an imperfection equal to zero at the extremities is drawn. Thus, it is supposed that the two points of reference for the measurements are the two extremities of the column. Thanks to this data providing the profile of the imperfections along the column, the global imperfection of the column and also the local imperfections observed around the global one are deduced. The following graphs show these profiles for each column:

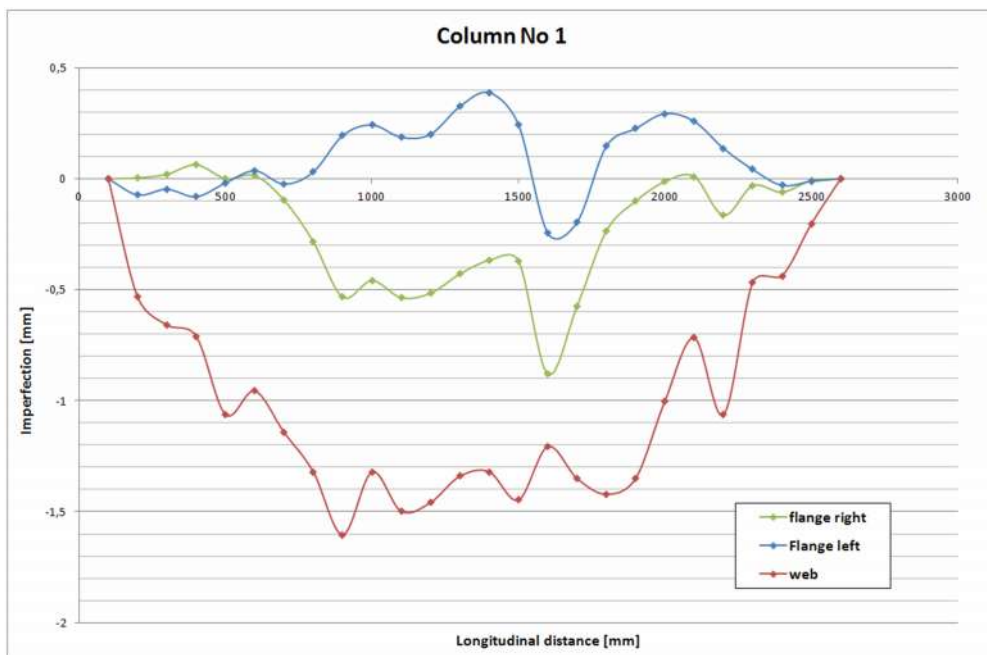


Figure 8: Test 1 – Amplitude of the imperfections along the web and both flanges

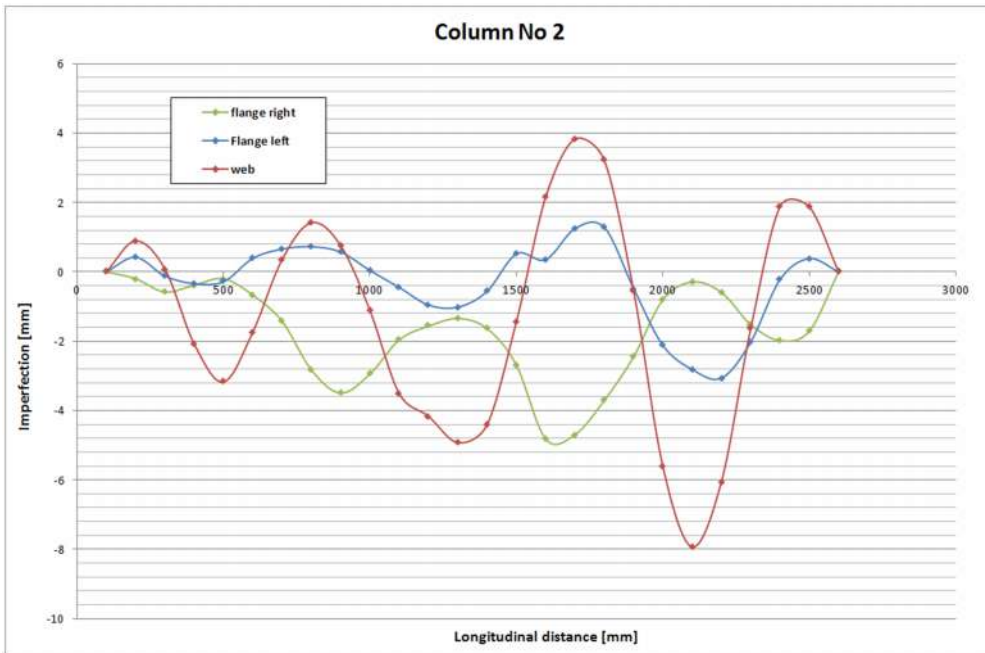


Figure 9: Test 2 – Amplitude of the imperfections along the web and both flanges

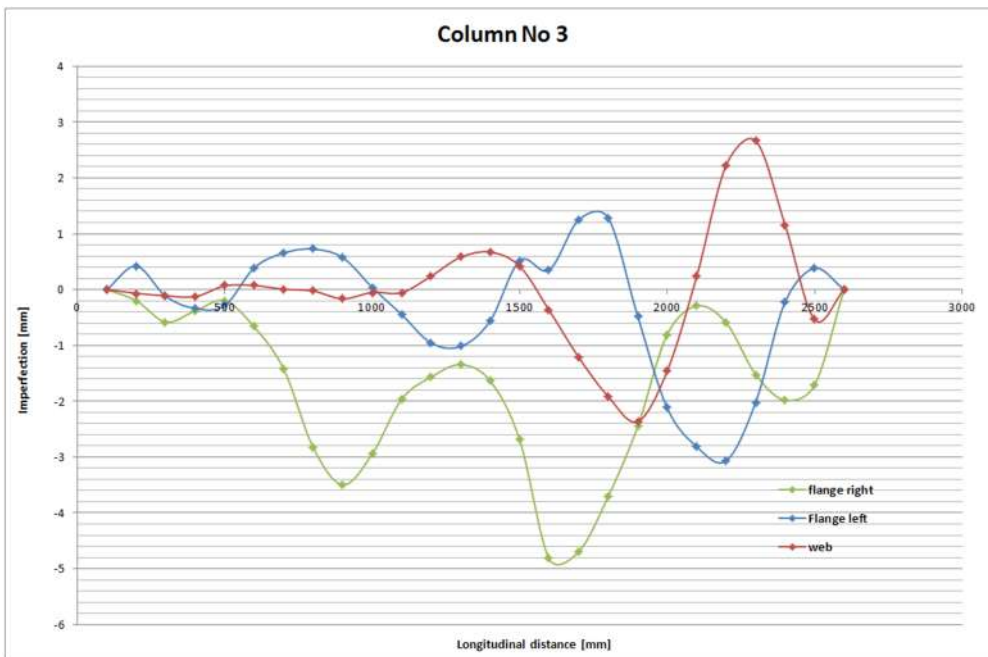


Figure 10: Test 3 – Amplitude of the imperfections along the web and both flanges

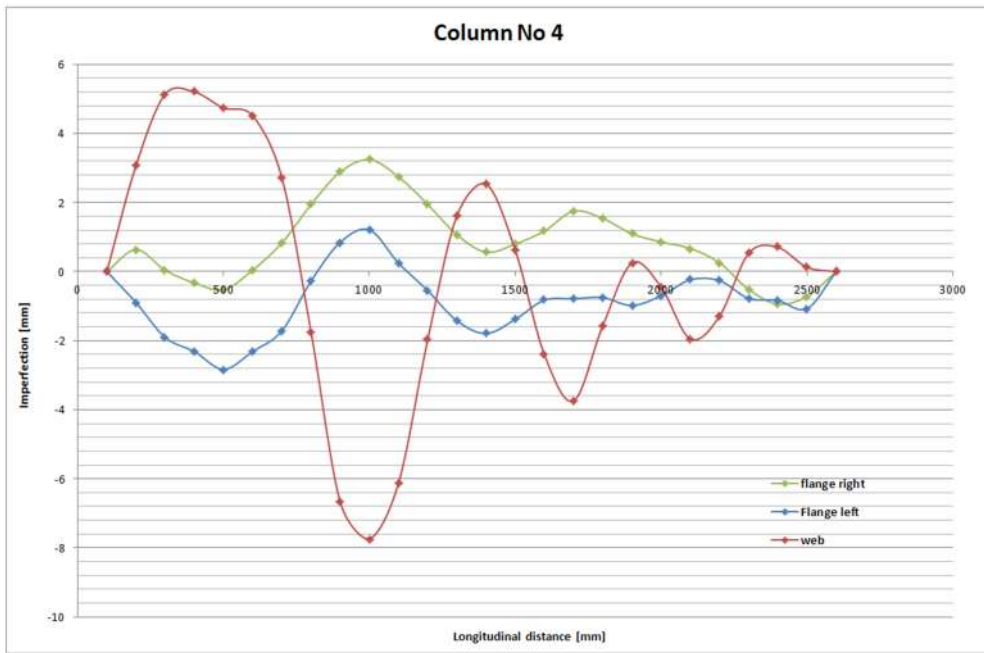


Figure 11: Test 4 – Amplitude of the imperfections along the web and both flanges

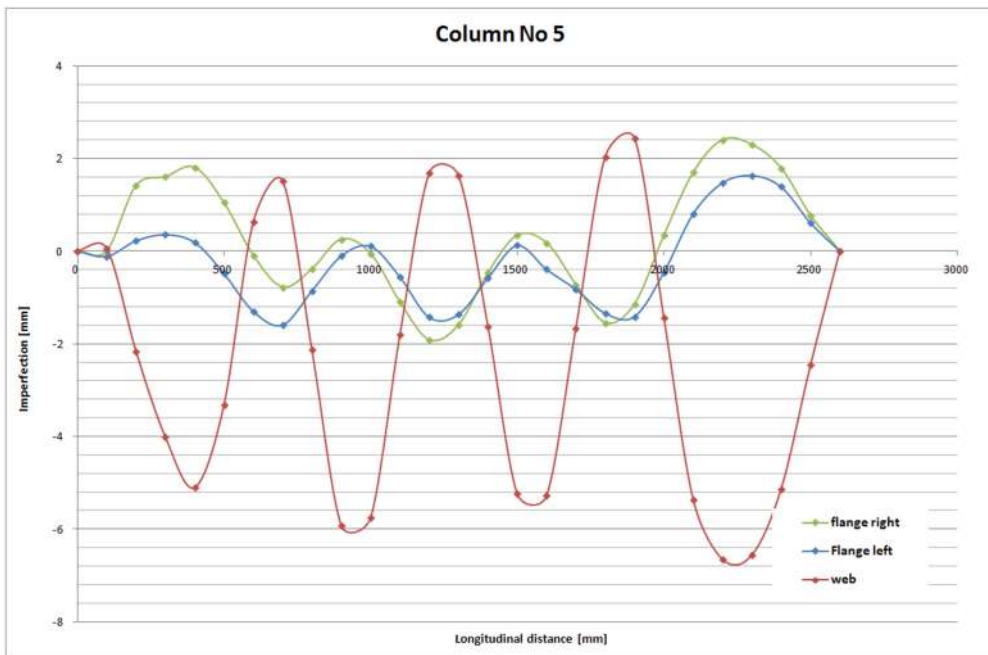


Figure 12: Test 5 – Amplitude of the imperfections along the web and both flanges

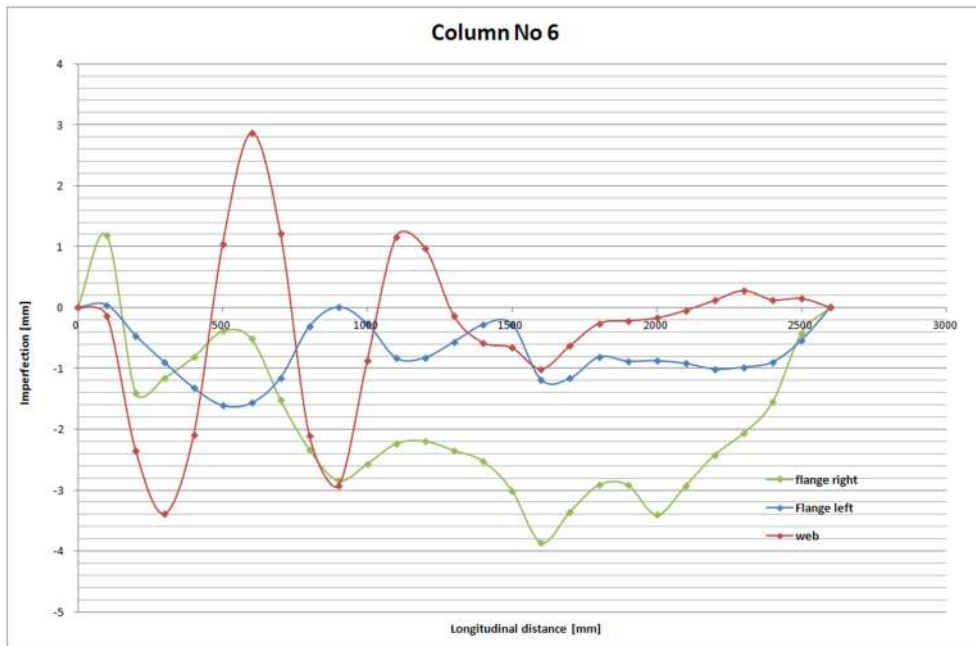


Figure 13: Test 6 – Amplitude of the imperfections along the web and both flanges

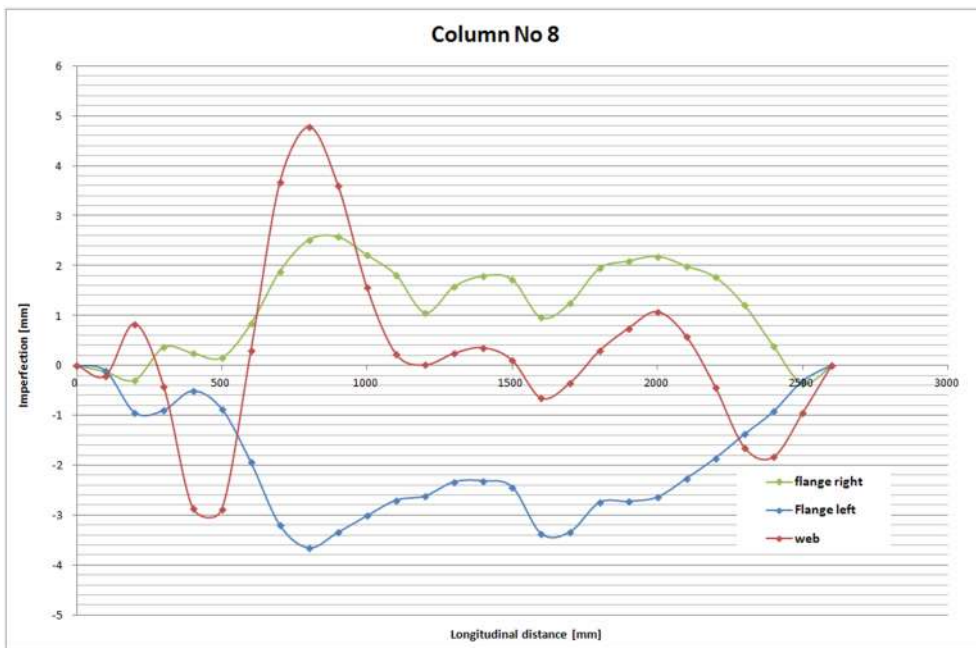


Figure 14: Test 8 – Amplitude of the imperfections along the web and both flanges

The fire tests consist in applying a mechanical load until reaching the load ratio (percentage of the cold failure load selected to reach a temperature of at least 450°C in the column) for the steel members and then heating the latter at least until mechanical failure. The column is heated electrically along its whole length using flexible ceramic pad heaters. This procedure is the same for the eight tested columns.

The tested columns are set in the steel frame of the laboratory which is made with jacks to apply the mechanical load on the tested columns pushing up the lower beam of the frame. A special preparation has been done because it is necessary to make some holes in the steel profiles madding up the frame to fix the pinned supports located at the extremities of the specimens. Some 20 mm diameter bolts are used to fix the specimen to the pinned support and also to fix the pinned supports to the steel testing frame. The frame and some details are described in the following figure:

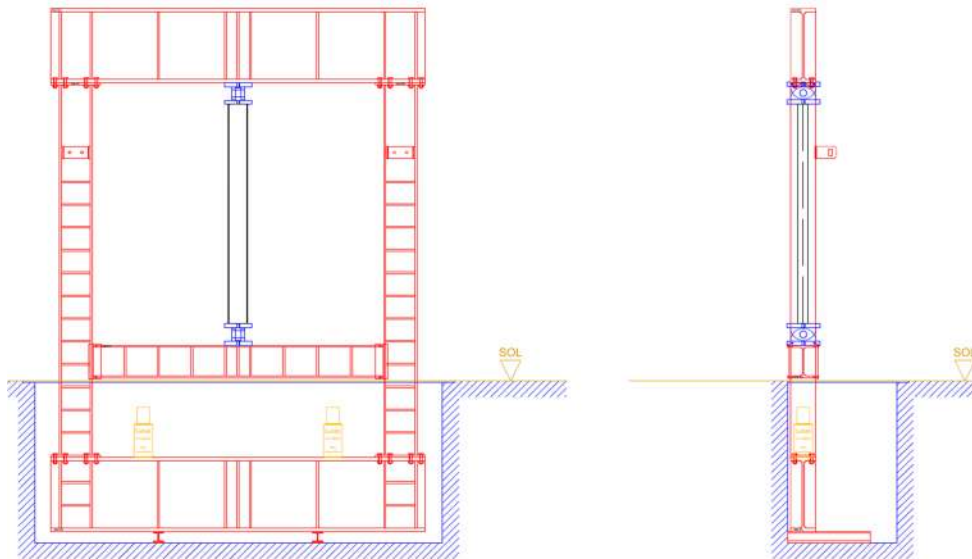


Figure 15: Testing frame for the experimental tests

A photograph of the steel frame is also available hereafter:



Figure 16: Testing frame for the experimental tests with the equipped column

The extremities of the columns are fixed using pinned supports which enable the rotation in only one direction, see Figure 17. This kind of supports allows controlling the failure mode of each tested column:

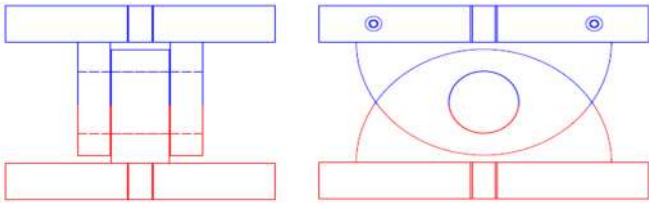


Figure 17: Scheme of pinned supports

In addition, this support cannot overreach the temperature of 200°C. But the columns (and thus its end-plates) will be heated up to a maximum of 650°C. So a thermal disconnection between the steel end-plate of the tested columns and the steel pinned support is installed. A layer of 35 mm of thickness of the material PROMATECT-H that allows ensuring sufficient compression strength in its heated state for the most critical of our experimental tests and that provides a lambda value at 650°C of around 0.235 W/m.K measured with hotwire system is placed between the end-plates and the pinned-supports. Details are available in the following figures:

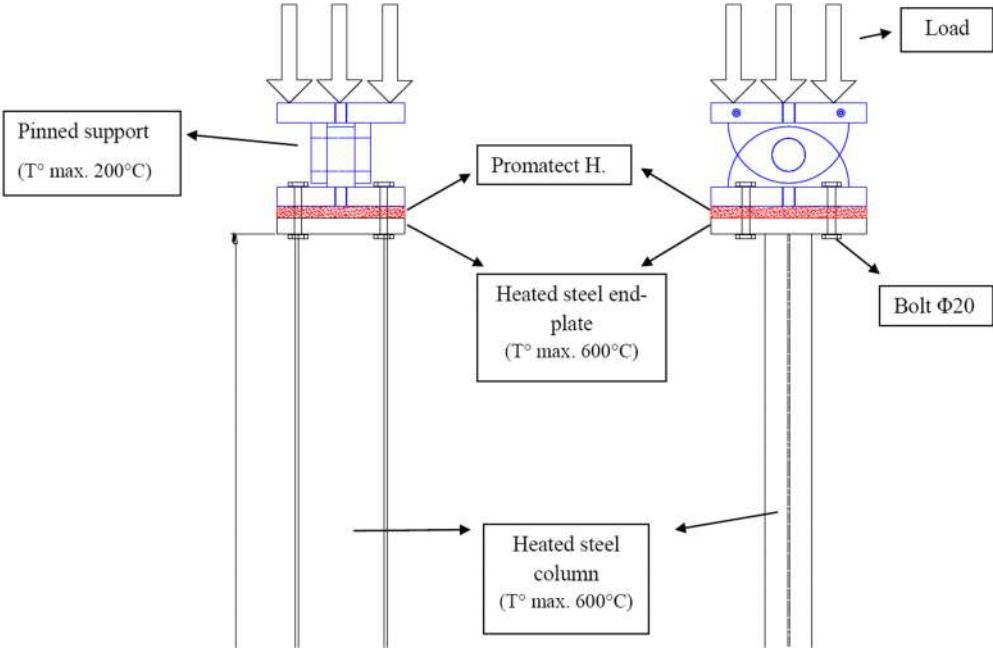


Figure 18: Layout of the insulating and resistant material PROMATECT-H



Figure 19: Pinned support with thermal disconnection

The columns are heated up using electrical elements; more precisely, flexible ceramic pad heaters are set along the profile providing a uniform increase of the temperature in the profile. The planning heating velocity is around $5^{\circ}\text{C}/\text{min}$. The heating is ordered from the supplier Stork Technical Service STS. The different components of the heating equipment are briefly described hereafter.

The Manning's power unit provides a 60 volts supply for powering various types of low voltage heating elements. The unit consists of an air natural three phase transformer, switching is made by contactors. The output channels are controlled by means of energy regulators and six temperature controllers, provision is made for connection to external control from any compatible programmer/control unit. Each channel has its own auto/manual switch so that it can be operated either automatically, via an external compatible programmer unit, or manually by means of the internal energy regulator and temperature controller:



Figure 20: Mannings 65 kV.A power unit with six temperature controllers

The Mannings six channels Automatic P256 Programmer/Controller is developed to be used in conjunction with Mannings' heat treatment Transformer Units to provide automatic temperature process control of up to six Transformer Unit output channels. Each control channel can either be operated for manual temperature control of the work piece, or in automatic mode. In automatic mode, the channel controller ensures that the control zone temperature closely follows the temperature rise, hold and fall and hold period parameters programmed by the operator.



Figure 21: Six channels automatic P256 programmer/controller

By the mean of a microprocessor which controls programming, LCD display and push button operation, programming and operation of the unit are kept simple and user friendly. The LCD display provides visual indication of the running heat treatment program status and control zone output. In addition, individual control zone neon's indicate when a control zone contactor is energized.

Mannings ceramic pad heating elements are constructed from high grade sintered alumina ceramic beads, Nickel-Chrome core wire and Nickel cold tail wire. The construction allows the heating element to be flexible and provides high heat transfer efficiency. In order to be able to heat all the eight different columns of the experimental tests, two sizes of the ceramic pad heating elements are used: 610 x 85 mm and 1220 x 45 mm.

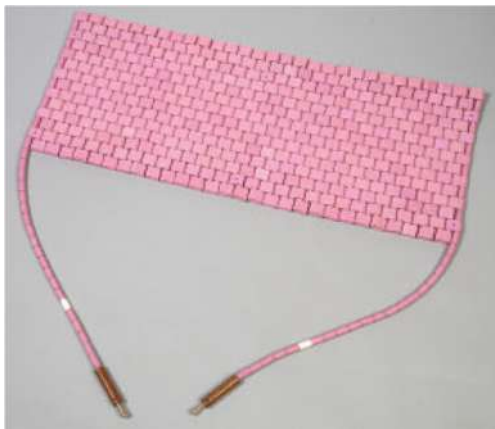


Figure 22: Ceramic pad heating elements

The temperatures are recorded during the whole duration of each test and at several positions along the web and the flanges of the columns by means of several thermocouples:

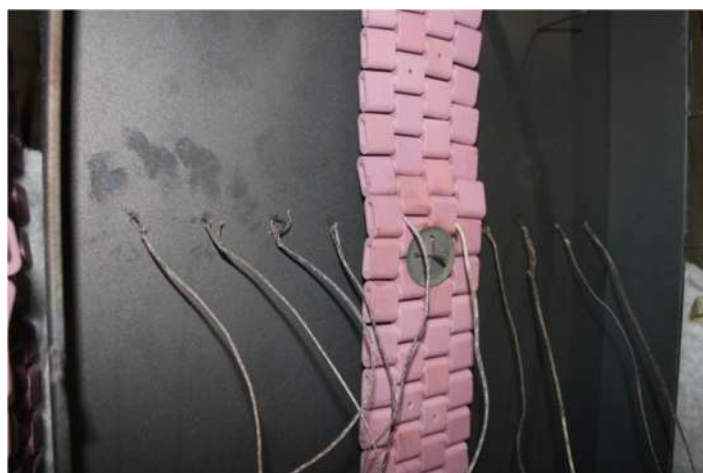


Figure 23: Thermocouples

Calculation of the mean temperature in the steel of the column is possible and the exact temperatures at several positions in order to observe the temperatures distribution and gradients induced along the column by the pad heaters are known. For each test and depending on the geometry of the column, the location of the thermocouple is slightly adapted.

Several displacements are measured by means of displacement transducers. The vertical global extension of the whole column subjected to the fire and to the load is obtained by the mean of the displacements measured by two displacement transducers located at the bottom face of the lower beam of the testing frame. The global deflections at mid-span of the column in the direction of the strong axis and of the weak axis are also measured by means of displacements transducers, see Figure 24. More precisely, the transversal displacement in the direction of the weak axis is measured at the middle of the width of the web whereas the transversal displacement in the direction of the strong axis is measured at the middle of the width of the flange:



Figure 24: Displacement transducer

Moreover, a visual examination is undertaken in order to observe the local displacements of section walls once the insulation surrounding the column is removed.

1.1.2 Progress and results of the experiments

As the arrangement of the pad heating elements depends on the geometry of the column, there are some differences between the eight tests and the layout of these pads is presented for each test.

After connecting all sensing devices (thermocouples, displacement transducers) to the measuring equipment, after connecting the heating pads and controlling thermocouples to the transformer, and after putting the insulating materials, the column is ready for the experiment and the test is conducted.

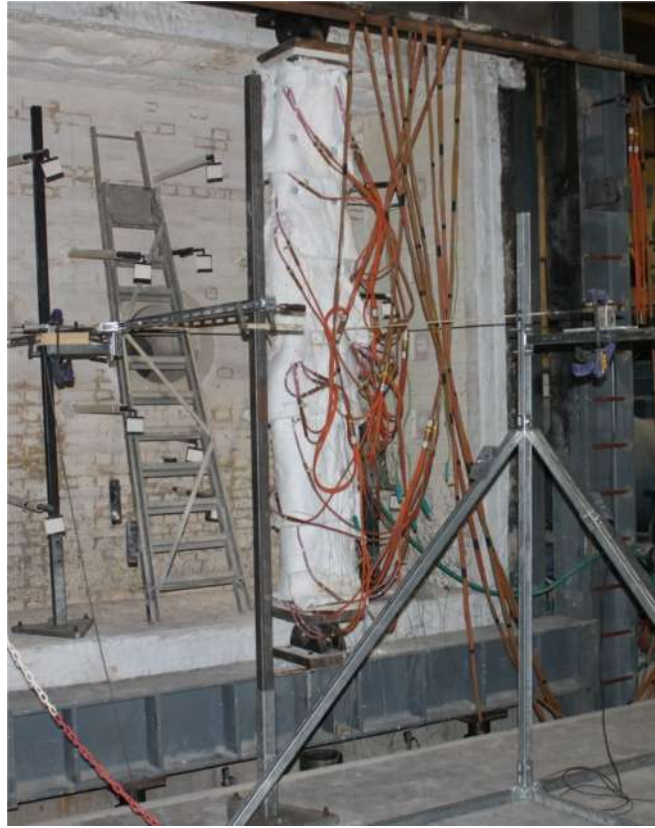


Figure 25: Equipped column with all sensing devices, heating pads and insulation

1.1.2.1 *Blank test*

Some blank tests are performed before launching the real experimental tests in order to master the heating and loading methodologies and equipments. The load is applied on the column with two jacks pushing up the lower beam of the testing frame; it is the usual way to apply the load in the vertical furnace of the laboratory of Liege and this method is thus well known and mastered. The blank tests aimed at the observation of the temperature provided by the ceramic heating pads and then the distribution of the temperature into the steel columns. LINDAB provided two times the set of the welded columns to be tested by the ULg in this project. The first set was provided without certificate and samples to realize the material tests for the steel of the columns. All the columns were thus reproduced a second time. The column of test 3 of the first set is used to perform preliminary heating tests.

Some preliminary tests are performed to study the heating of the steel by using the heating pads. The first test is made putting the heating pads against the steel web of the column. Moreover, a velocity of heating of $100^{\circ}\text{C}/\text{h}$ is imposed thanks to the automatic mode available with the equipments that allows giving a temperature profile which is followed the most closely by the activation of the heating pads on the basis of information from the thermocouples which are displayed on the measuring device. In automatic mode, the channel controller ensures that the control temperature closely follows the temperature rise (in this case $100^{\circ}\text{C}/\text{h}$), hold and fall and hold period parameters programmed by the operator. The temperature is recorded at three different positions below and around the heating pad to study the variation of the temperatures of the steel; one thermocouple is directly set below the heating

pad (i.e. between the pad and the steel), one thermocouple at 1 cm from the pad, and a last one is put just at the middle distance between two resistances, see Figure 26:

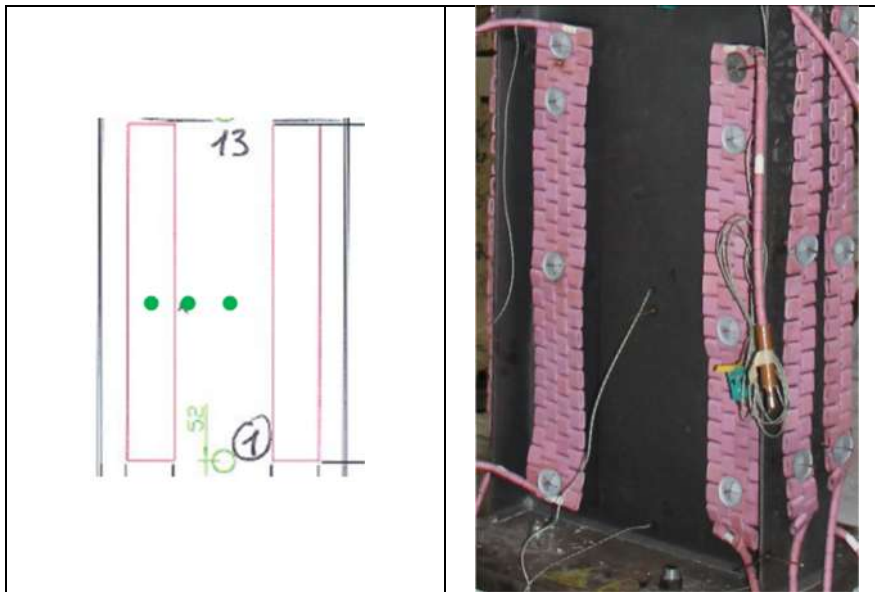


Figure 26: Location of the thermocouples along the height of the web of the column below and between two resistances (the pads are put directly against the steel)

The temperature distribution obtained with this setup is presented in the following figure:

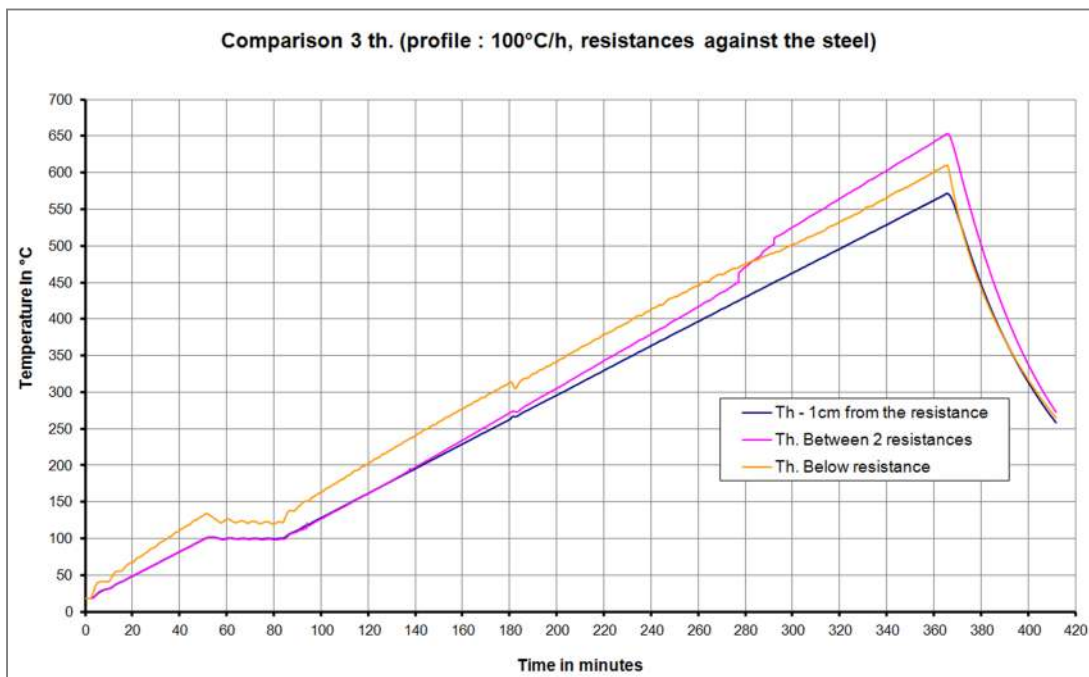


Figure 27: Evolution of temperature in function of time in the three thermocouples

The biggest variation of the temperatures observed between these three thermocouples is presented in the next figure:

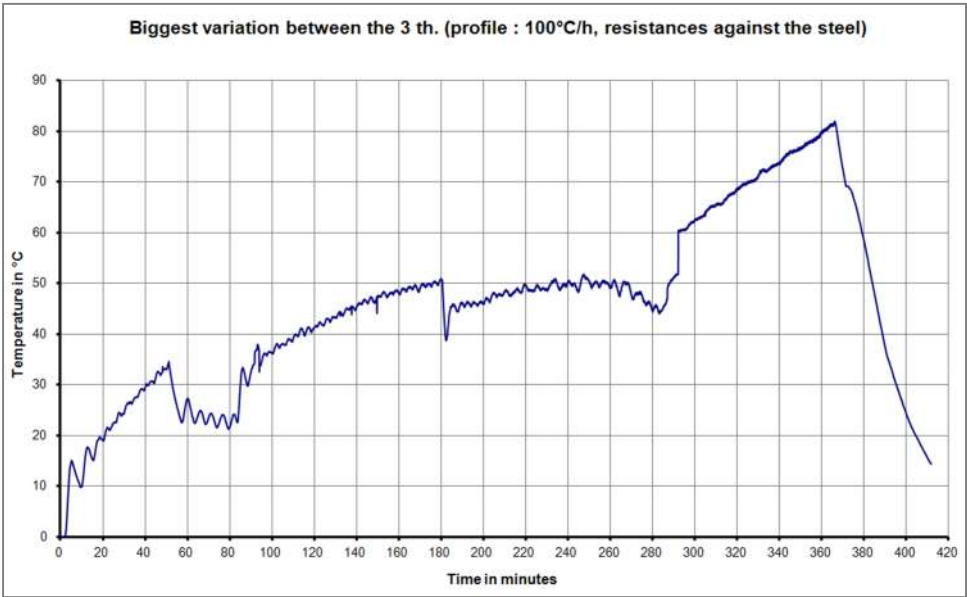


Figure 28: Most important variation between the temperatures of the three thermocouples

A significant temperature gradient is observed with maximum amplitude of 80°C while the maximum distance between the thermocouple is only 13 cm. This result is not very convincing because the objective is to reach the most uniform temperature along the whole column.

A second test is performed putting in this case the resistance at a distance of 25 mm from the surface of the steel of the web in order to use the convection and also the radiation from the resistances to heat the steel column. The thermocouples are set at the same positions than in the previous test:



Figure 29: Location of the resistance (25 mm from the steel surface)

The temperature distribution obtained with this setup is presented in the following figure:

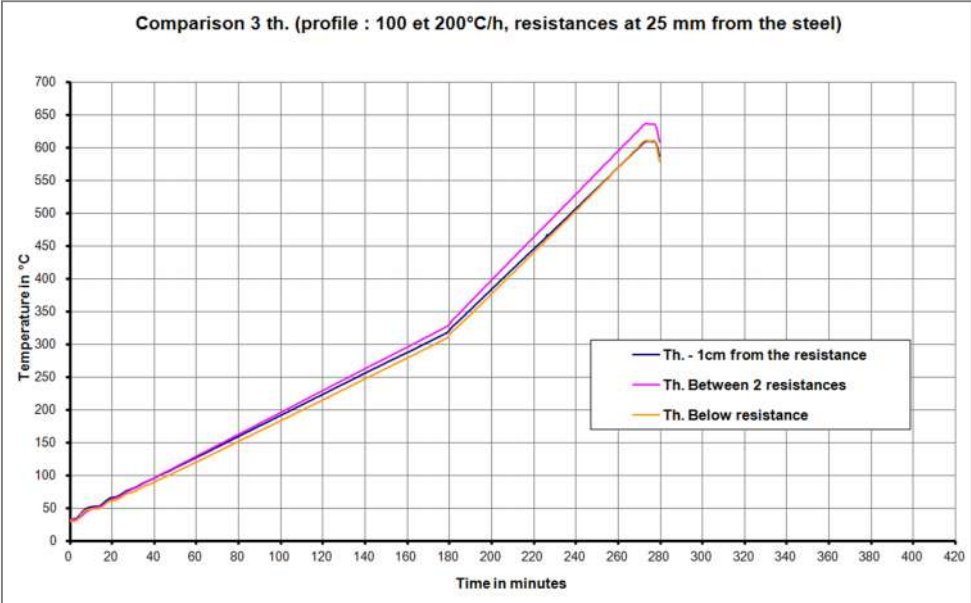


Figure 30: Temperature comparison between the three thermocouples with the resistance at 25 mm from the steel

The biggest variation of the temperatures observed between these three thermocouples is presented in the following figure. It is observed that the gradient is largely smaller than in the previous case with the resistance put against the steel (maximum gradient of 29°C):

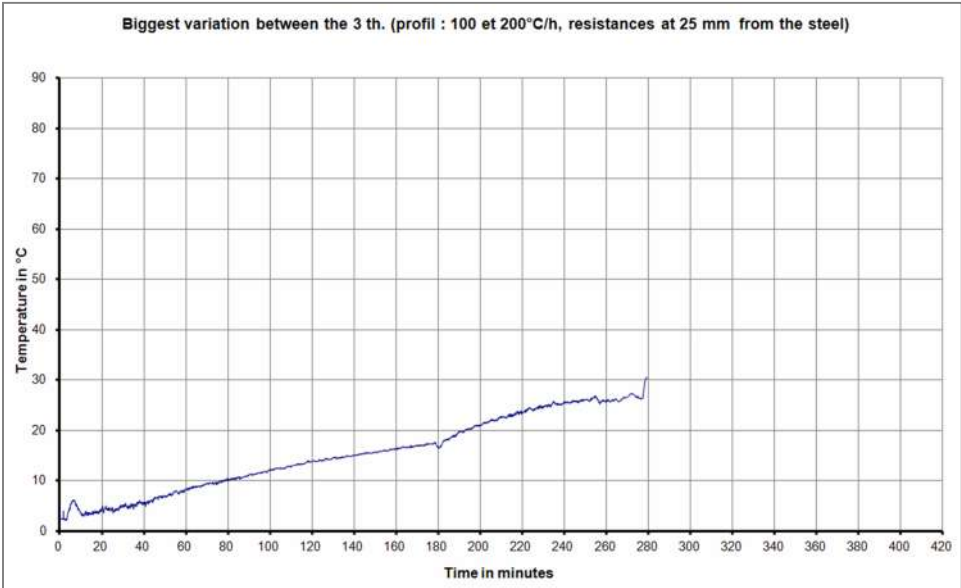


Figure 31: Maximum variation between the temperatures of the three thermocouples

Finally the column of the blank test is tested as in the real experimental configuration. The column is loaded and then heated up with a velocity of 400°C/h until mechanical failure. In order to improve the uniformity of the heating of the whole column, it is divided in six control zones gathering a certain number of resistances. Each zone is managed by a channel control and the imposed increase of temperature to all the zones are the same (constant velocity of 400°C/h). The cold failure load, the selected value of the applied load and the failure temperature computed with SAFIR software are given in the table here below with the main dimensions of the column No 3:

Cold failure load (kN)	Load applied for the test (kN)	Experimental Failure temperature (°C)	Failure temperature SAFIR (°C) <i>Before the test</i>
408	204	345	420

Table 3: Main results of blank test

The temperature profiles given by the six control thermocouples are presented in the following figure:

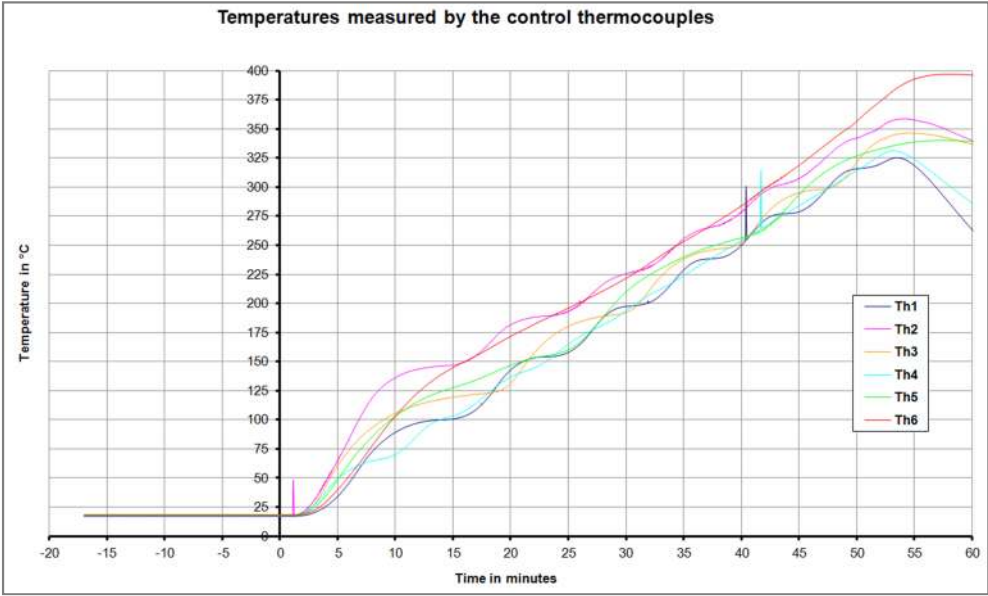


Figure 32: Profile of the obtained temperatures for the six thermocouples

The mechanical failure occurs at a temperature of 345°C (mean temperature between the six temperatures of the control thermocouples). The failure occurs earlier than the failure temperature calculated with SAFIR because the fixation of one of the control thermocouples broke down and the temperature recorded by this thermocouple was lower than the real temperature of the steel in the zone. So the global failure is induced by an excessive heating of the resistances of the zone No 1. However, it is observed that the automatic mode is successful because the temperature of the six zones is consistent with the instructions (temperature rise of 400°C/h) imposed by the automatic controller. The failure mode of the blank test is illustrated hereafter:

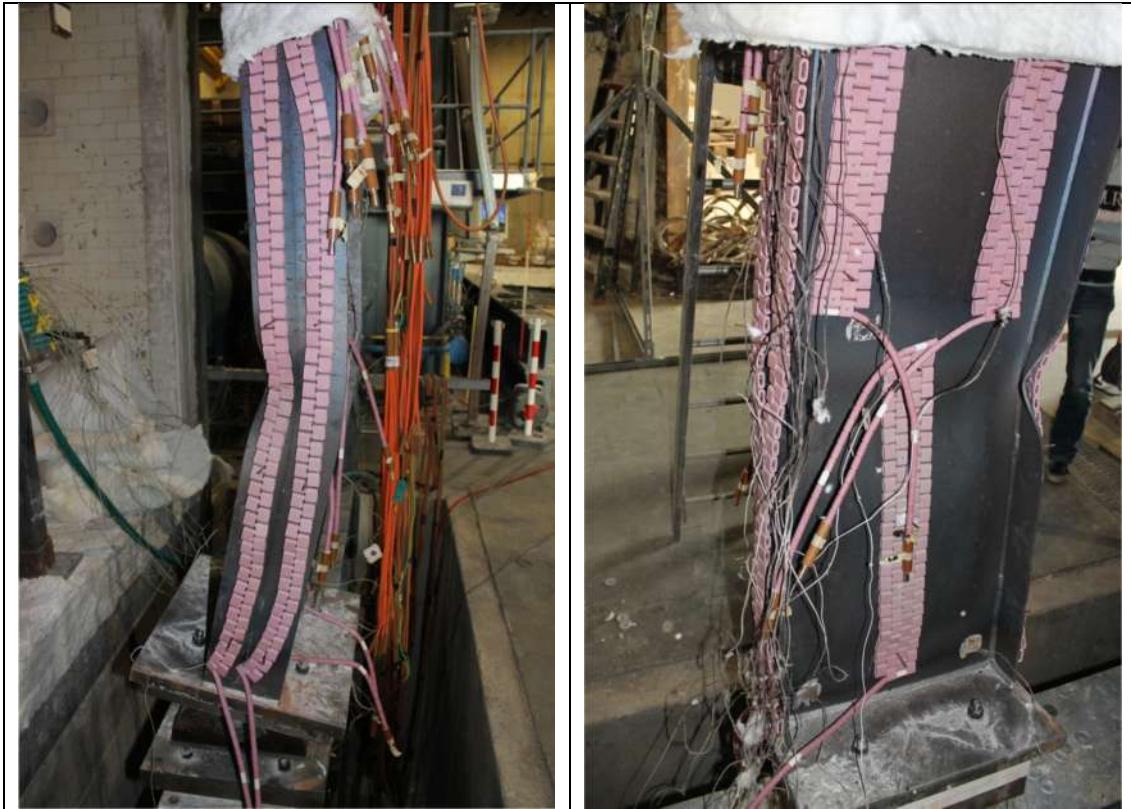


Figure 33: Failure mode of column of blank test

The transversal displacements in function of time are shown in next diagram:

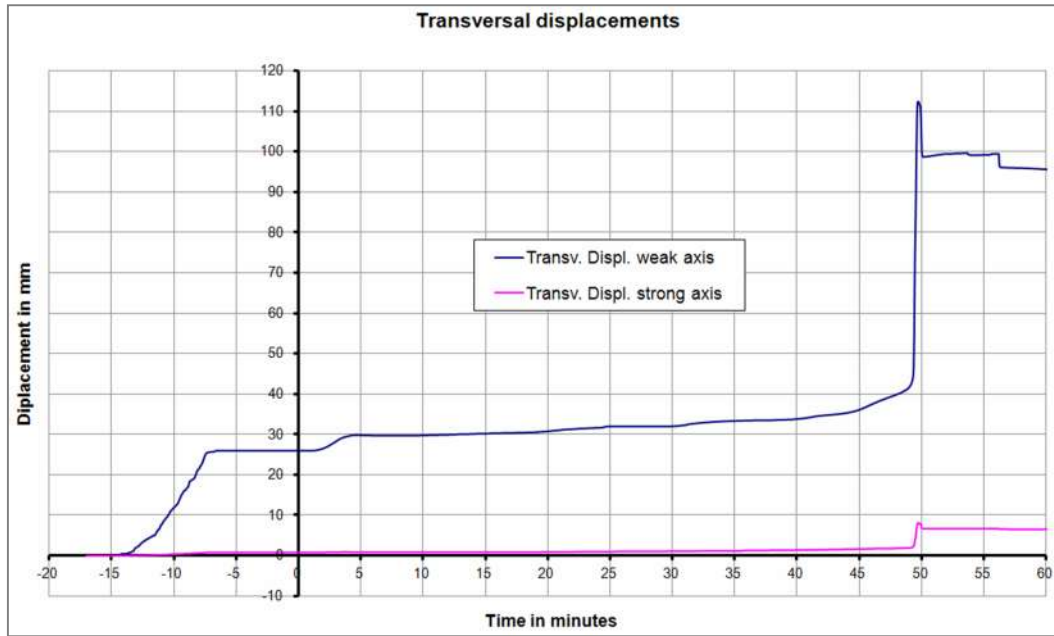


Figure 34: Transversal displacement in the direction of the strong axis in function of time

1.1.2.2 Test 1

The dimensions of the hot-rolled IPE240A are given in the following table:

h_w (mm)	t_w (mm)	b (mm)	t_f (mm)	H (mm)
237	5.2	120	8.3	2700

Table 4: Global dimensions of first tested column

The applied load for the test and the expected failure temperature calculated with SAFIR are given in the table below:

Cold failure load (kN)	Load applied for the test (kN)	Experimental Failure temperature (°C)	Failure temperature SAFIR (°C) <i>Before the test</i>
410.3	144.5	610	541

Table 5: Applied load and failure temperature for test 1

The location of the resistances and the definition of the control zones are presented on the scheme here below. Only five areas are used in this test because the web of the column is only 220 mm width and allows putting only two resistances on its width:

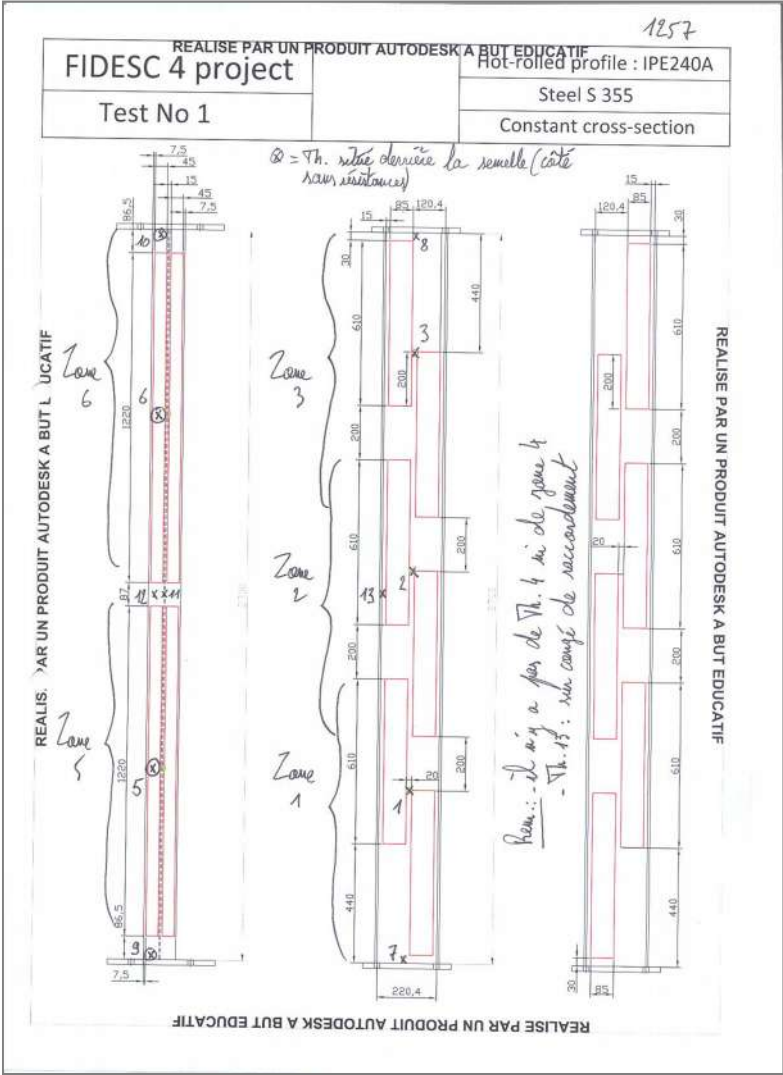


Figure 35: Definition of the control zones and position of the control thermocouples

The temperature of the control thermocouples as a function of time is shown in the following figure:

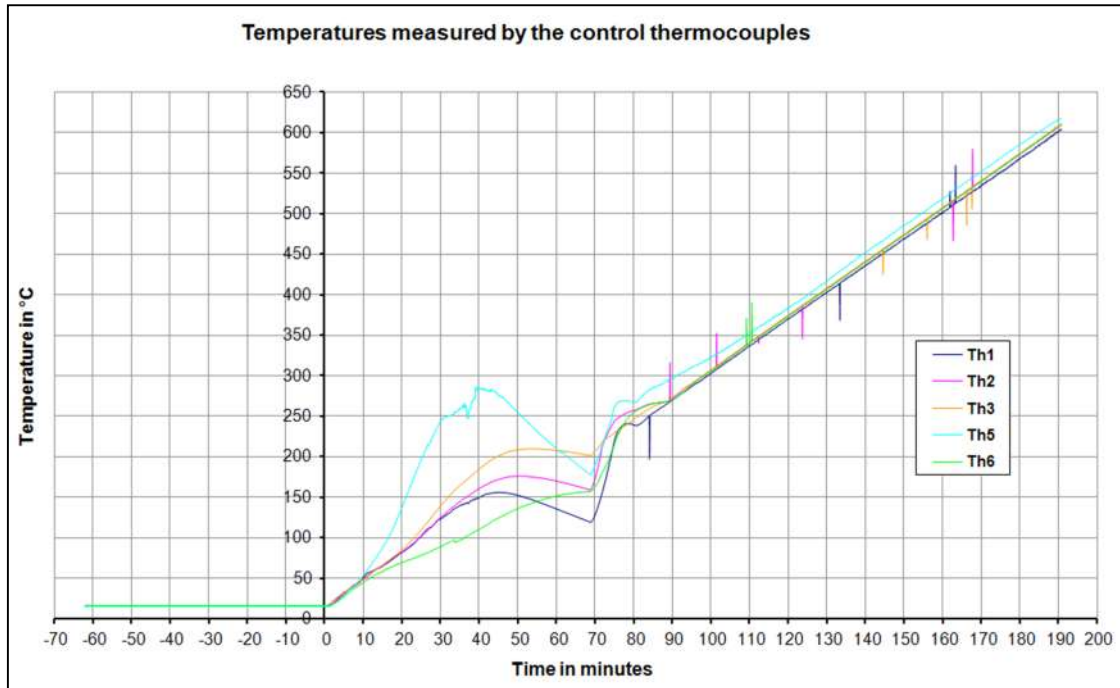


Figure 36: Recorded temperature by the five control thermocouples

It is observed that the control temperature curves are very close to each other and the instruction is thus well followed after the 80th minute. At the beginning of the heating, some differences appear. It is due to the calibration of the different zones and resistances. The heating and loading process is stopped at the 190th minute:

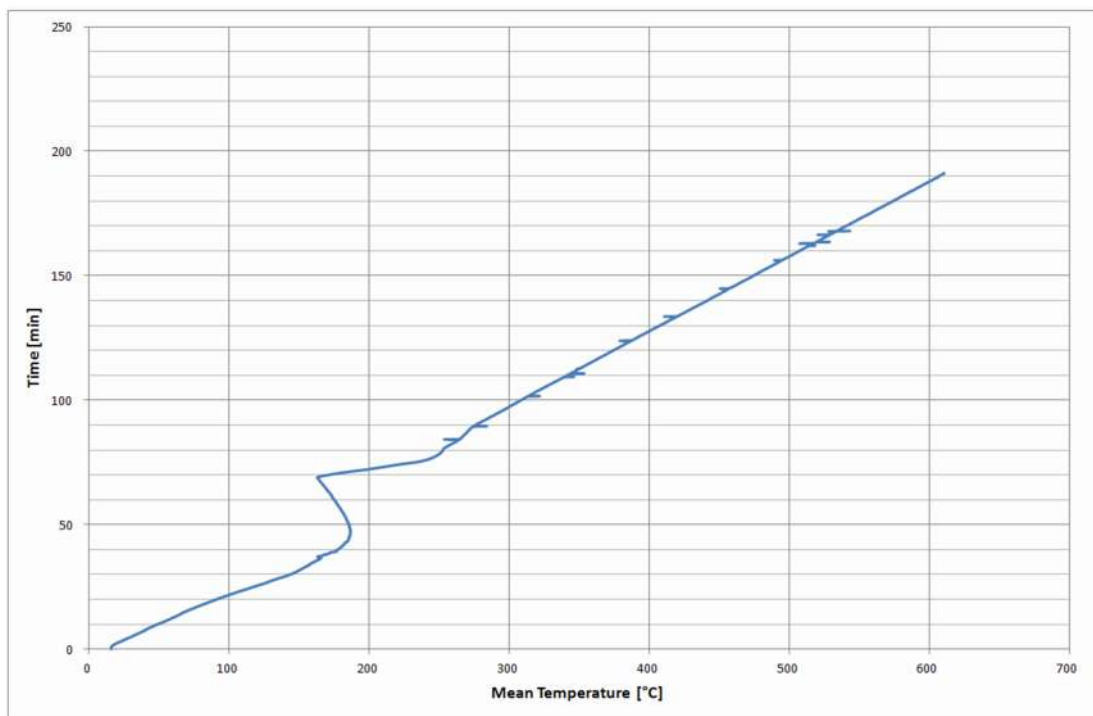


Figure 37: Time in function of the mean temperature

By calculating the mean between these five temperatures, the evolution of the transversal and axial displacements as a function of the mean temperature of the column is displayed in the next figure:

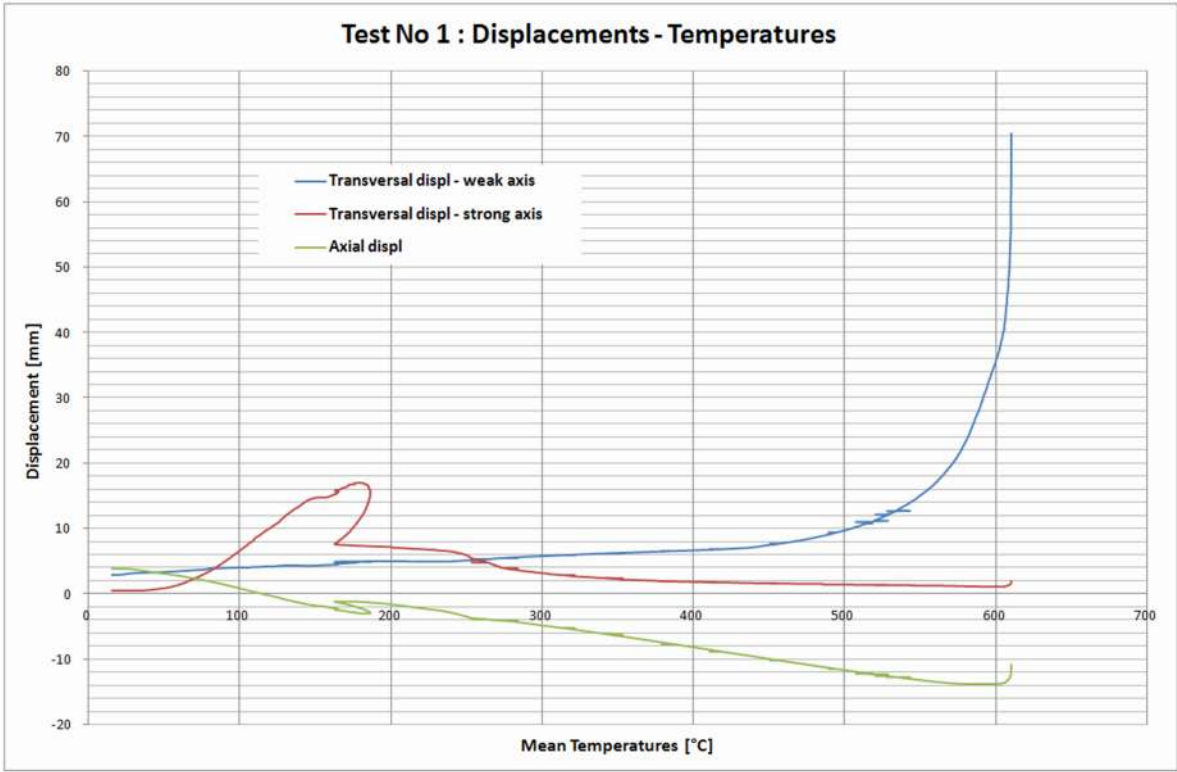


Figure 38: Displacements (mm) in function of the mean temperature (°C)

The real properties are determined by performing material tests on samples of the steel of the web and of the flange. For test 1, these material tests are performed by partner 5. The steel grades of the flange and of the web are the following:

	Upper yield strength (MPa)	$f_{y,mean}$ (MPa)	Bottom yield strength (MPa)	$f_{y,mean}$ (MPa)
Web	452 - 447	449.5	445 - 436	441.5
Flanges	408 - 396	402	396 - 391	393.5

Table 6: Summarized material properties of test 1

The deformed shape of column of test 1 after failure is shown in the following pictures:



Figure 39: Deformed shape after test 1

1.1.2.3 Test 2

The dimensions of the welded 450x4+150x5 are given in the following table:

h_w (mm)	t_w (mm)	b (mm)	t_f (mm)	H (mm)
450	4	150	5	2700

Table 7: Global dimensions of second tested column

The applied load for the test and the expected failure temperature calculated with SAFIR are given in the table below:

Cold failure load (kN)	Load applied for the test (kN)	Experimental Failure temperature (°C)	Failure temperature SAFIR (°C) <i>Before the test</i>
408	122.4	608	578

Table 8: applied load and failure temperature for test 2

The location of the resistances and the definition of the control zones are presented on the scheme here below. In this case, six zones are used because the web of the column was 450 mm width and allows putting three resistances on its width.

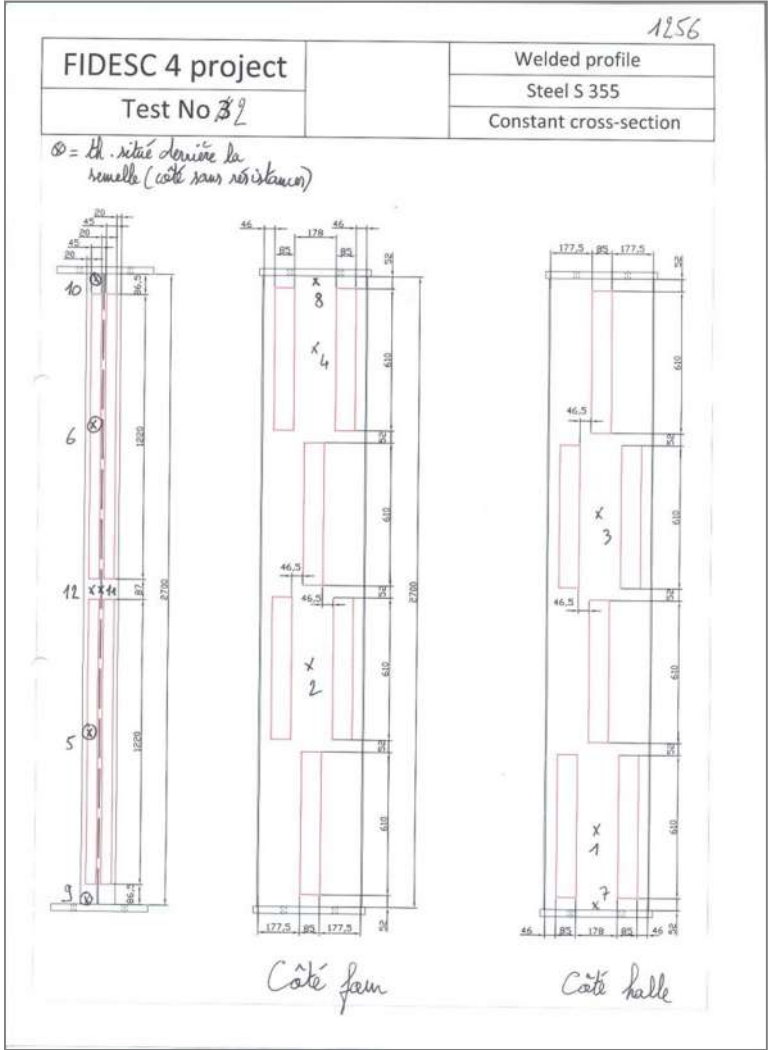


Figure 40: Definition of the control zones and position of the control thermocouples

The temperature of the control thermocouples as a function of time is shown in the following figure:

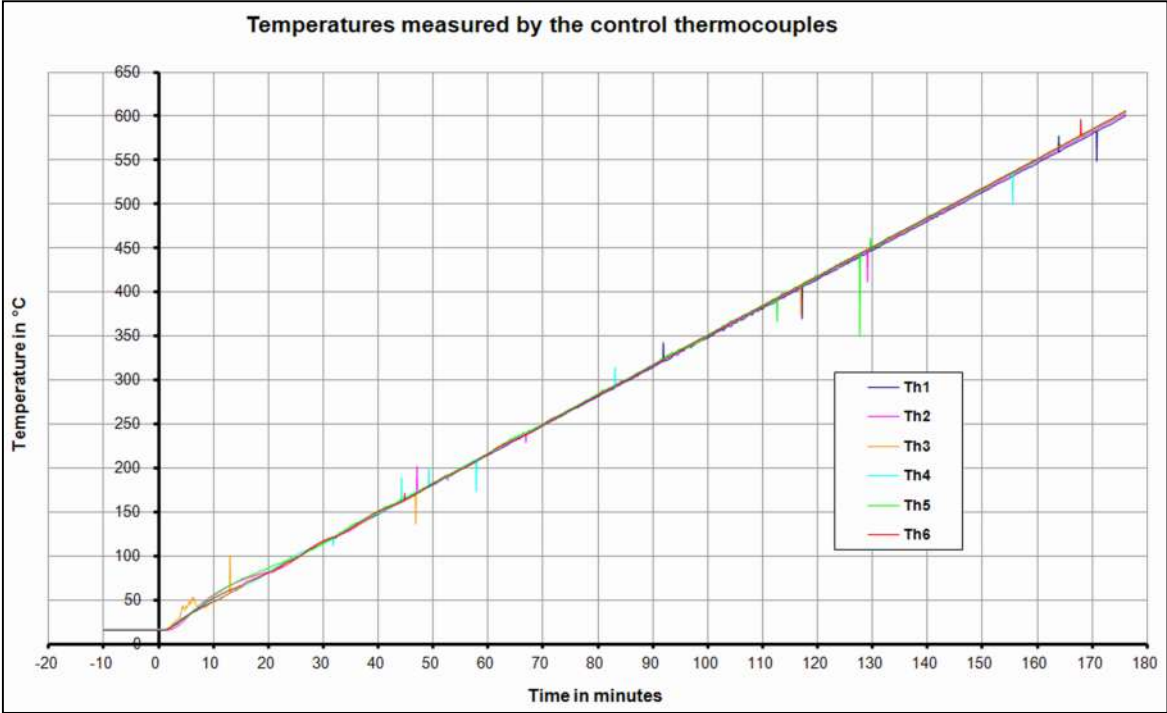


Figure 41: Recorded temperature by the six control thermocouples

It is observed that the control temperature curves are very close to each other and the instruction is thus well followed. The heating and loading process is stopped at the 176th minute:

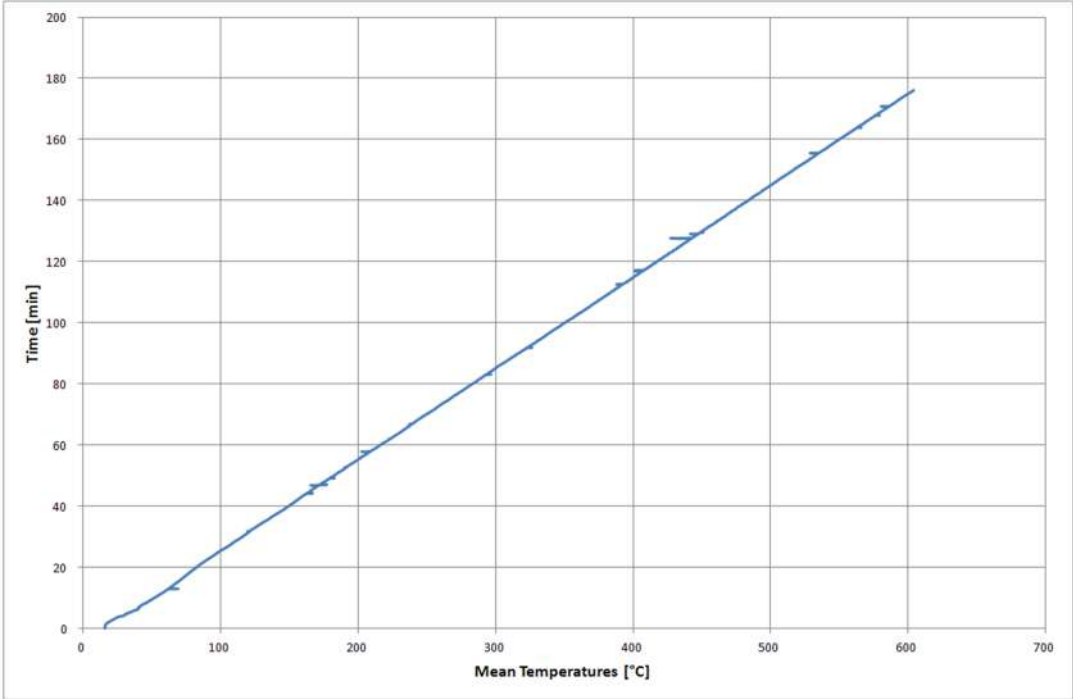


Figure 42: Time in function of the mean temperature

By calculating the mean between these six temperatures, the evolution of the transversal and axial displacements as a function of the mean temperature of the column is displayed in the next figure:

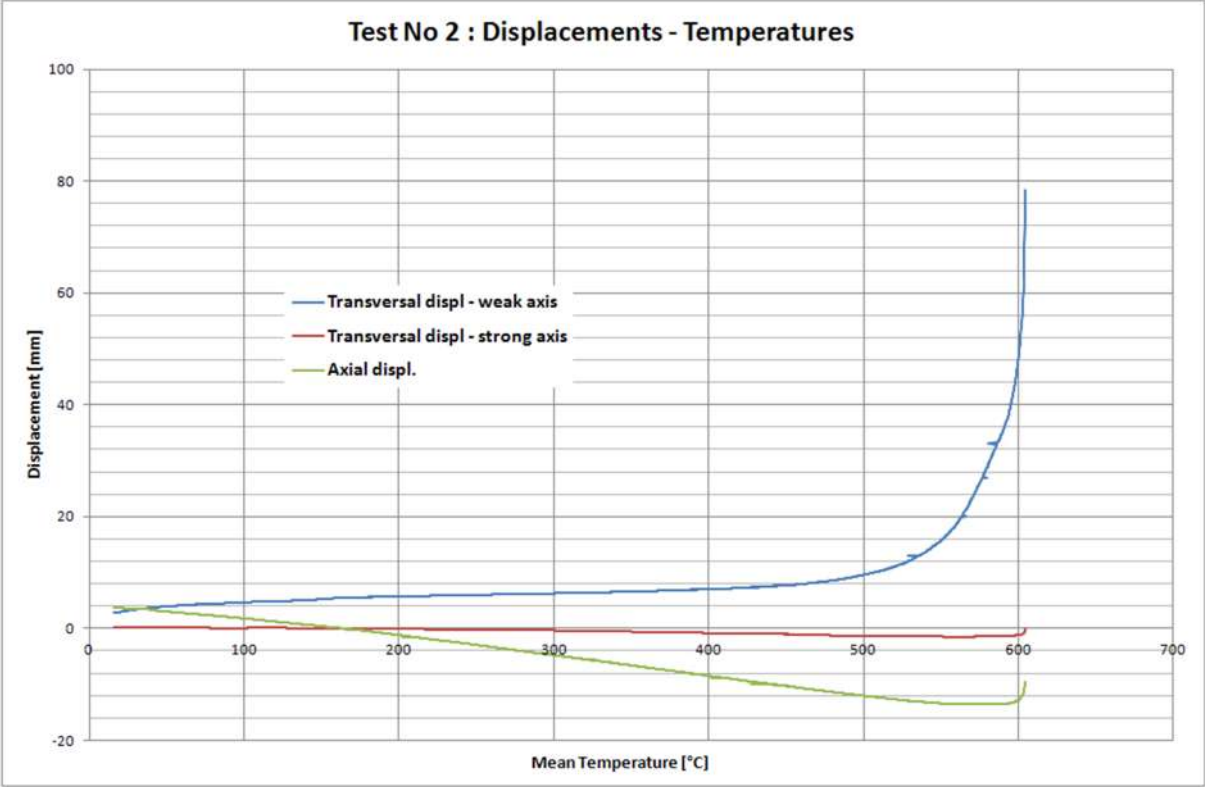


Figure 43: Displacements (mm) in function of the mean temperature (°C)

The real properties are determined by performing material tests on samples of the steel of the web and of the flange. For test 2, these material tests are performed by partner 2 and a certificate is provided with the welded columns. The steel grades of the flange and of the web are the following:

	yield strength (MPa)
Web – at the lead end of the plate	482
Web – at the tail end of the plate	447
Flanges	404

Table 9: Summarized material properties of test 2

The deformed shape of column of test 2 after failure is shown in the following pictures:



Figure 44: Deformed shape after test 2

1.1.2.4 Test 3

The dimensions of the welded 450x4+150x5 are given in the following table:

h_w (mm)	t_w (mm)	b (mm)	t_f (mm)	H (mm)
450	4	150	5	2700

Table 10: Global dimensions of third tested column

The applied load for the test and the expected failure temperature calculated with SAFIR are given in the table below:

Cold failure load (kN)	Load applied for the test (kN)	Experimental Failure temperature (°C)	Failure temperature SAFIR (°C) <i>Before the test</i>
408	204	452	420

Table 11: applied load and failure temperature for test 3

The location of the resistances and the definition of the control zones are presented on the scheme here below. In this case, six zones are used because the web of the column was 450 mm width and allows putting three resistances on its width.

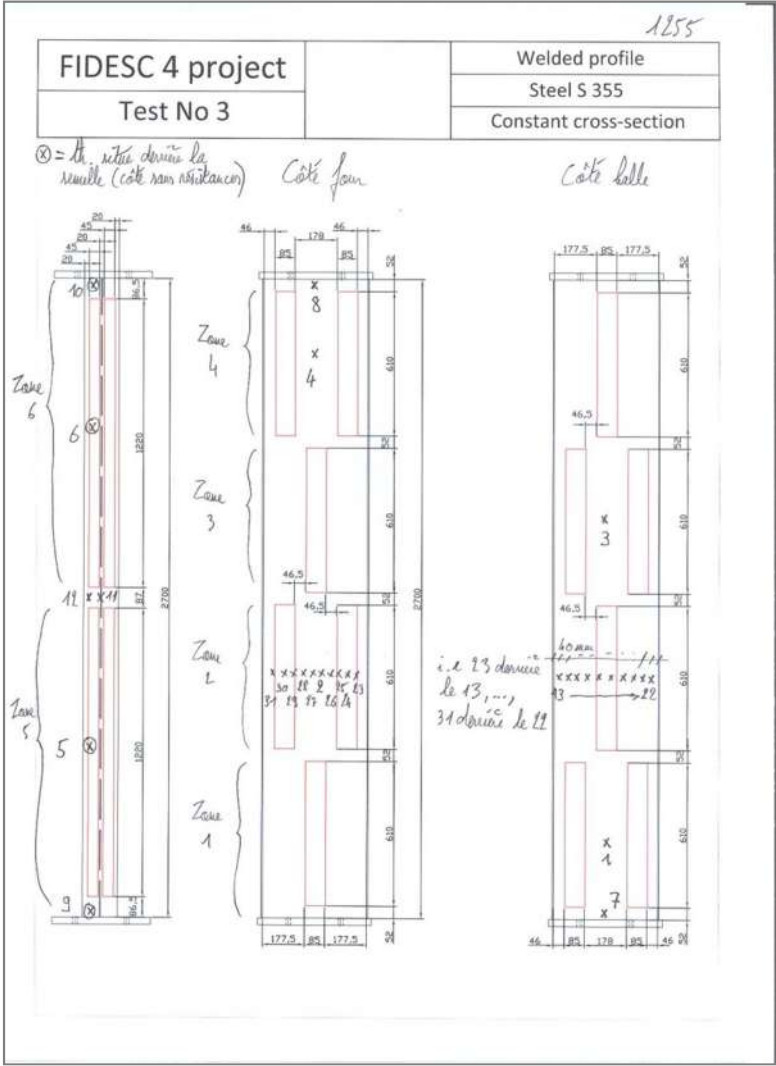


Figure 45: Definition of the control zones and position of the control thermocouples

The temperature of the control thermocouples as a function of time is shown in the following figure:

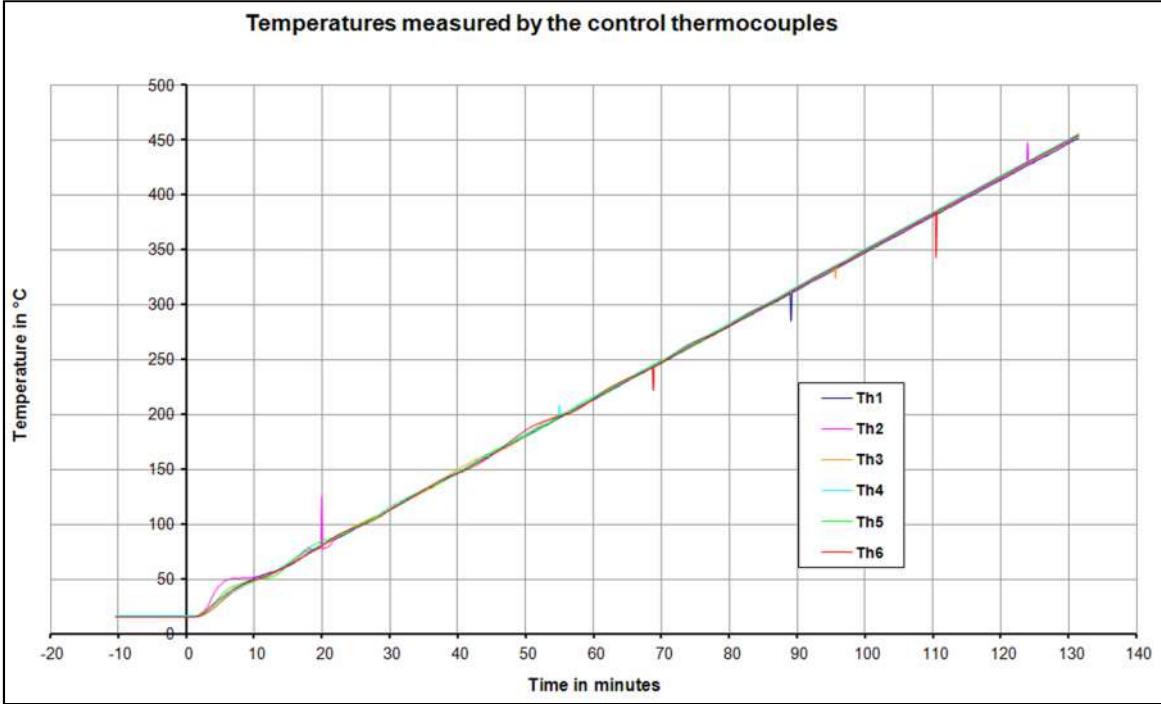


Figure 46: Recorded temperature by the six control thermocouples

It is observed that the control temperature curves are very close to each other and the instruction is thus well followed. The heating and loading process is stopped at the 131th minute:

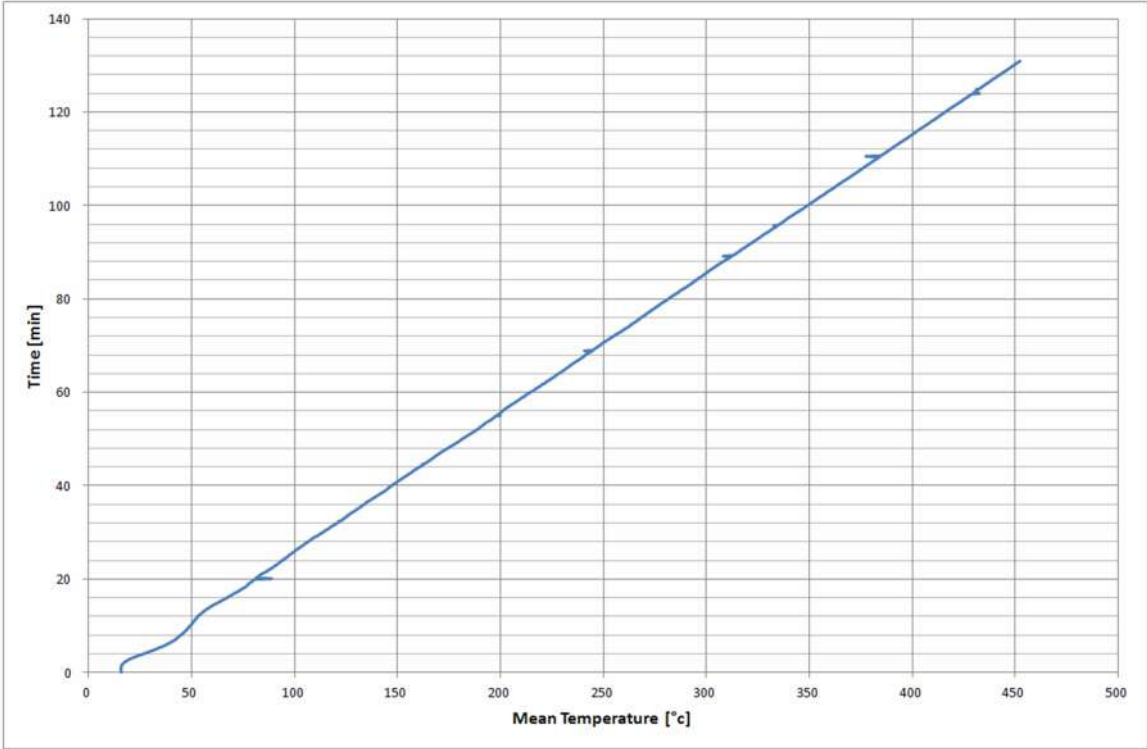


Figure 47: Time in function of the mean temperature

By calculating the mean between these six temperatures, the evolution of the transversal and axial displacements as a function of the mean temperature of the column is displayed in the next figure:

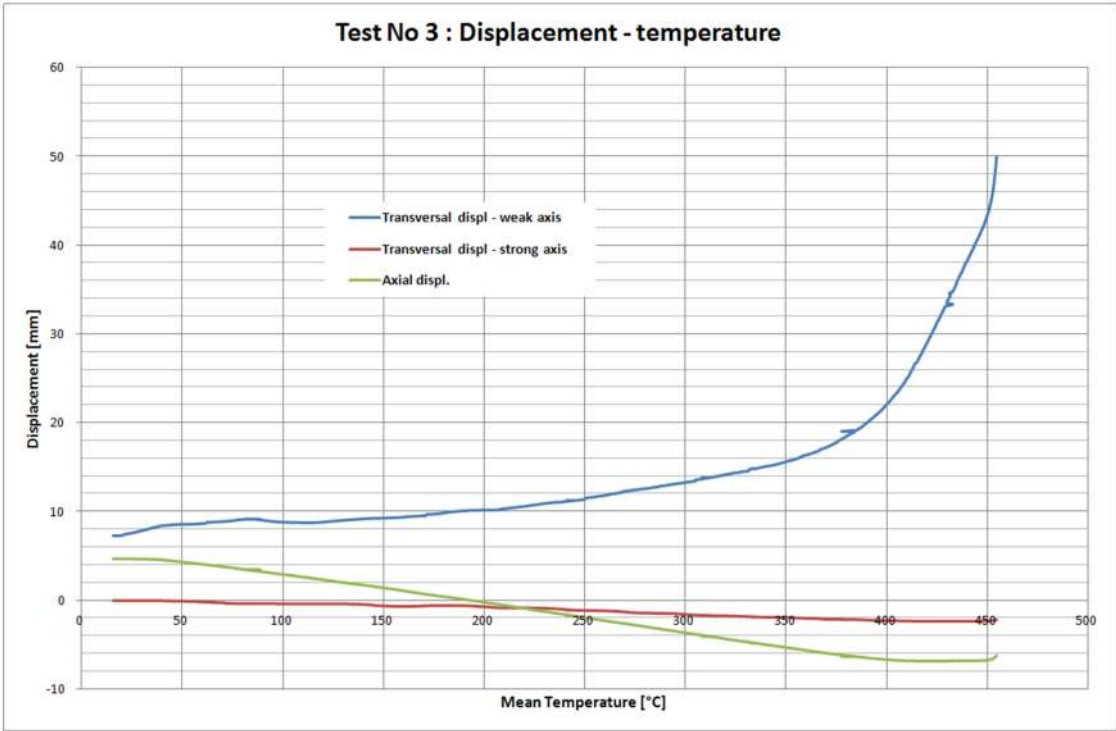


Figure 48: Displacements (mm) in function of the mean temperature (°C)

The real properties are determined by performing material tests on samples of the steel of the web and of the flange. For test 3, these material tests are performed by partner 2 and a certificate is provided with the welded columns. The steel grades of the flange and of the web are the following:

	yield strength (MPa)
Web – at the lead end of the plate	482
Web – at the tail end of the plate	447
Flanges	404

Table 12: Summarized material properties of test 3

The deformed shape of column of test 3 after failure is shown in the following pictures:



Figure 49: Deformed shape after test 3

1.1.2.5 Test 4

The dimensions of the welded 500-300x4+150x5 are given in the following table:

h_w (mm)	t_w (mm)	b (mm)	t_f (mm)	H (mm)
300 (small base)	4	150	5	2700
500 (large base)				

Table 13: Global dimensions of fourth tested column

The applied load for the test and the expected failure temperature calculated with SAFIR is given in the table below:

Cold failure load (kN)	Load applied for the test (kN)	Experimental Failure temperature (°C)	Failure temperature SAFIR (°C) <i>Before the test</i>
696	348	520	502

Table 14: Applied load and failure temperature for test 4

The location of the resistances and the definition of the control zones are presented on the scheme here below. In this case, six zones are used because with a particular disposition of the resistances due to the variable width of the web.

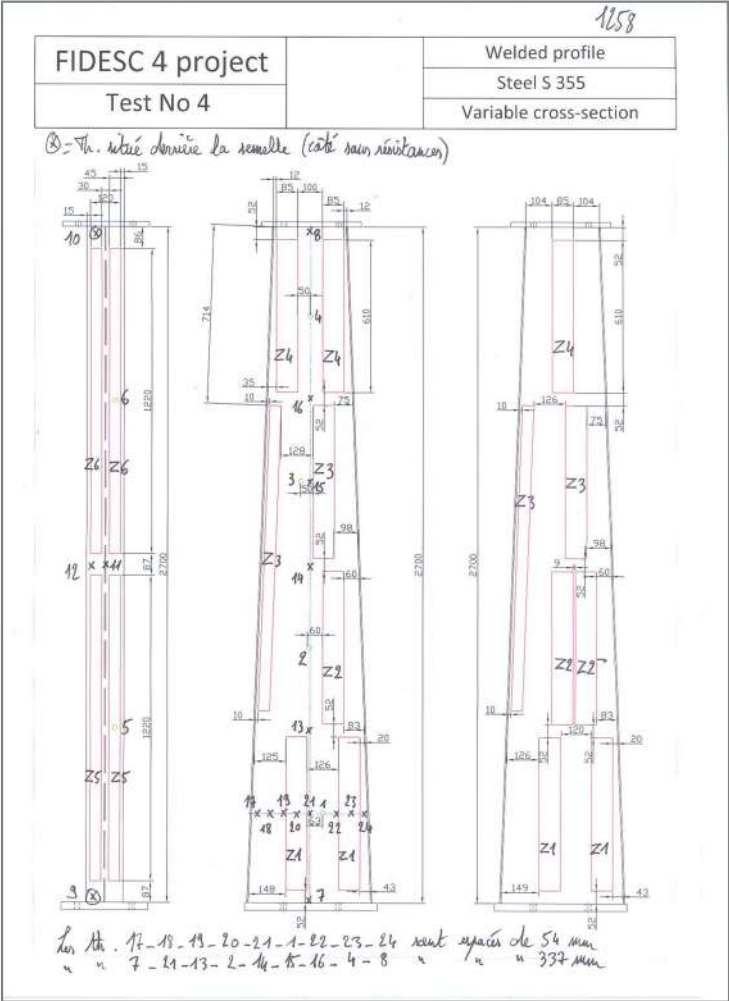


Figure 50: Definition of the control zones and position of the control thermocouples

The temperature of the control thermocouples as a function of time is shown in the following figure:

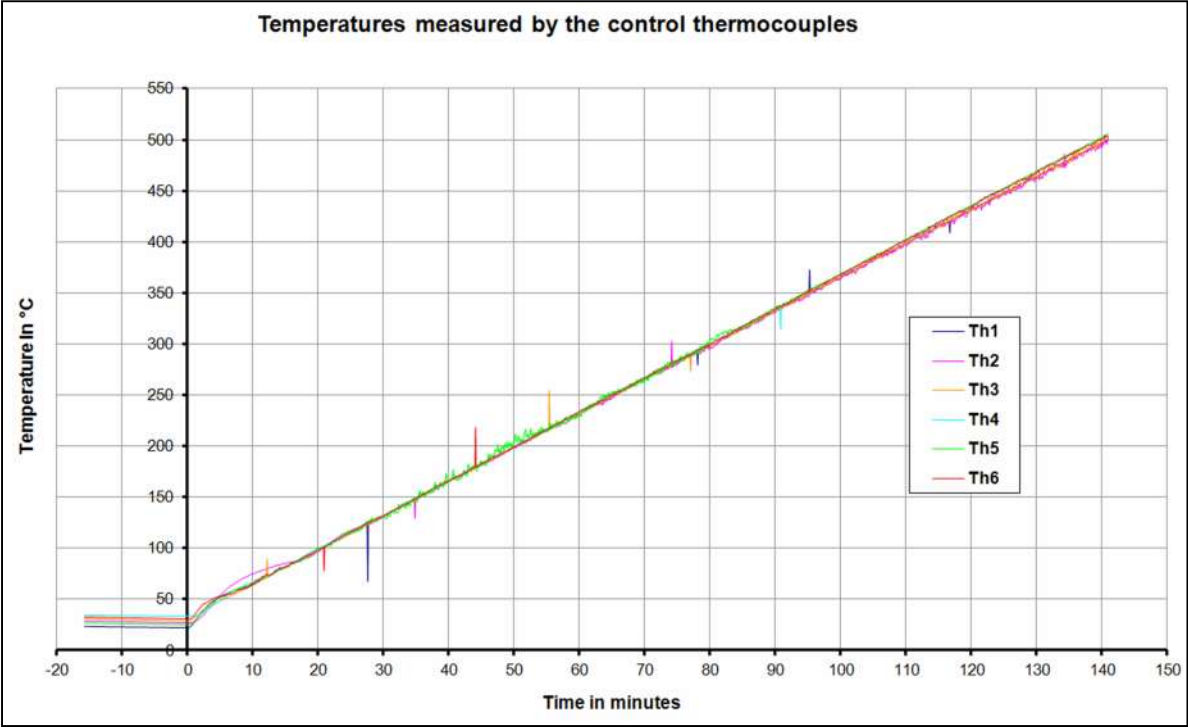


Figure 51: Recorded temperature by the six control thermocouples

It is observed that the control temperature curves are very close to each other and the instruction is thus well followed in the six areas. The heating and loading process is stopped at the 141th minute:

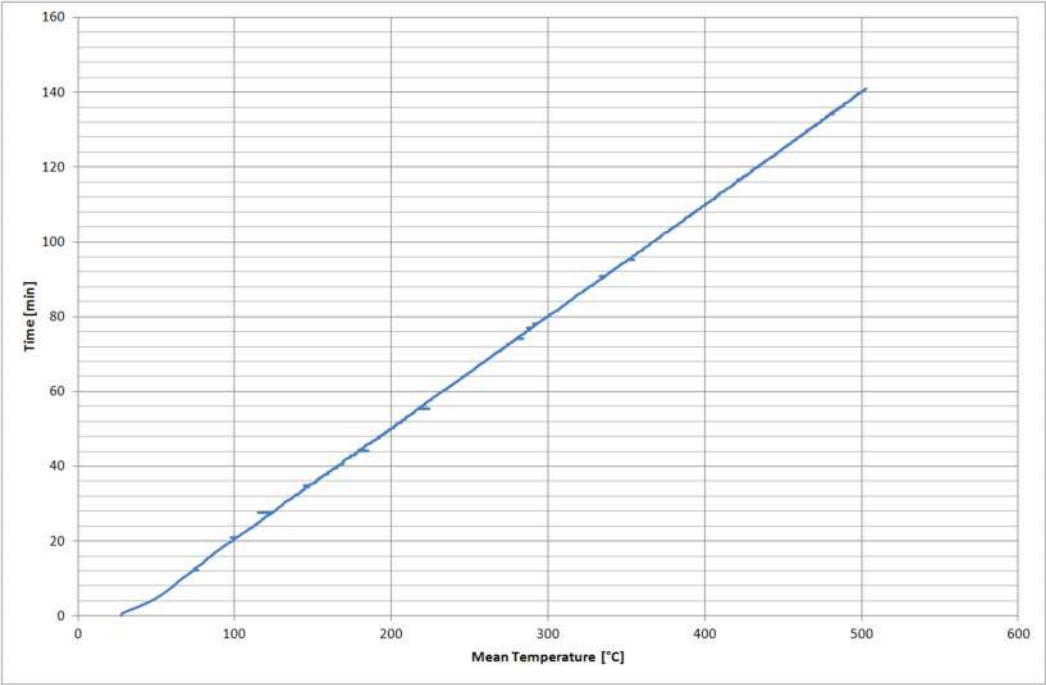


Figure 52: Time in function of the mean temperature

By calculating the mean between these six temperatures, the evolution of the transversal and axial displacements as a function of the mean temperature of the column is displayed in the next figure:

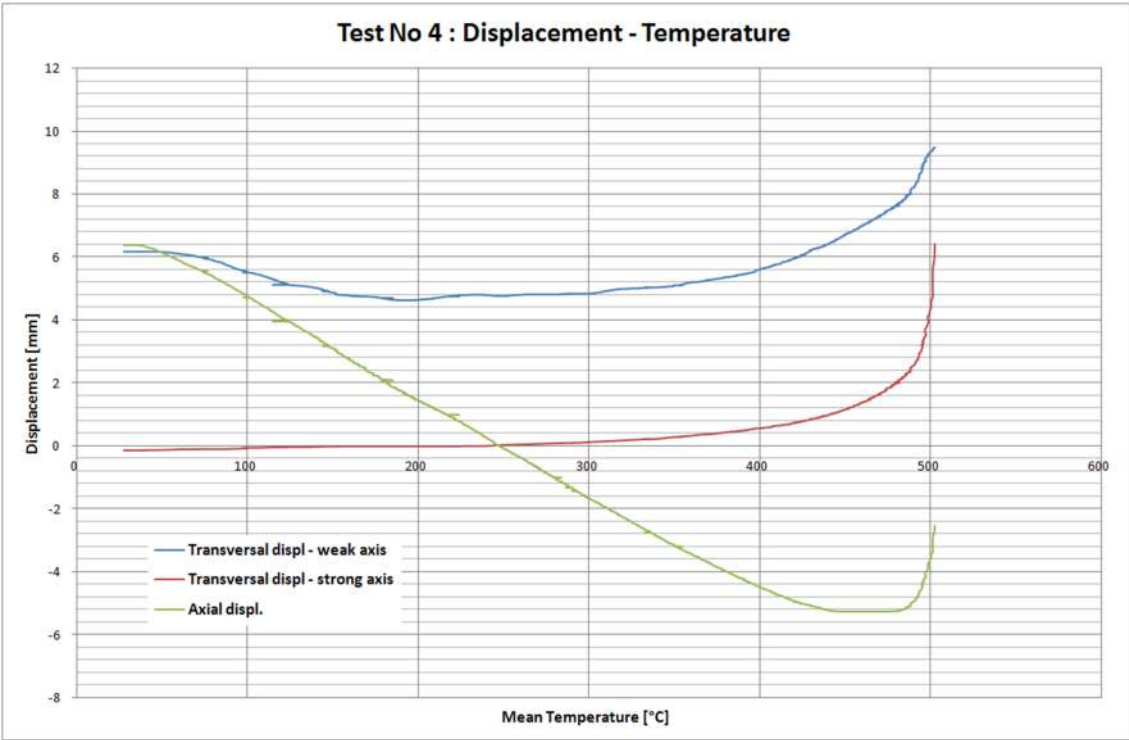


Figure 53: Displacements (mm) in function of the mean temperature (°C)

For the test 4, no certificate for the steel of this column is available and no material tests are performed. It is considered that the steel grades of the flange and of the web are the same than for the test 3 (see Table 12) even if the steel of the web and of the flange are a product of a different steel plate.

The deformed shape of column of test 4 after failure is shown in the following pictures:



Figure 54: Deformed shape after test 4

1.1.2.6 Test 5

The dimensions of the welded 360x4+150x5 are given in the following table:

h_w (mm)	t_w (mm)	b (mm)	t_f (mm)	H (mm)
360	4	150	5	2700

Table 15: Global dimensions of fifth tested column

The applied load for the test and the expected failure temperature calculated with SAFIR are given in the table below:

Cold failure load (kN)	Load applied for the test (kN)	Experimental Failure temperature (°C)	Failure temperature SAFIR (°C) <i>Before the test</i>
462.5	231.3	509	506

Table 16: Applied load and failure temperature for test 5

The location of the resistances and the definition of the control zones are presented on the scheme here below. In this case, six zones are used because the web of the column is 360 mm width and allowed putting three resistances along its width:

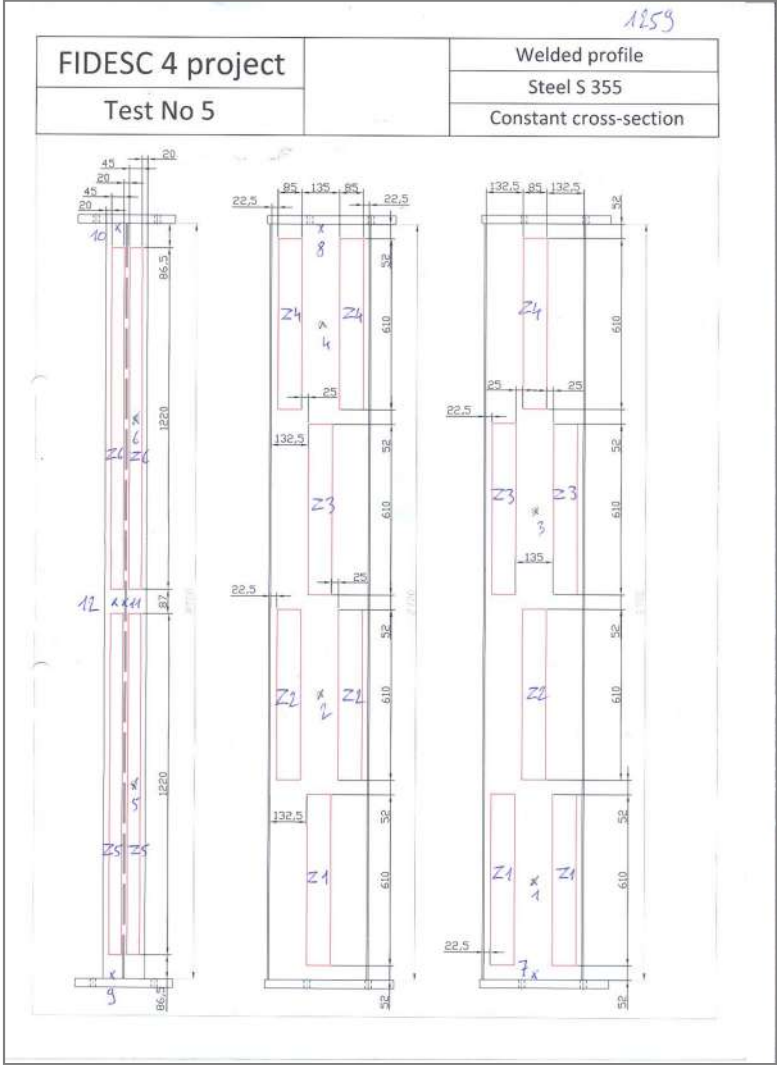


Figure 55: Definition of the control zones and position of the control thermocouples

The temperature of the control thermocouples as a function of time is shown in the following figure:

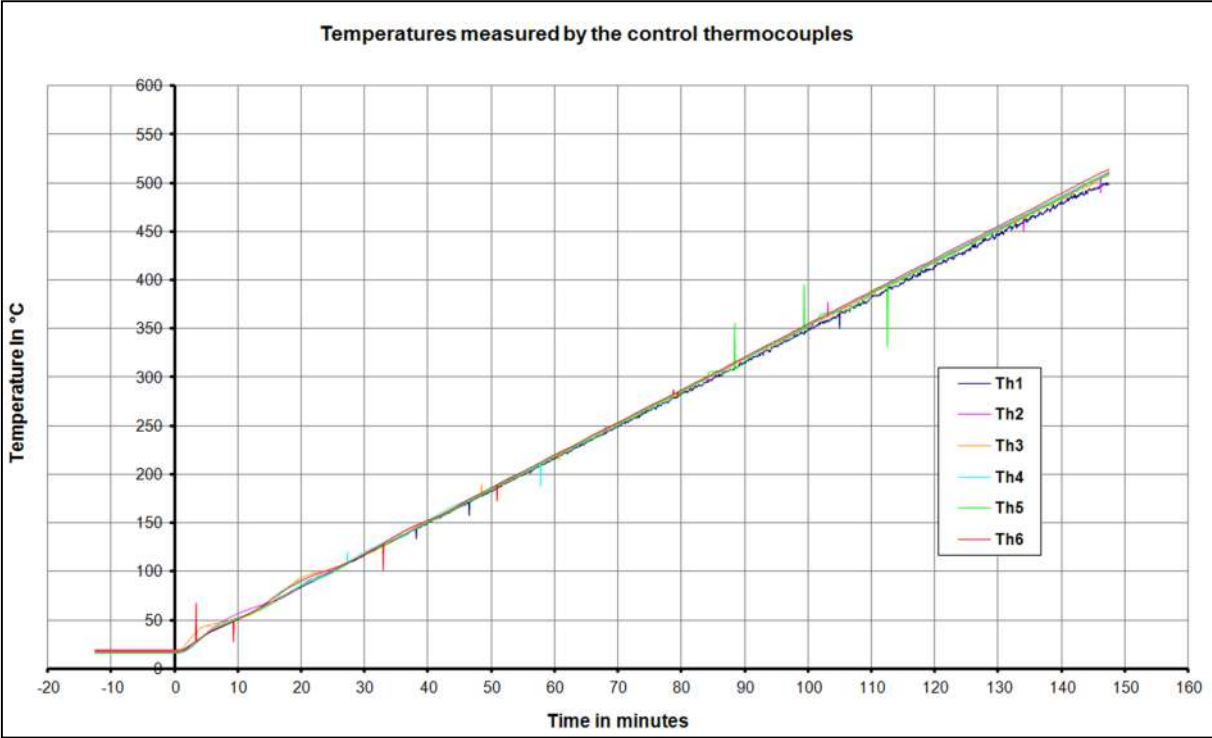


Figure 56: Recorded temperature by the six control thermocouples

It is observed that the control temperature curves are very close to each other and the instruction is thus well followed by the six zones. The heating and loading process is stopped at the 147th minute:

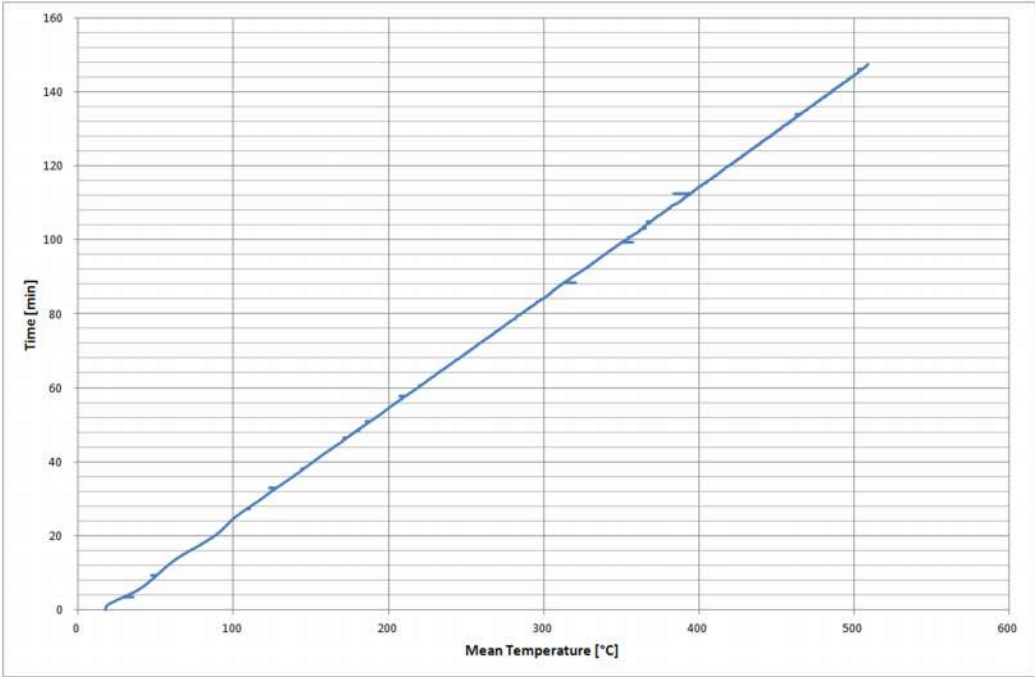


Figure 57: Time in function of the mean temperature

By calculating the mean between these six temperatures, the evolution of the transversal and axial displacements as a function of the mean temperature of the column is displayed in the next figure:

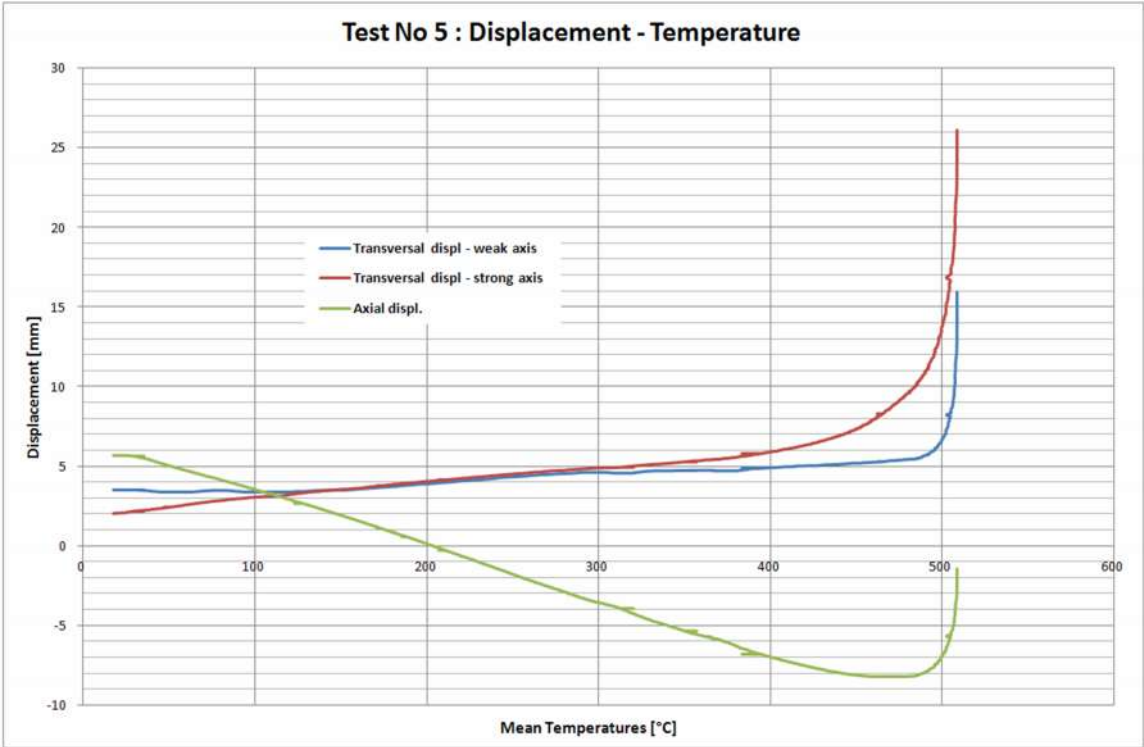


Figure 58: Displacements (mm) in function of the mean temperature (°C)

For the test 5, no certificate for the steel of this column is available and no material tests are performed. It is considered that the steel grades of the flange and of the web are the same than for the test 3 (see Table 12) even if the steel of the web and of the flange are a product of a different steel plate.

The deformed shape of column of test 5 after failure is shown in the following pictures:



Figure 59: Deformed shape after test 5

1.1.2.7 Test 6

The dimensions of the welded 360x4+150x5 are given in the following table:

h_w (mm)	t_w (mm)	b (mm)	t_f (mm)	H (mm)
360	4	150	5	2700

Table 17: Global dimensions of third tested column

The applied load for the test and the expected failure temperature calculated with SAFIR is given in the table below. The eccentricity of the load is larger than for test 5:

Cold failure load (kN)	Load applied for the test (kN)	Experimental Failure temperature (°C)	Failure temperature SAFIR (°C) <i>Before the test</i>
332.8	166.4	530	503

Table 18: Applied load and failure temperature for test 6

The location of the resistances and the definition of the control zones are presented on the scheme here below. In this case, six zones are used because the web of the column was 360 mm width and allows putting three resistances on its width.

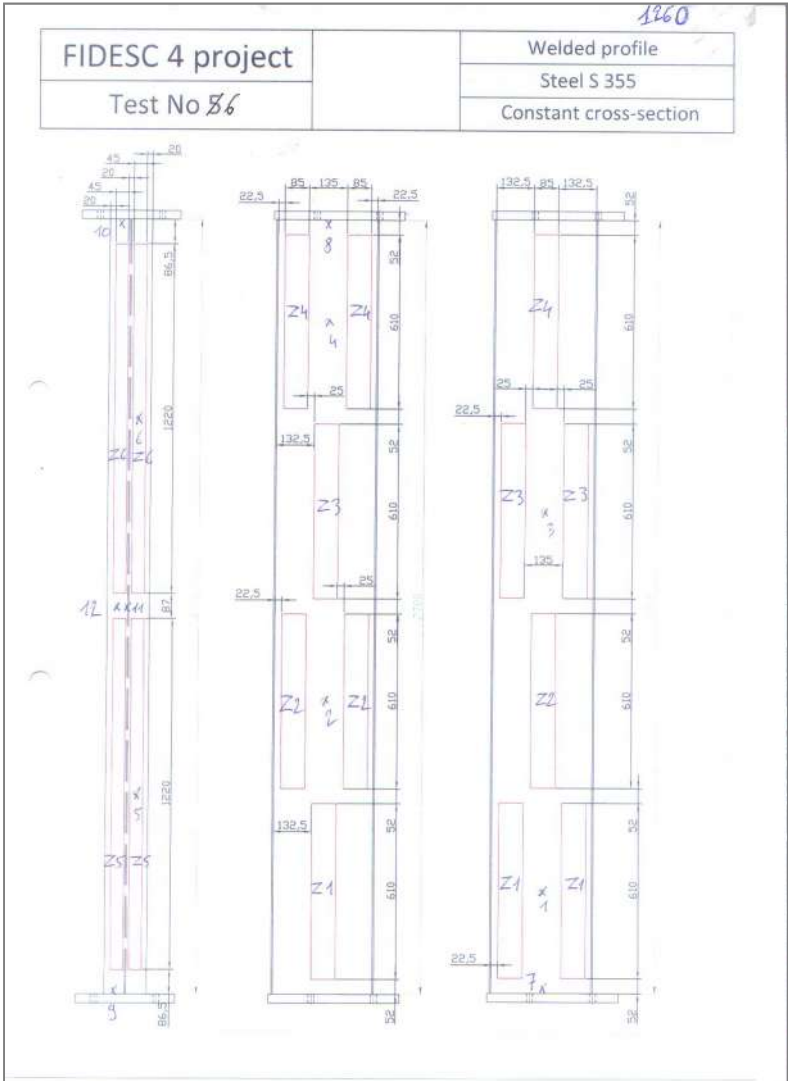


Figure 60: Definition of the control zones and position of the control thermocouples

The temperature of the control thermocouples as a function of time is shown in the following figure:

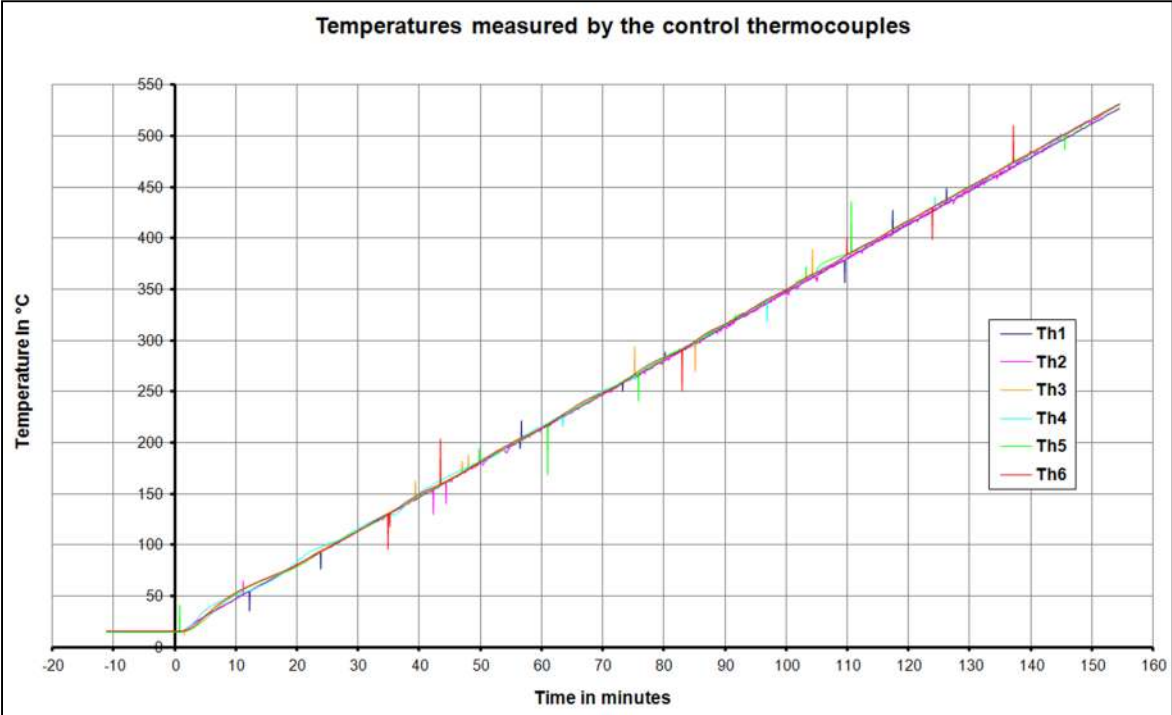


Figure 61: Recorded temperature by the six control thermocouples

It is observed that the control temperature curves are very close to each other and the instruction is thus well followed in the six zones. The heating and loading process is stopped at the 154th minute:

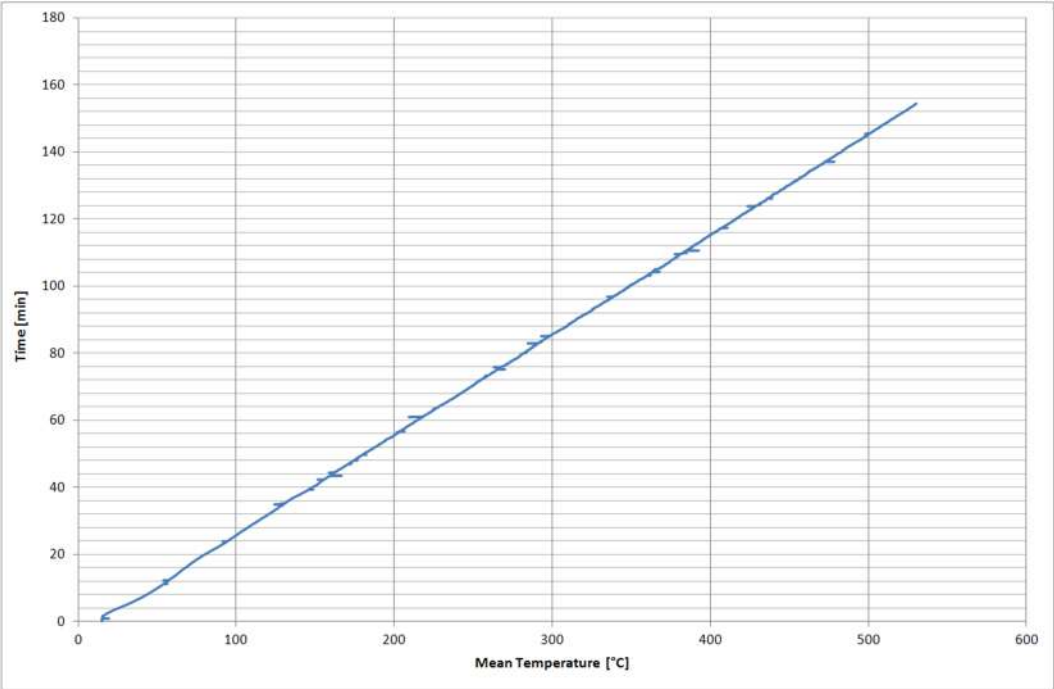


Figure 62: Time in function of the mean temperature

By calculating the mean between these six temperatures, the evolution of the transversal and axial displacements as a function of the mean temperature of the column is displayed in the next figure:

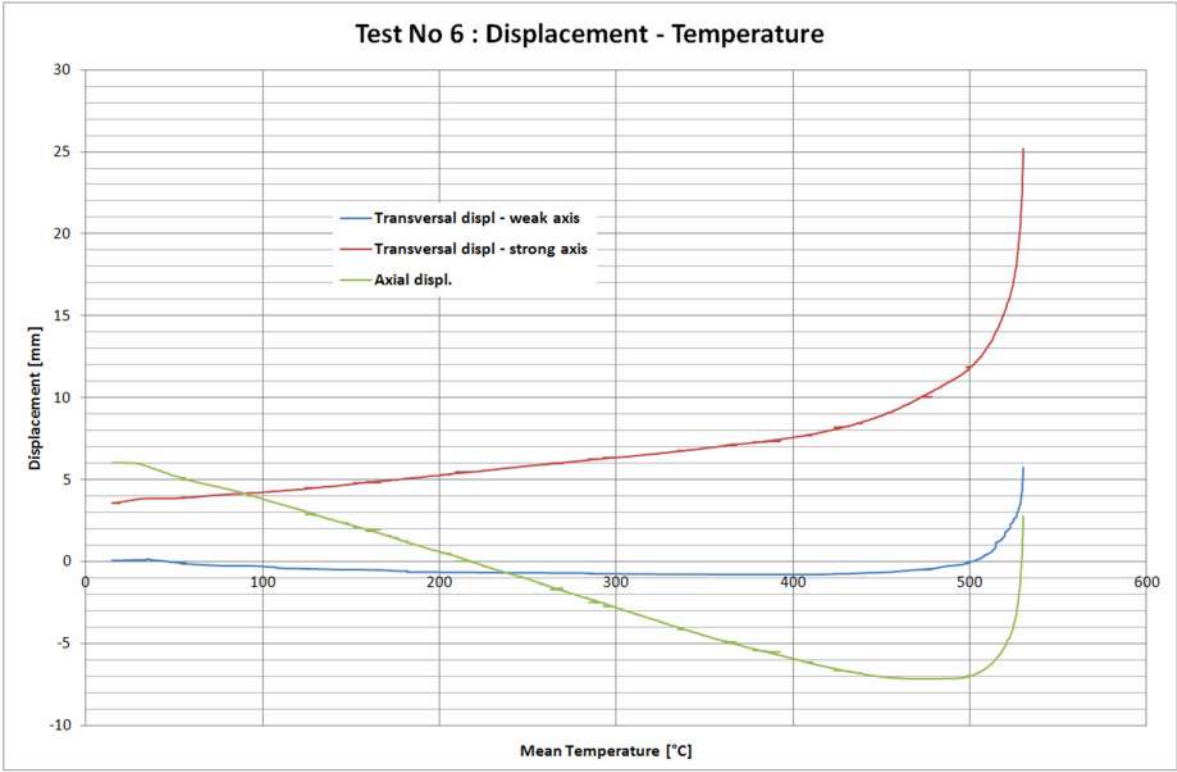


Figure 63: Displacements (mm) in function of the mean temperature (°C)

The real properties are determined by performing material tests on samples of the steel of the web and of the flange. For test 6, these material tests are performed by partner 2 and a certificate is provided with the welded columns. The steel grades of the flange and of the web are the following:

	yield strength (MPa)
Web – at the lead end of the plate	482
Web – at the tail end of the plate	447
Flanges	404

Table 19: Summarized material properties of test 6

The deformed shape of column of test 6 after failure is shown in the following pictures:



Figure 64: Deformed shape after test 6

1.1.2.8 Test 7

The dimensions of the hot-rolled HE340A are given in the following table:

h_w (mm)	t_w (mm)	b (mm)	t_f (mm)	H (mm)
320	8.5	300	11.5	2700

Table 20: Global dimensions of seventh tested column

The applied load for the test and the expected failure temperature calculated with SAFIR is given in the table below:

Cold failure load (kN)	Load applied for the test (kN)	Experimental Failure temperature (°C)	Failure temperature SAFIR (°C) <i>Before the test</i>
1902	760.8	622.8	630.2

Table 21: Applied load and failure temperature for test 7

The temperature of the control thermocouples as a function of time is shown in the following figure:

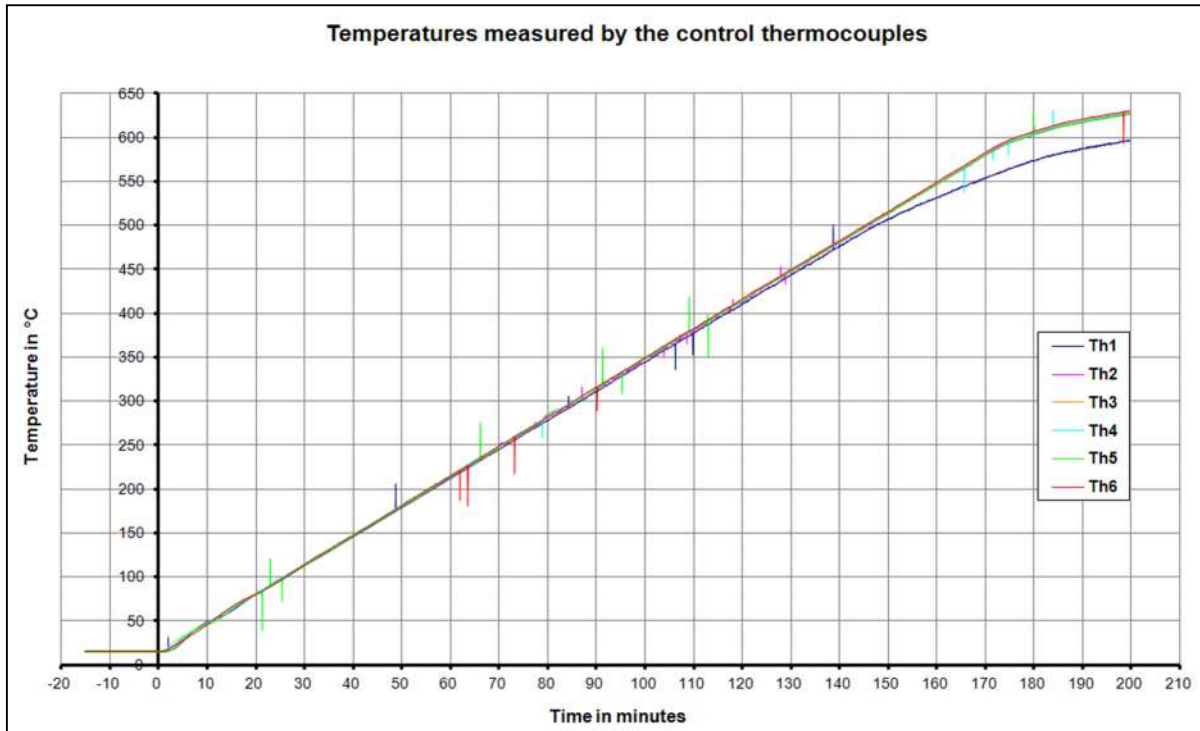


Figure 66: Recorded temperature by the five control thermocouples

It is observed that the control temperature curves are very close to each other and the instruction is thus well followed by the six zones up to the 145th minute. The control thermocouple of the zone 1 presents an increasing deviation from the 145th minute to the 180th minute with a maximum value of 30°C. The heating and loading process was stopped at the 199th minute:

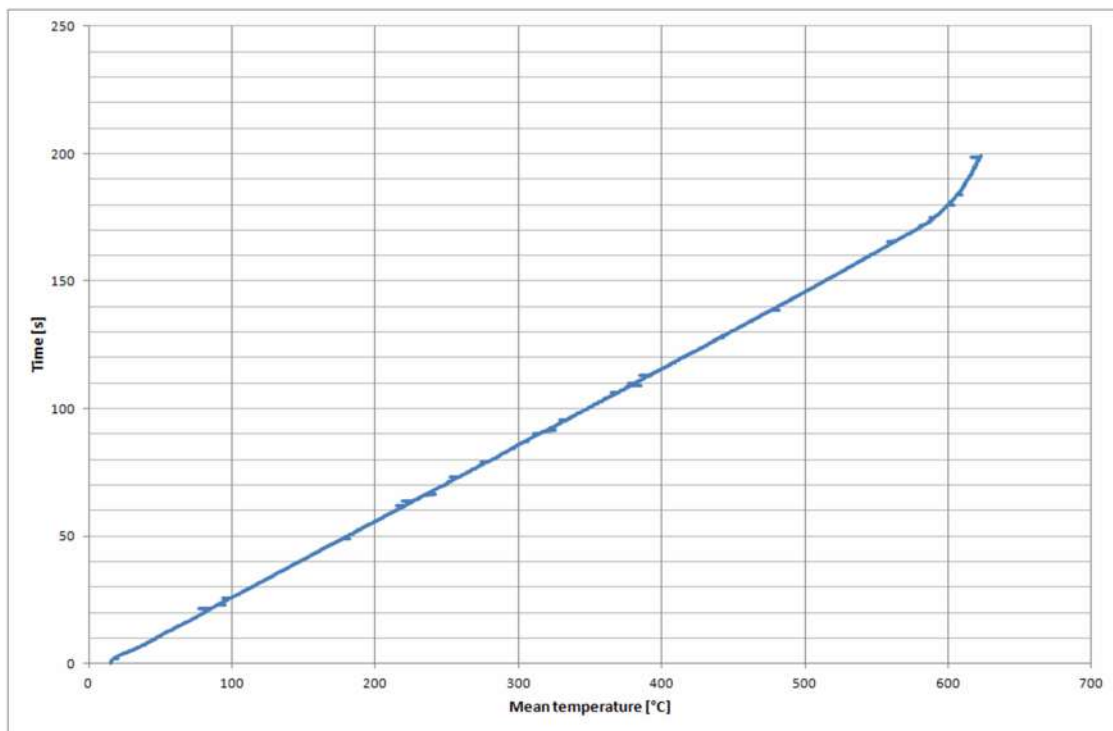


Figure 67: Time in function of the mean temperature

By calculating the mean between these six temperatures, the evolution of the transversal and axial displacements as a function of the mean temperature of the column is displayed in the next figure:

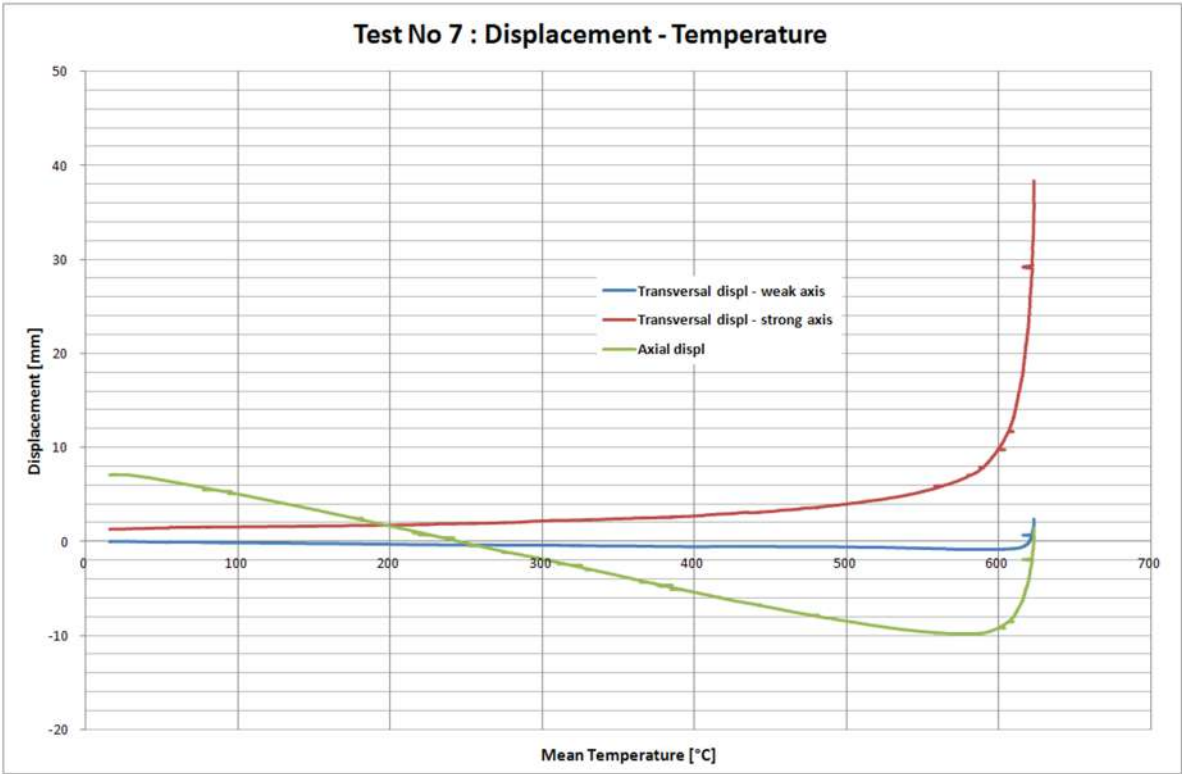


Figure 68: Displacements (mm) in function of the mean temperature (°C)

The real properties are determined by performing material tests on samples of the steel of the web and of the flange. For test 7, these material tests are performed by partner 5. The steel grades of the flange and of the web are the following:

	Upper yield strength (MPa)	$f_{y,mean}$ (MPa)	Bottom yield strength (MPa)	$f_{y,mean}$ (MPa)
Web	591 - 581	585.5	577 - 569	573
Flanges	538	-	523	-

Table 22: Summarized material properties of test 7

The deformed shape of column of test 7 after failure is shown in the following pictures:



Figure 69: Deformed shape after test 7

1.1.2.9 Test 8

The dimensions of the welded 500-300x4+150x5 are given in the following table:

h_w (mm)	t_w (mm)	b (mm)	t_f (mm)	H (mm)
300 (small base)	4	150	5	2700
500 (large base)				

Table 23: Global dimensions of eighth tested column

The applied load for the test and the expected failure temperature calculated with SAFIR is given in the table below:

Cold failure load (kN)	Load applied for the test (kN)	Experimental Failure temperature (°C)	Failure temperature SAFIR (°C) <i>Before the test</i>
438	219	505	510

Table 24: applied load and failure temperature for test 8

The location of the resistances and the definition of the control zones are presented on the scheme here below. In this case, six zones are used because the web of the column was 360 mm width and allowed putting three resistances along its width.

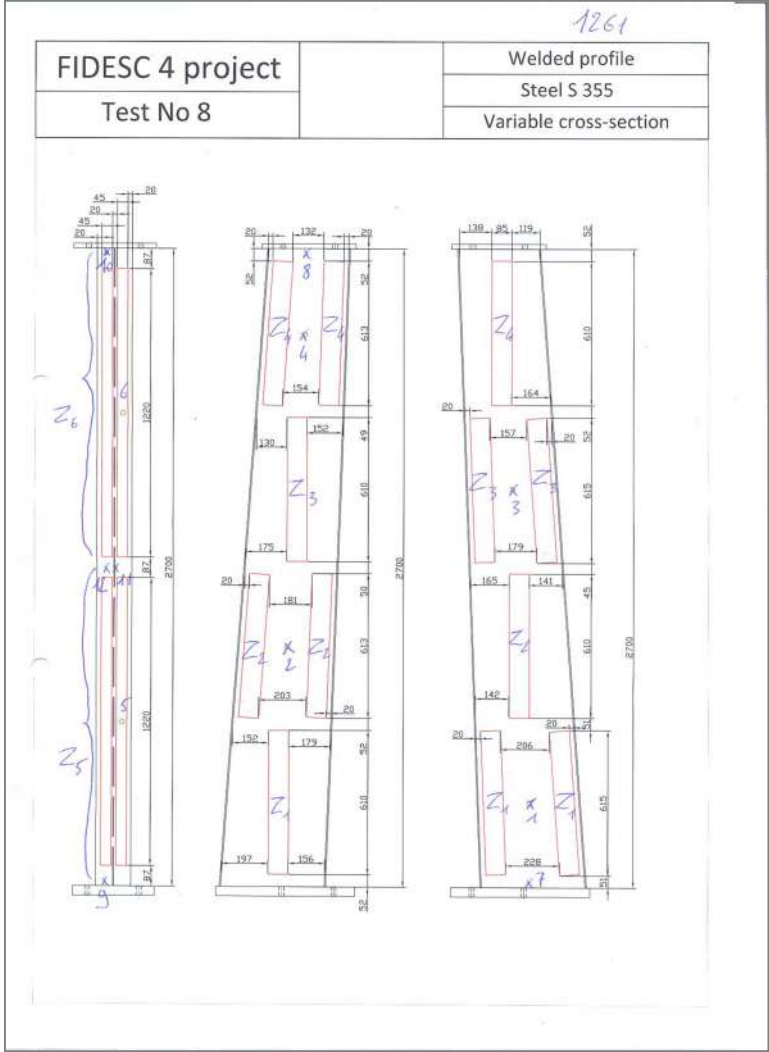


Figure 70: Definition of the control zones and position of the control thermocouples

The temperature of the control thermocouples as a function of time is shown in the following figure:

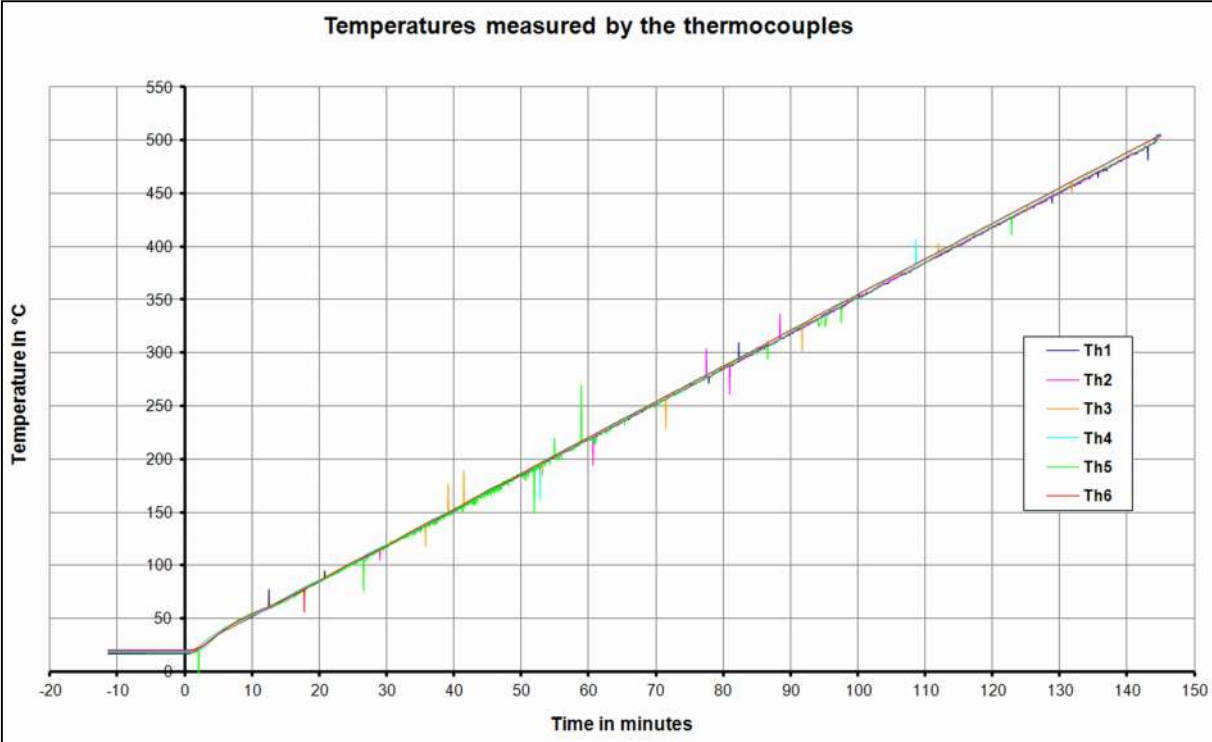


Figure 71: Recorded temperature by the six control thermocouples

It is observed that the control temperature curves are very close to each other and the instruction is thus well followed in the six areas. The heating and loading process is stopped at the 145th minute:

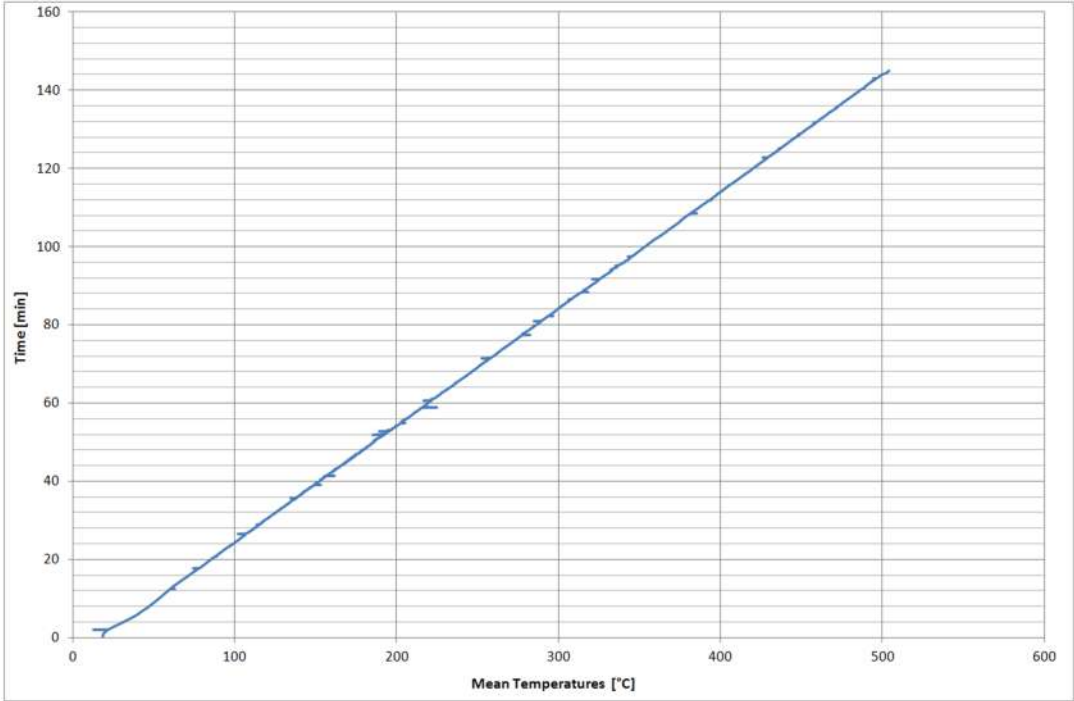


Figure 72: Time in function of the mean temperature

By calculating the mean between these six temperatures, the evolution of the transversal and axial displacements as a function of the mean temperature of the column is displayed in the next figure:

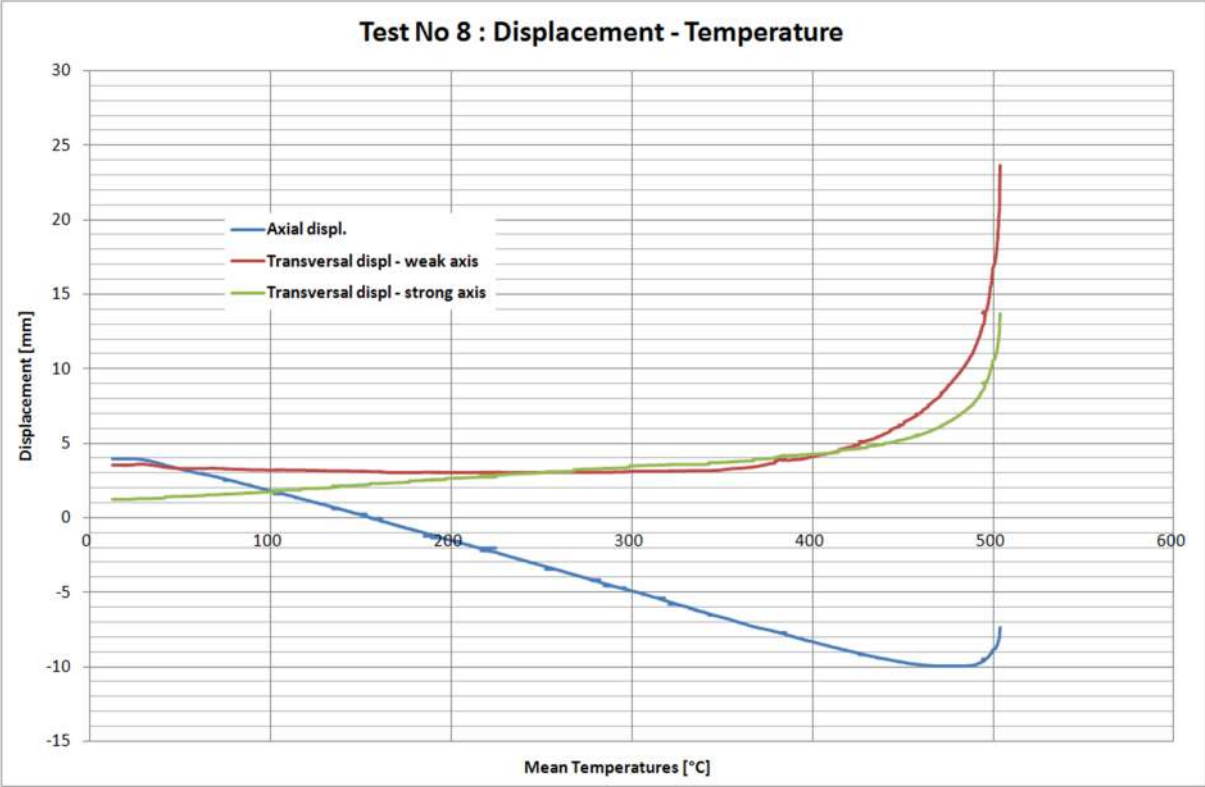


Figure 73: Displacements (mm) in function of the mean temperature (°C)

The real properties are determined by performing material tests on samples of the steel of the web and of the flange. For test 8, these material tests are performed by partner 2. The steel grades of the flange and of the web are the following:

	yield strength (MPa)
Web – at the lead end of the plate	482
Web – at the tail end of the plate	447
Flanges	404

Table 25: Summarized material properties of test 8

The deformed shape of column of test 8 after failure is shown in the following pictures:



Figure 74: Deformed shape after test 8

In order to summarize the progress and the results of the experiment, the following diagram illustrates the experimental failure temperatures and the failure temperatures calculated with SAFIR prior to the experimental tests:

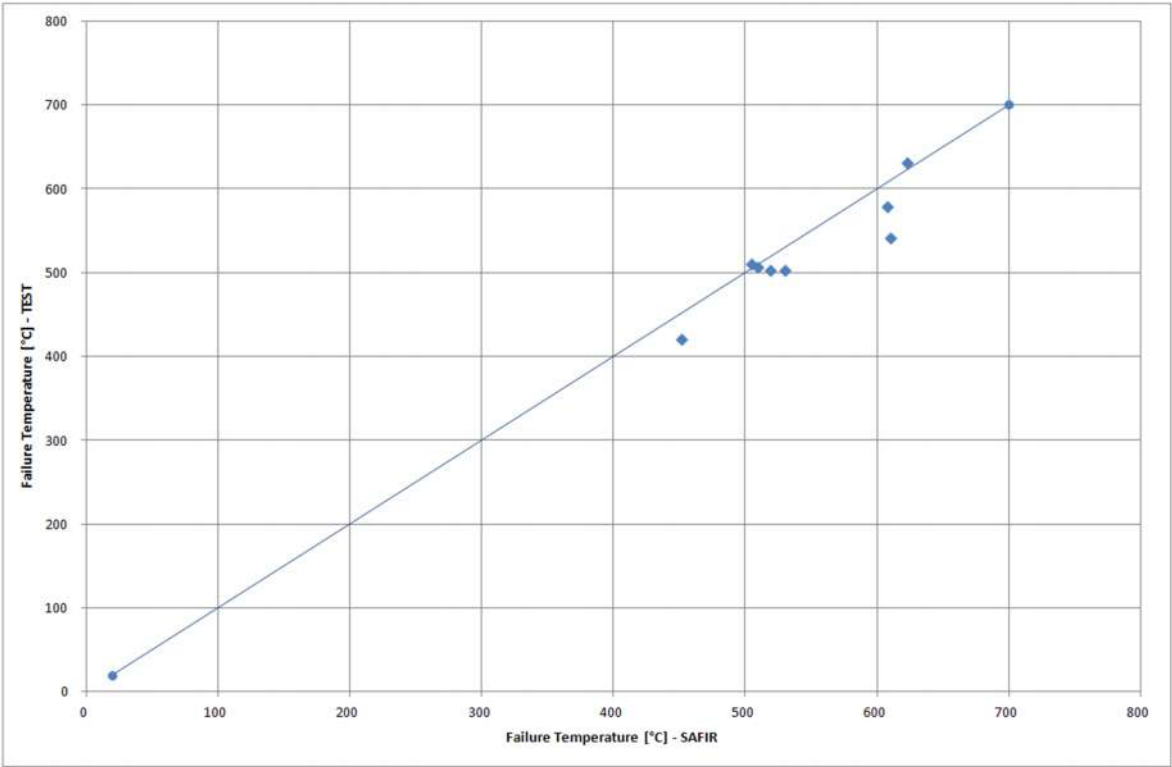


Figure 75 : Comparison between experimental and numerical results

1.1.3 Development of numerical models and correlation with experimental results

The numerical simulations are conducted in order to catch with the experimental results from the fire tests. The objective is to simulate the tests using the measured properties of the steel of the columns, the measured global and local imperfections, the measured temperature distribution along the column, the measured value of the load and the measured eccentricities of the load applied with the testing frame.

The real properties of the steel of each column were presented in the previous chapter 1.1.2 for each tested column. The maximum value obtained from the material tests is considered in the simulations. The used values are reminded for each simulation.

The measurement of the global and local imperfections of the specimens is manually performed, see 1.1.1. Thus, the geometry of the mesh of each column in these simulations takes into account these measured imperfections. A global imperfection along the weak axis deduced by the general shape of the profile of the imperfection along the web of the columns is deduced. Around this deformed shape, local sinusoidal imperfections perpendicular to the plane of the web and of the flange along the web and along the flange are added. The amplitude of these sinusoidal imperfections is the maximum value observed in the profile of imperfections around the global imperfection of the web and flange.

Besides, the temperatures along the profile are recorded during the tests in five or six zones along the column by means of five or six control thermocouples. It allows applying the recorded evolution of temperatures along the profile. From this data, it is observed that the instruction of heating up at a velocity of 200°C/hour is closely followed by all the control zones of the columns for each test. In the simulations, the steel of the column is heated at a constant velocity of 200°C/hour along the whole column of each test.

The applied loads during the tests are presented in the previous paragraph 1.1.2.

Finally, these simulations take account of the differences between the theoretically-planned eccentricities of the load and the effective eccentricities of the load measured during the tests.

Indeed, two mean types of imprecision may affect the value of the eccentricity of the columns compared to the pinned supports:

- The imprecisions due to the fabrication process
- The imprecisions due to the setting of the column between the pinned supports of the testing frame

The imprecision due to the fabrication may result from an error of positioning of the column compared to the steel end plates and/or from an error of positioning of the holes into the end plates.

The imprecision due to the setting of the column into the frame may result from a slack between the holes of the end plates and the holes of the pinned supports and also from the thread bars used to fix the end plates to the pinned supports. Indeed, the holes in the end plates of the column have a diameter of 20 mm. The holes in the pinned supports have a diameter of 21 mm and the thread bars have a diameter of 16 mm. These slacks may thus generate an offset from 0 to 4.5 mm.

The last characteristic to be taken into account is the length of the column. The length of the columns between the end plates is 2.7 m for all the tested ones. However, the columns are ended by a steel plate at each extremity and these end plates themselves are fixed to the pinned supports. That is why the length of the column to be considered between the points of application of the load includes the 2,7 m length of the column, the thickness of the two end plates (depends on the column) and the two half thicknesses of the pinned supports ($2 \times (265 \text{ mm} / 2)$) more the thickness of the insulating PROMATECT ($2 \times 35 \text{ mm}$).

In order to take into account this feature, a vertical line of shell elements with a length equal to the measured over-length along the axis of the column is modelled. To introduce the eccentricities of the load we use a horizontal line of shell elements perpendicular to the vertical one and with a length equal

to the measured eccentricity of the load. These shell elements have a big thickness of 100 mm to prevent their mechanical failure.

The transversal displacement in the direction of the weak axis is recorded at the mid-height of the column and at the mid-width of the web. The transversal displacement in the direction of the strong axis is recorded at the mid-height of the column and at the mid-width of the flange. The vertical displacement is recorded for the central node of the node line where the load is applied.

1.1.3.1 Test 1

The maximum steel grades of the flanges and of the web obtained by the material tests and used for the numerical simulations are given in the following table:

	f_y (MPa)
Web	449.5
Flanges	402.0

Table 26: Material properties for the numerical simulations

The global initial imperfections deduced from the manual measurement along the web and the flanges of the column are presented in Table 27. A global imperfection in the direction of the weak axis only, with a half sinusoidal shape, is set. The amplitude of this global imperfection is deduced from the profile of imperfection measured along the web. Around this global imperfection, some local imperfections are imposed to the web and to the flanges along the column. They have a sinusoidal shape in the direction perpendicular to the plane of the flange for the flanges and perpendicular to the web for the webs respectively.

Amplitude of the global imperfection in the direction of the weak axis (mm)	Amplitude of the local imperfection of the web (mm)	Amplitude of the local imperfection of the flange (mm)
1.5	0.2	0.3

Table 27: Amplitude of imperfections

The eccentricities between the axis of the pinned supports and the axis of the column were measured once the column was equipped and placed into the testing frame:

Eccentricity at the bottom basis (mm)	Eccentricity at the top basis (mm)
5	5

Table 28: Effective eccentricities

The modelled over-lengths of the column for bottom end and upper end are:

- Bottom end: $132.5 + 35 + 20/2 = 177.5$ mm
- Upper end: $132.5 + 32 + 20/2 = 177.5$ mm

The next table illustrates the results obtained in the fire test compared with the results obtained with both computer codes ABAQUS and SAFIR:

Failure temperature (°C)					
Test	ABAQUS	ϵ (%)	Test	SAFIR	ϵ (%)
610	587.3	-3.7	610	572.1	-6.2

Table 29: Failure temperature of simulations compared with experimental test

The following diagram illustrates the displacements of the column in function of the mean temperature for both experimental test and SAFIR simulation:

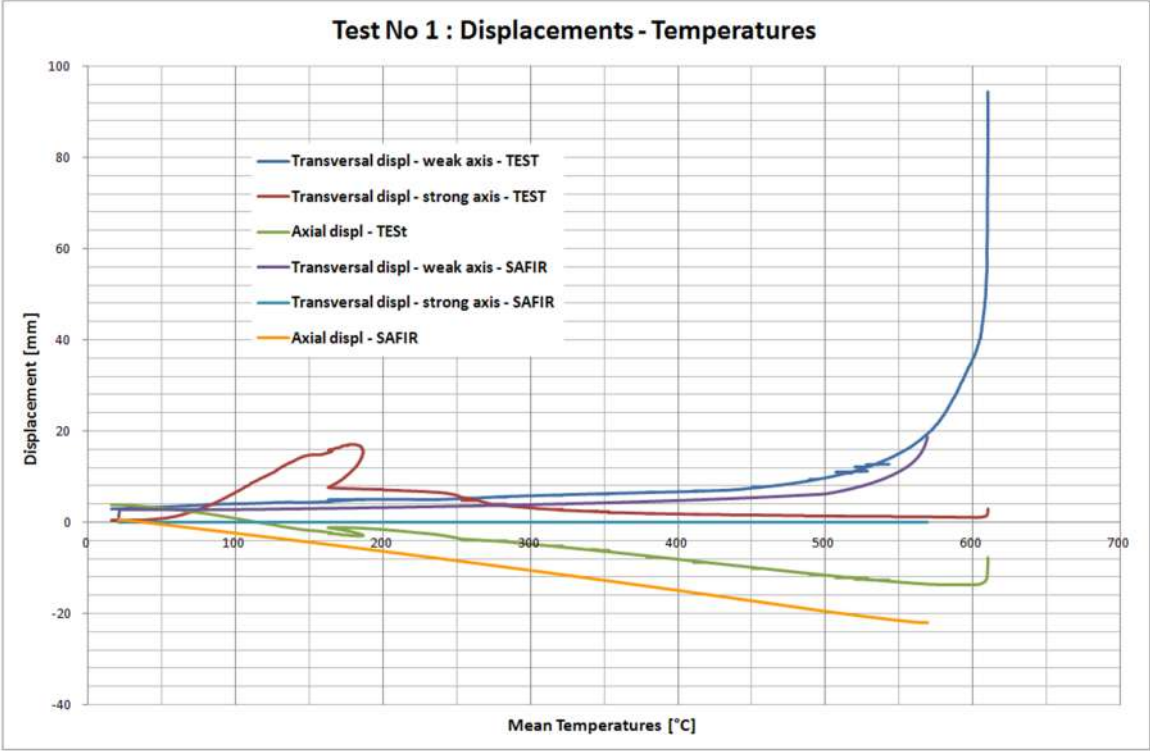


Figure 76: Displacements (mm) in function of temperature (°C) – SAFIR comparison

The following diagram illustrates the displacements of the column in function of the mean temperature for both experimental test and ABAQUS simulation:

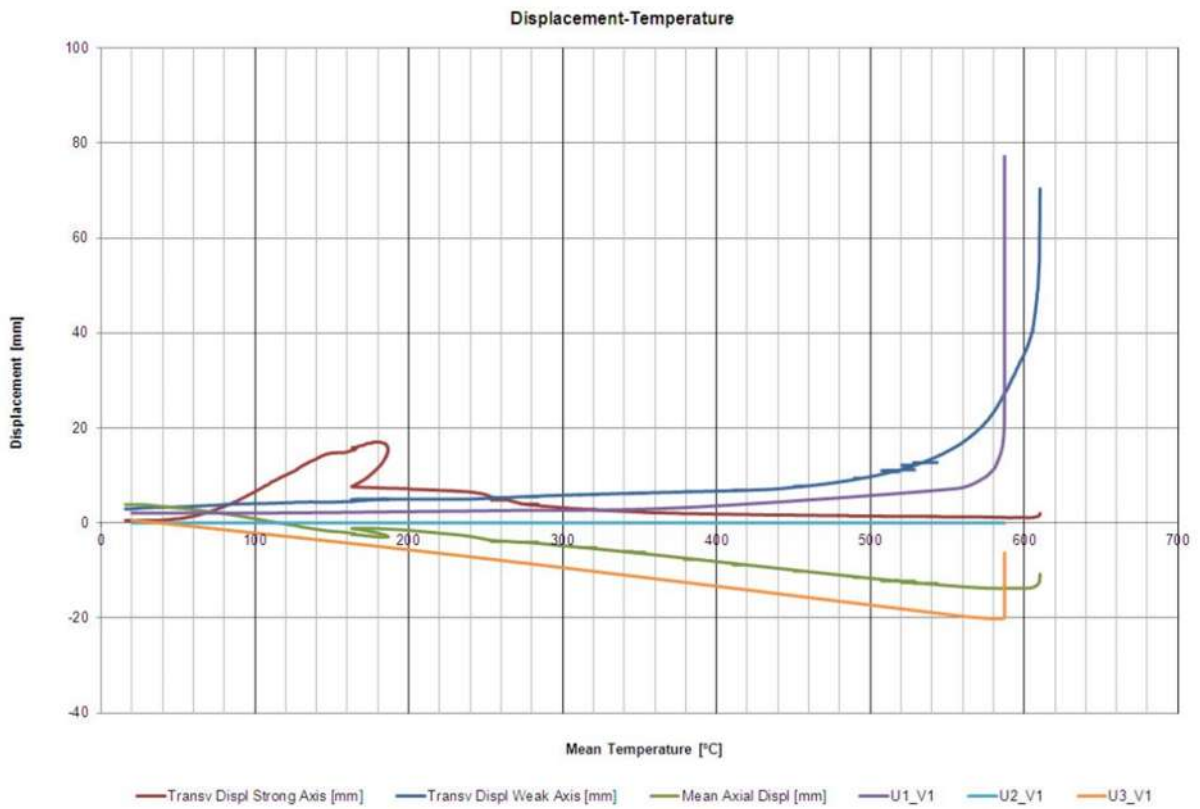


Figure 77: Displacements (mm) in function of temperature (°C) – ABAQUS comparison

The failure mode obtained numerically with SAFIR is a global buckling along the weak axis as the experimental failure mode:

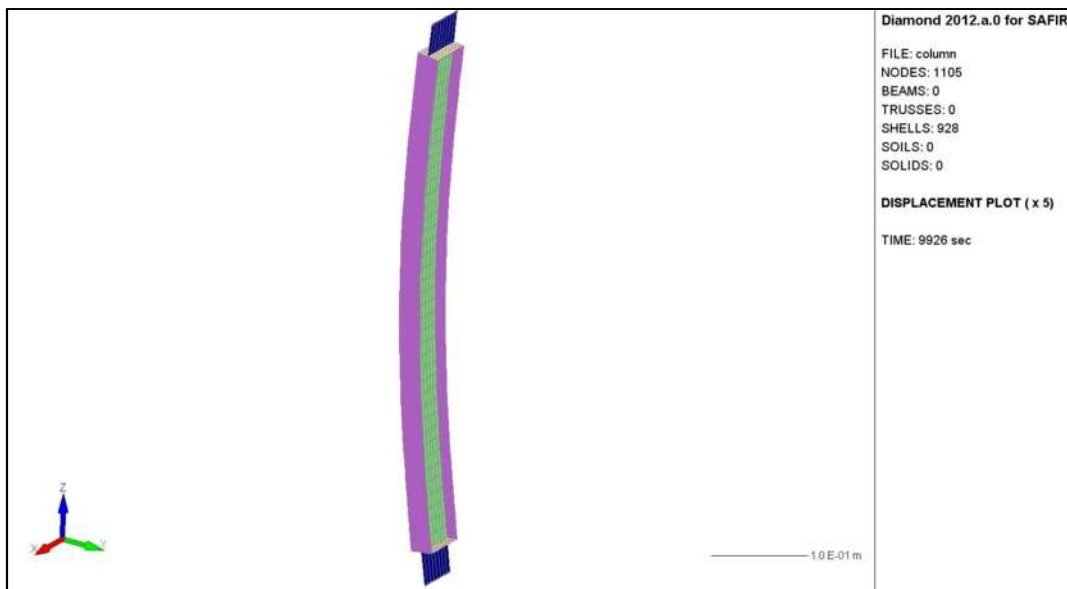


Figure 78: Numerical failure mode obtained with SAFIR

The failure mode obtained numerically with ABAQUS is a global buckling along the weak axis as the experimental failure mode:

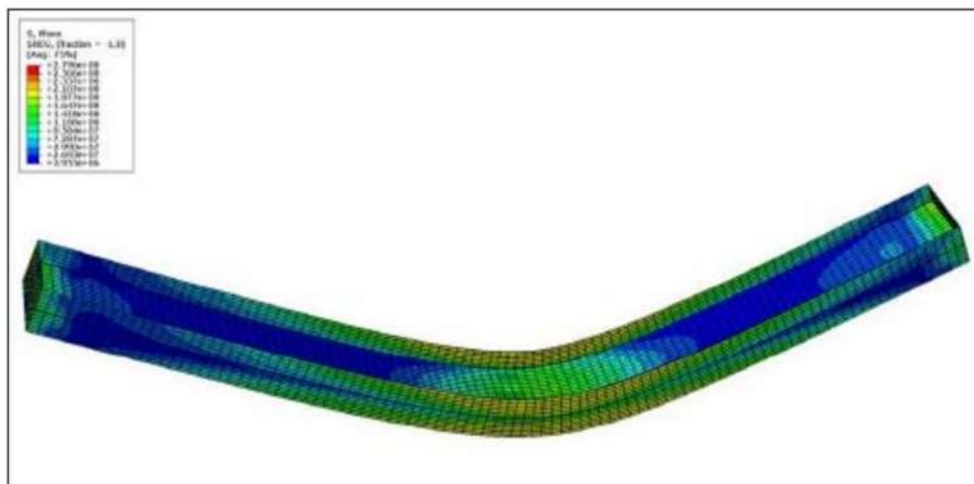


Figure 79: Numerical failure mode obtained with ABAQUS

1.1.3.2 Test 2

The maximum steel grades of the flanges and of the web obtained by the material tests and used for the numerical simulations are given in the following table:

	f_y (MPa)
Web	482
Flanges	404

Table 30: Material properties for the numerical simulations

The global initial imperfections deduced from the manual measurement along the web and the flanges of the column are presented in Table 31. A global imperfection in the direction of the weak axis only, with a half sinusoidal shape, is set. The amplitude of this global imperfection is deduced from the profile of imperfection measured along the web. Around this global imperfection, some local imperfections are imposed to the web and to the flanges along the column. They have a sinusoidal shape in the direction perpendicular to the plane of the flange for the flanges and perpendicular to the web for the webs respectively.

Amplitude of the global imperfection in the direction of the weak axis (mm)	Amplitude of the local imperfection of the web (mm)	Amplitude of the local imperfection of the flange (mm)
2.7	3.2	2.4

Table 31: Amplitude of imperfections

The eccentricities between the axis of the pinned supports and the axis of the column were measured once the column was equipped and placed into the testing frame:

Eccentricity at the bottom basis (mm)	Eccentricity at the top basis (mm)
5	5

Table 32: Effective eccentricities

The modelled over-lengths of the column for bottom end and upper end are:

- Bottom end: $132.5 + 35 + 30/2 = 182.5$ mm
- Upper end: $132.5 + 32 + 30/2 = 182.5$ mm

The next table illustrates the results obtained in the fire test compared with the results obtained with both computer codes ABAQUS and SAFIR:

Failure temperature (°C)					
Test	ABAQUS	ε (%)	Test	SAFIR	ε (%)
608	597.3	-1.8	608	594.7	-2.2

Table 33: Failure temperature of simulations compared with experimental test

The following diagram illustrates the displacements of the column in function of the mean temperature for both experimental test and SAFIR simulation:

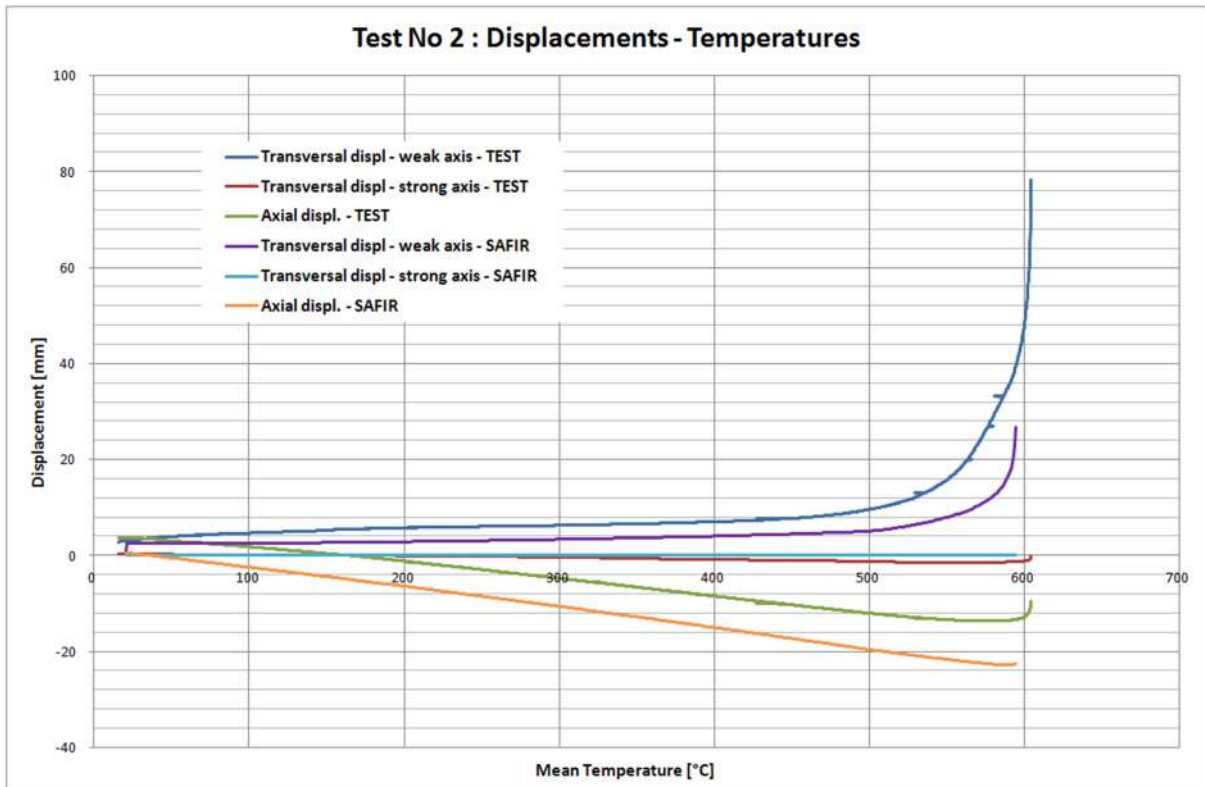


Figure 80: Displacements (mm) in function of temperature (°C) – SAFIR comparison

The following diagram illustrates the displacements of the column in function of the mean temperature for both experimental test and ABAQUS simulation:

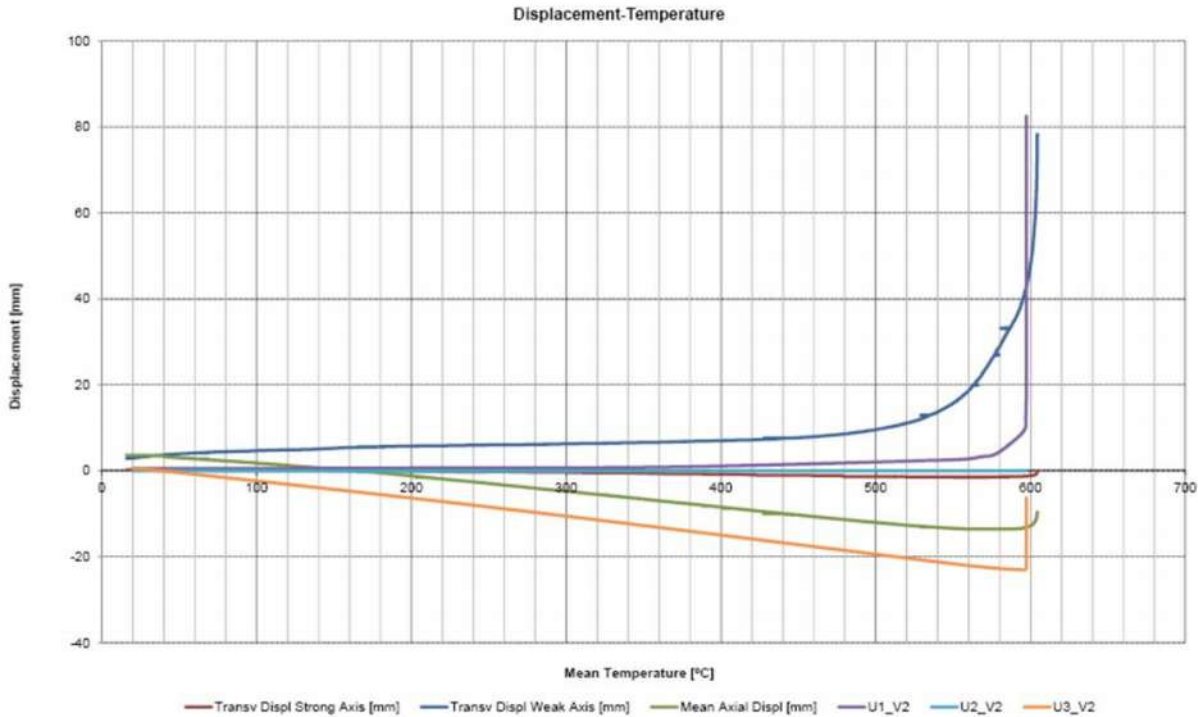


Figure 81: Displacements (mm) in function of temperature (°C) – ABAQUS comparison

The failure mode obtained numerically is a global buckling along the weak axis with a local buckling of the flange at mid-height of the column:

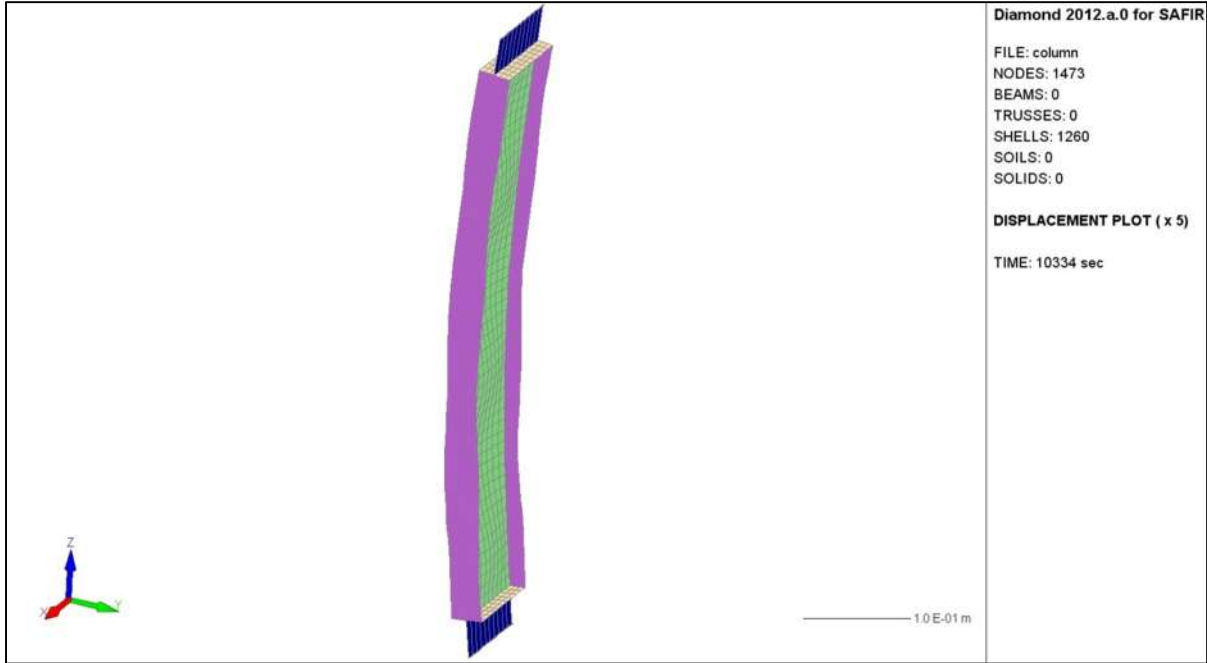


Figure 82: Numerical failure mode obtained with SAFIR

The failure mode obtained numerically with ABAQUS is a global buckling along the weak axis as the experimental failure mode:

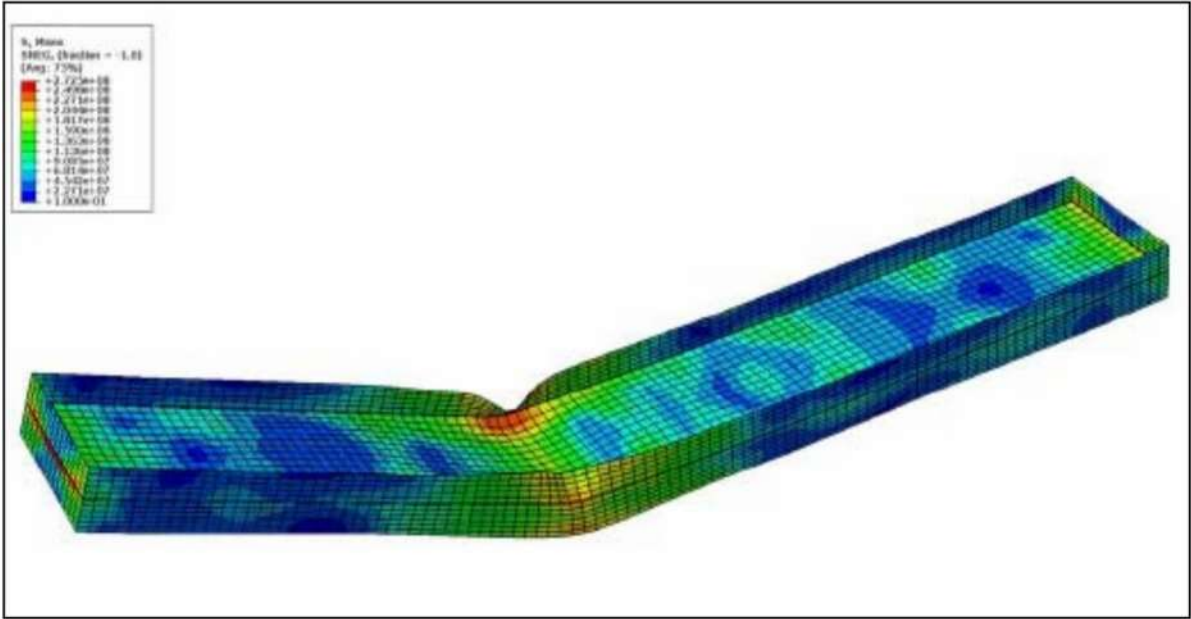


Figure 83: Numerical failure mode obtained with ABAQUS

1.1.3.3 Test 3

The maximum steel grades of the flanges and of the web obtained by the material tests and used for the numerical simulations are given in the following table:

	f_y (MPa)
Web	482
Flanges	404

Table 34: Material properties for the numerical simulations

The global initial imperfections deduced from the manual measurement along the web and the flanges of the column are presented in Table 31. A global imperfection in the direction of the weak axis only, with a half sinusoidal shape, is set. The amplitude of this global imperfection is deduced from the profile of imperfection measured along the web. Around this global imperfection, some local imperfections are imposed to the web and to the flanges along the column. They have a sinusoidal shape in the direction perpendicular to the plane of the flange for the flanges and perpendicular to the web for the webs respectively.

Amplitude of the global imperfection in the direction of the weak axis (mm)	Amplitude of the local imperfection of the web (mm)	Amplitude of the local imperfection of the flange (mm)
5.4	2.7	4.7

Table 35: Amplitude of imperfections

The eccentricities between the axis of the pinned supports and the axis of the column were measured once the column was equipped and placed into the testing frame:

Eccentricity at the bottom basis (mm)	Eccentricity at the top basis (mm)
4	13

Table 36: Effective eccentricities

The modelled over-lengths of the column for bottom end and upper end are:

- Bottom end: $132.5 + 35 + 30/2 = 182.5$ mm
- Upper end: $132.5 + 32 + 30/2 = 182.5$ mm

The next table illustrates the results obtained in the fire test compared with the results obtained with both computer codes ABAQUS and SAFIR:

Failure temperature (°C)					
Test	ABAQUS	ϵ (%)	Test	SAFIR	ϵ (%)
452	445.6	-1.4	452	459	1.5

Table 37: Failure temperature of simulations compared with experimental test

The following diagram illustrates the displacements of the column in function of the mean temperature for both experimental test and SAFIR simulation:

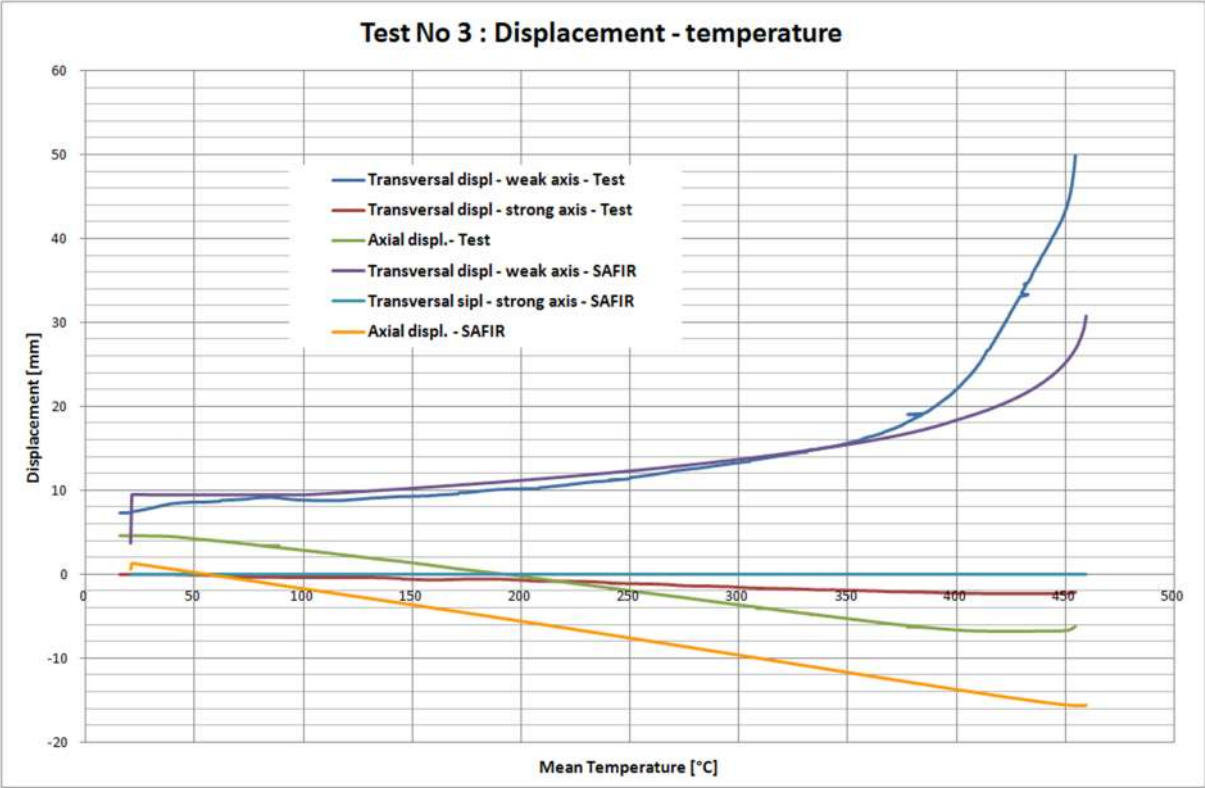


Figure 84: Displacements (mm) in function of temperature (°C) – SAFIR comparison

The following diagram illustrates the displacements of the column in function of the mean temperature for both experimental test and ABAQUS simulation:

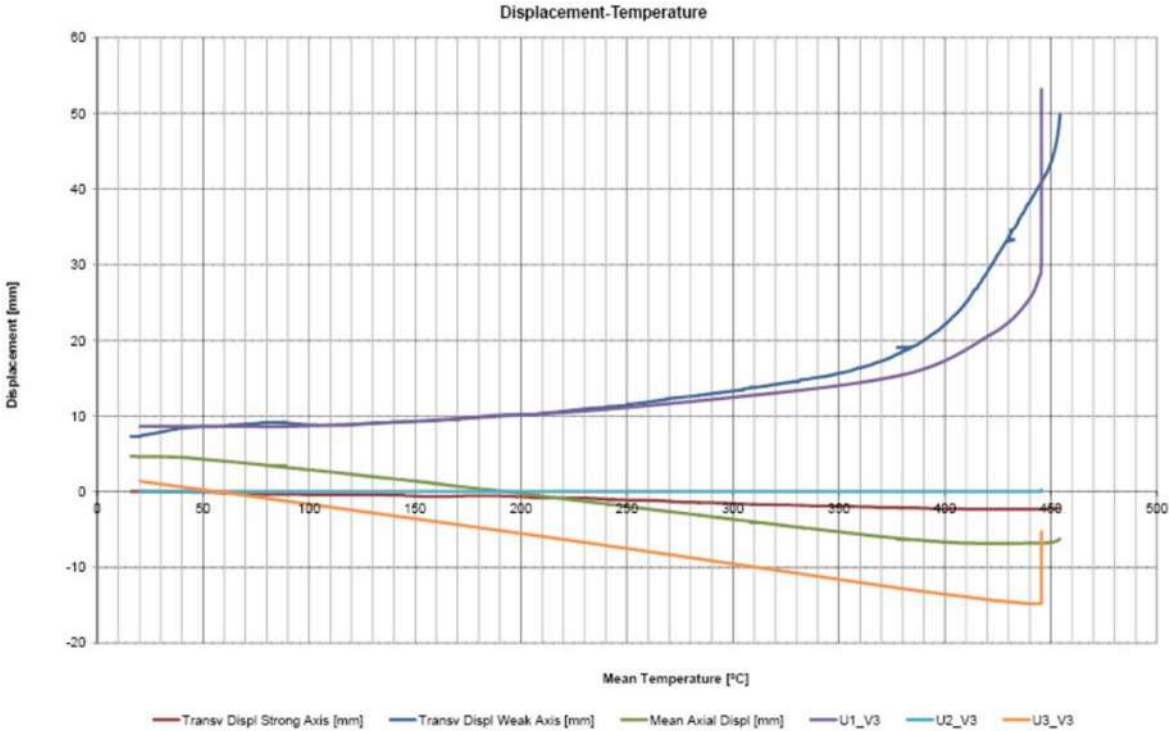


Figure 85: Displacements (mm) in function of temperature (°C) – ABAQUS comparison

The failure mode obtained numerically is a global buckling along the weak axis with a local buckling of the flange at mid-height of the column:

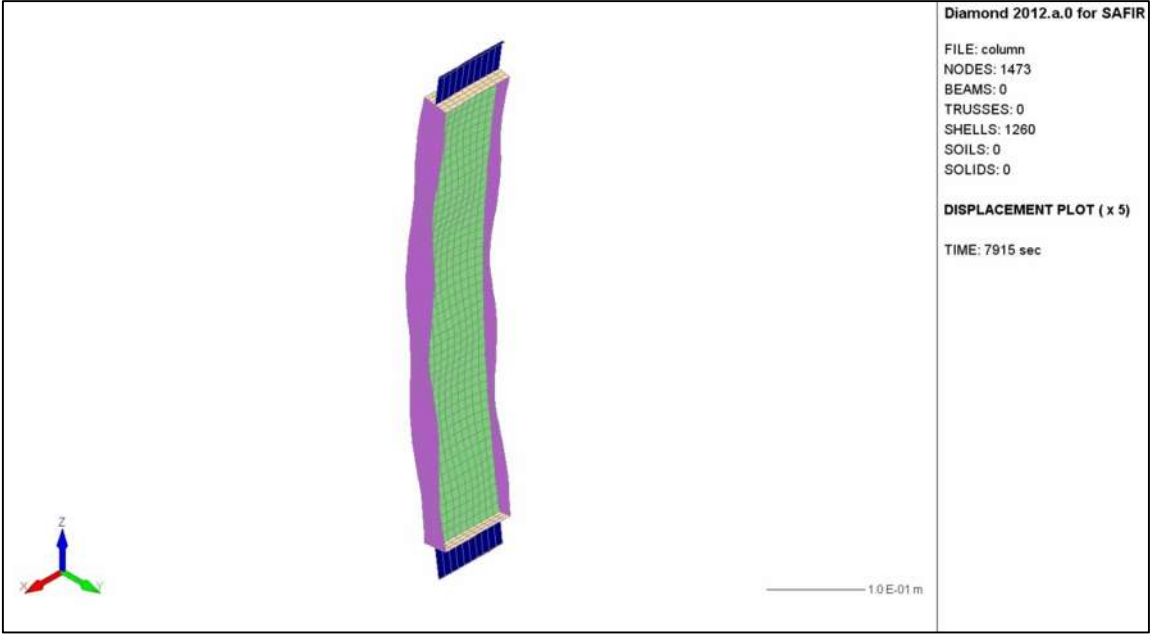


Figure 86: Numerical failure mode obtained with SAFIR

The failure mode obtained numerically with ABAQUS is a global buckling along the weak axis as the experimental failure mode:

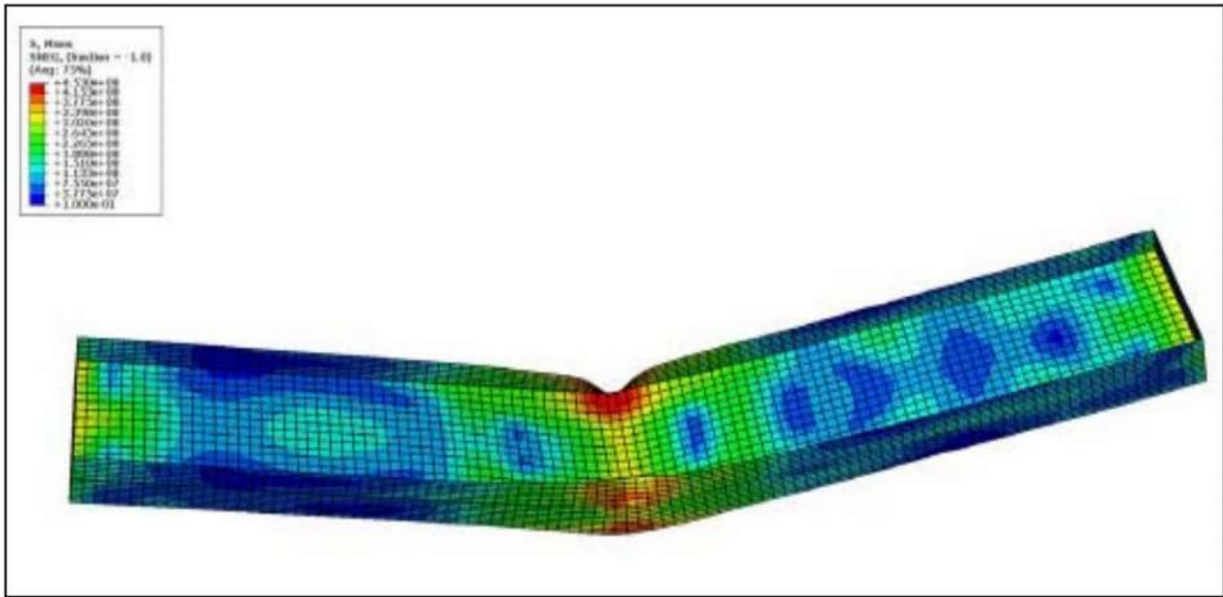


Figure 87: Numerical failure mode obtained with ABAQUS

1.1.3.4 Test 4

The maximum steel grades of the flanges and of the web obtained by the material tests and used for the numerical simulations are given in the following table:

	f_y (MPa)
Web	464.5
Flanges	404

Table 38: Material properties for the numerical simulations

The global initial imperfections deduced from the manual measurement along the web and the flanges of the column are presented in Table 39. A global imperfection in the direction of the weak axis only, with a half sinusoidal shape, is set. The amplitude of this global imperfection is deduced from the profile of imperfection measured along the web. Around this global imperfection, some local imperfections are imposed to the web and to the flanges along the column. They have a sinusoidal shape in the direction perpendicular to the plane of the flange for the flanges and perpendicular to the web for the webs respectively.

Amplitude of the global imperfection in the direction of the weak axis (mm)	Amplitude of the local imperfection of the web (mm)	Amplitude of the local imperfection of the flange (mm)
1.8	4.5	1.5

Table 39: Amplitude of imperfections

The eccentricities between the axis of the pinned supports and the axis of the column were measured once the column was equipped and placed into the testing frame:

Eccentricity at the bottom basis (mm)	Eccentricity at the top basis (mm)
5	3.5

Table 40: Effective eccentricities

The modelled over-lengths of the column for bottom end and upper end are:

- Bottom end: $132.5 + 35 + 30/2 = 182.5$ mm
- Upper end: $132.5 + 32 + 20/2 = 177.5$ mm

The next table illustrates the results obtained in the fire test compared with the results obtained with both computer codes ABAQUS and SAFIR:

Failure temperature (°C)					
Test	ABAQUS	ϵ (%)	Test	SAFIR	ϵ (%)
519.5	533.9	2.8	519.5	535	2.9

Table 41: Failure temperature of simulations compared with experimental test

The following diagram illustrates the displacements of the column in function of the mean temperature for both experimental test and SAFIR simulation:

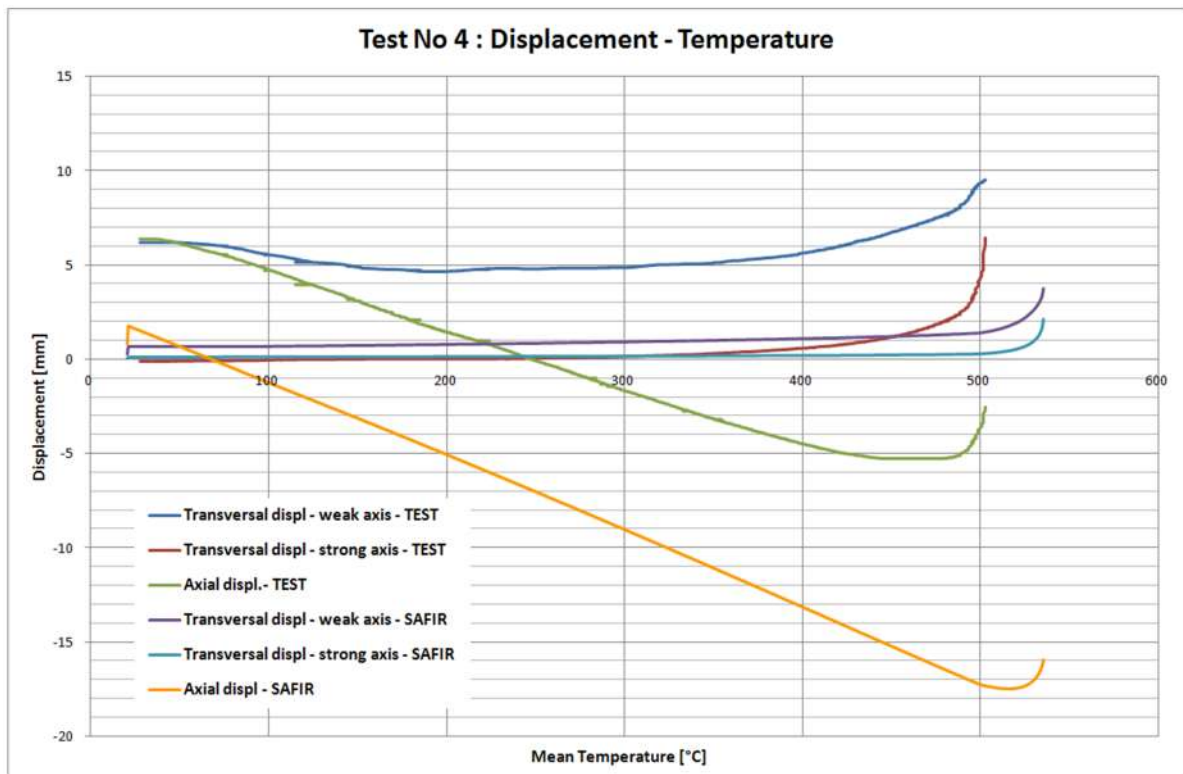


Figure 88: Displacements (mm) in function of temperature (°C) – SAFIR comparison

The following diagram illustrates the displacements of the column in function of the mean temperature for both experimental test and ABAQUS simulation:



Figure 89: Displacements (mm) in function of temperature (°C) – ABAQUS comparison

The failure mode obtained numerically is a global buckling along the weak axis with a local buckling of the flange at mid-height of the column:

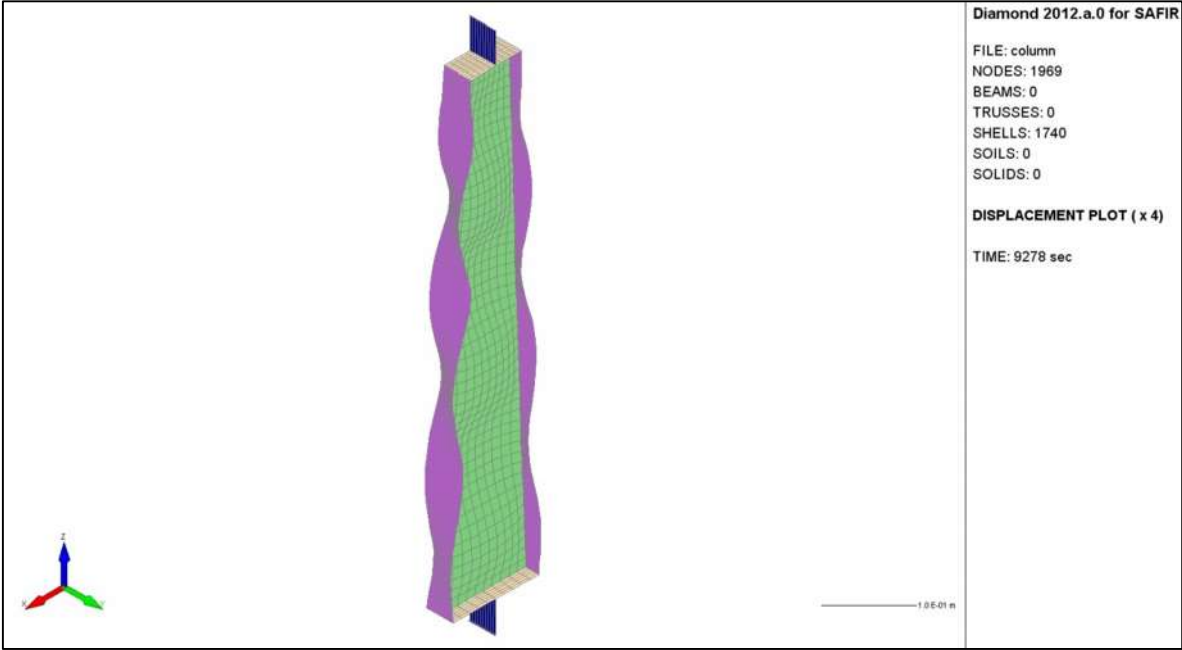


Figure 90: Numerical failure mode obtained with SAFIR

The failure mode obtained numerically with ABAQUS is a global buckling along the weak axis as the experimental failure mode:

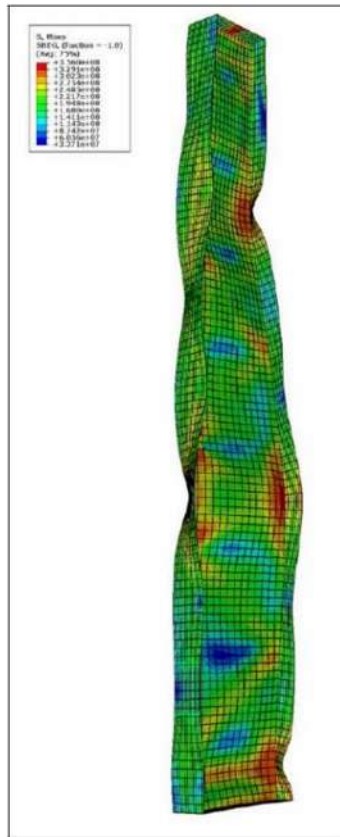


Figure 91: Numerical failure mode obtained with ABAQUS

1.1.3.5 Test 5

The maximum steel grades of the flanges and of the web obtained by the material tests and used for the numerical simulations are given in the following table:

	f_y (MPa)
Web	464.5
Flanges	404

Table 42: Material properties for the numerical simulations

The global initial imperfections deduced from the manual measurement along the web and the flanges of the column are presented in Table 43. A global imperfection in the direction of the weak axis only, with a half sinusoidal shape, is set. The amplitude of this global imperfection is deduced from the profile of imperfection measured along the web. Around this global imperfection, some local imperfections are imposed to the web and to the flanges along the column. They have a sinusoidal shape in the direction perpendicular to the plane of the flange for the flanges and perpendicular to the web for the webs respectively.

Amplitude of the global imperfection in the direction of the weak axis (mm)	Amplitude of the local imperfection of the web (mm)	Amplitude of the local imperfection of the flange (mm)
2.2	3.4	1.6

Table 43: Amplitude of imperfections

The eccentricities between the axis of the pinned supports and the axis of the column were measured once the column was equipped and placed into the testing frame:

Eccentricity at the bottom basis (mm)	Eccentricity at the top basis (mm)
71	71

Table 44: Effective eccentricities

The modelled over-lengths of the column for bottom end and upper end are:

- Bottom end: $132.5 + 35 + 30/2 = 182.5$ mm
- Upper end: $132.5 + 32 + 30/2 = 182.5$ mm

The next table illustrates the results obtained in the fire test compared with the results obtained with both computer codes ANSYS and SAFIR:

Failure temperature (°C)					
Test	ANSYS	ϵ (%)	Test	SAFIR	ϵ (%)
510	503.3	-1.3	510	526	3

Table 45: Failure temperature of simulations compared with experimental test

The following diagram illustrates the displacements of the column in function of the mean temperature for both experimental test and SAFIR simulation:

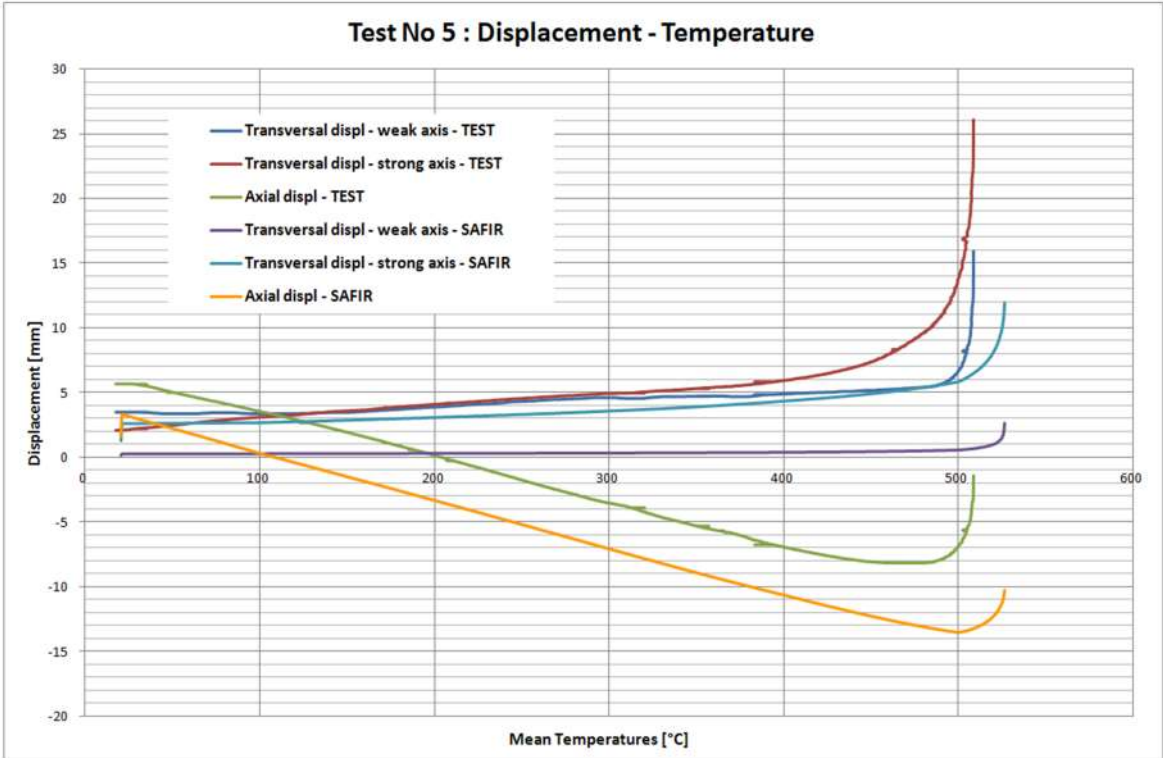


Figure 92: Displacements (mm) in function of temperature (°C) – SAFIR comparison

The following diagram illustrates the displacements of the column in function of the mean temperature for both experimental test and ANSYS simulation:

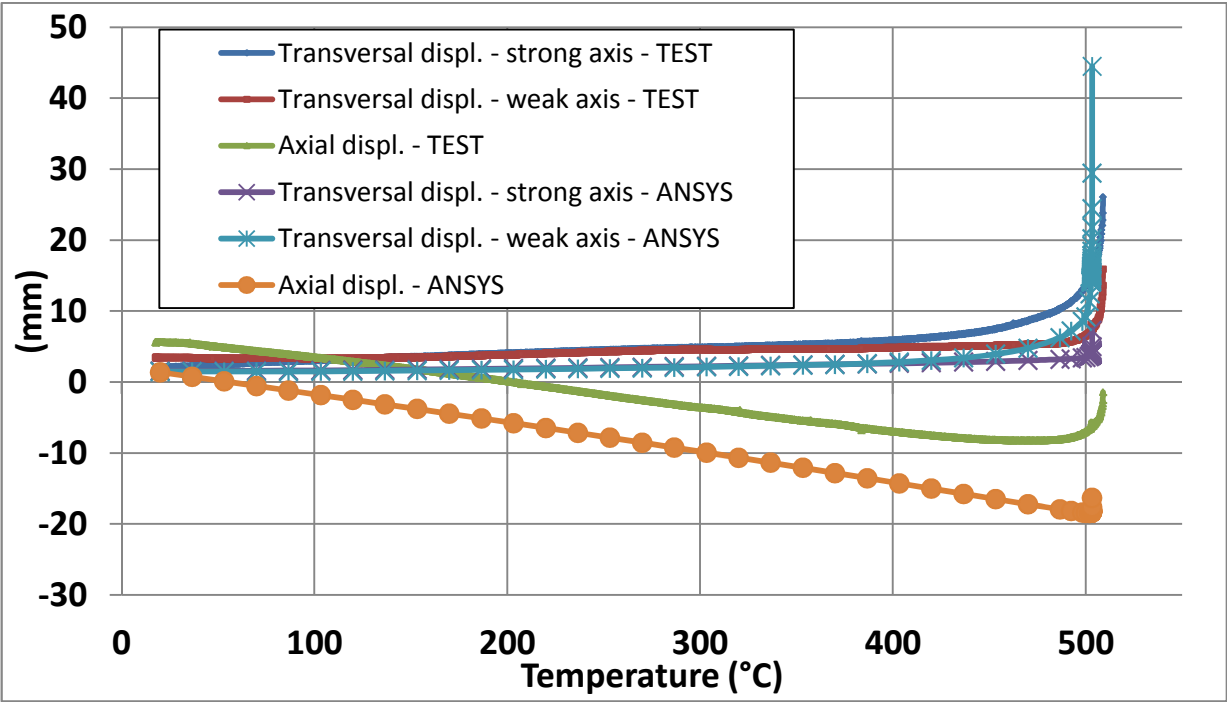


Figure 93: Displacements (mm) in function of temperature (°C) – ANSYS comparison

The failure mode obtained numerically is a global buckling along the weak axis with a local buckling of the flange at mid-height of the column:

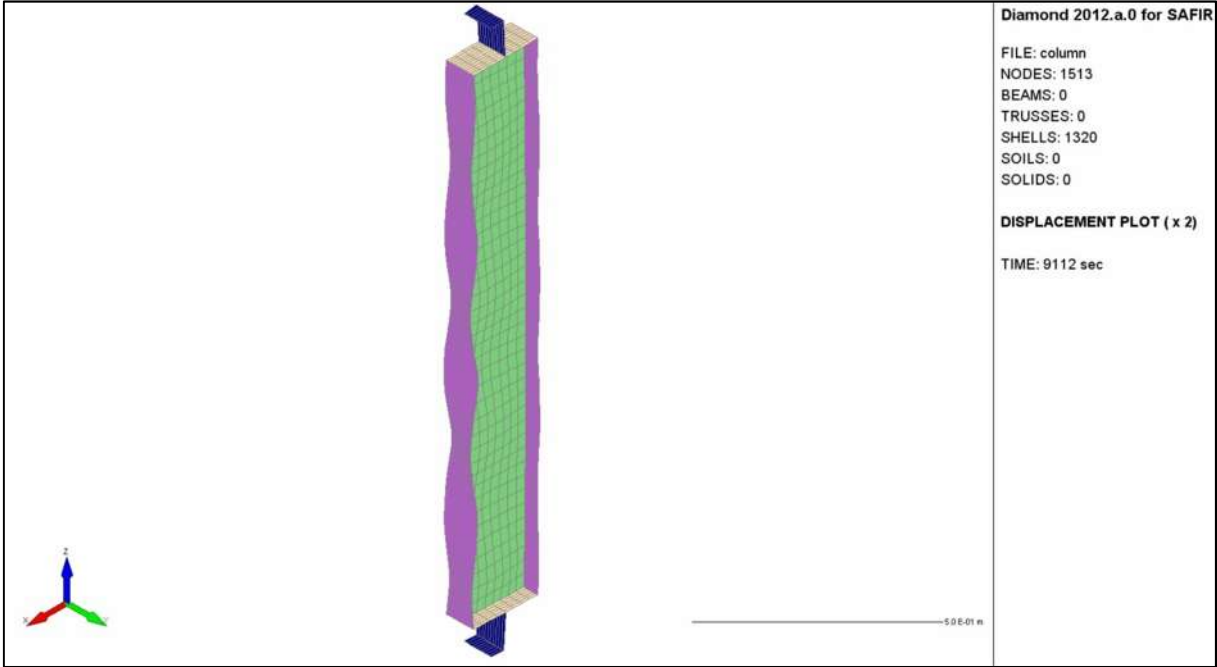


Figure 94: Numerical failure mode obtained with SAFIR

The failure mode obtained numerically with ANSYS is a global buckling along the weak axis as the experimental failure mode:

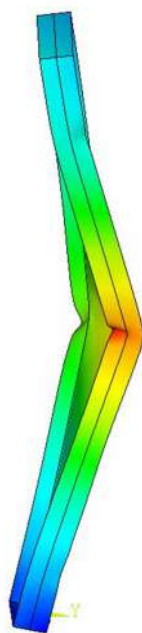


Figure 95: Numerical failure mode obtained with ANSYS

1.1.3.6 Test 6

The maximum steel grades of the flanges and of the web obtained by the material tests and used for the numerical simulations are given in the following table:

	f_y (MPa)
Web	482
Flanges	404

Table 46: Material properties for the numerical simulations

The global initial imperfections deduced from the manual measurement along the web and the flanges of the column are presented in Table 47. A global imperfection in the direction of the weak axis only, with a half sinusoidal shape, is set. The amplitude of this global imperfection is deduced from the profile of imperfection measured along the web. Around this global imperfection, some local imperfections are imposed to the web and to the flanges along the column. They have a sinusoidal shape in the direction perpendicular to the plane of the flange for the flanges and perpendicular to the web for the webs respectively.

Amplitude of the global imperfection in the direction of the weak axis (mm)	Amplitude of the local imperfection of the web (mm)	Amplitude of the local imperfection of the flange (mm)
1.0	2.5	1.2

Table 47: Amplitude of imperfections

The eccentricities between the axis of the pinned supports and the axis of the column were measured once the column was equipped and placed into the testing frame:

Eccentricity at the bottom basis (mm)	Eccentricity at the top basis (mm)
172	175

Table 48: Effective eccentricities

The modelled over-lengths of the column for bottom end and upper end are:

- Bottom end: $132.5 + 35 + 40/2 = 187.5$ mm
- Upper end: $132.5 + 32 + 40/2 = 187.5$ mm

The next table illustrates the results obtained in the fire test compared with the results obtained with both computer codes ANSYS and SAFIR:

Failure temperature (°C)					
Test	ANSYS	ϵ (%)	Test	SAFIR	ϵ (%)
530	530.8	0.2	530	531.5	0.3

Table 49: Failure temperature of simulations compared with experimental test

The following diagram illustrates the displacements of the column in function of the mean temperature for both experimental test and SAFIR simulation:

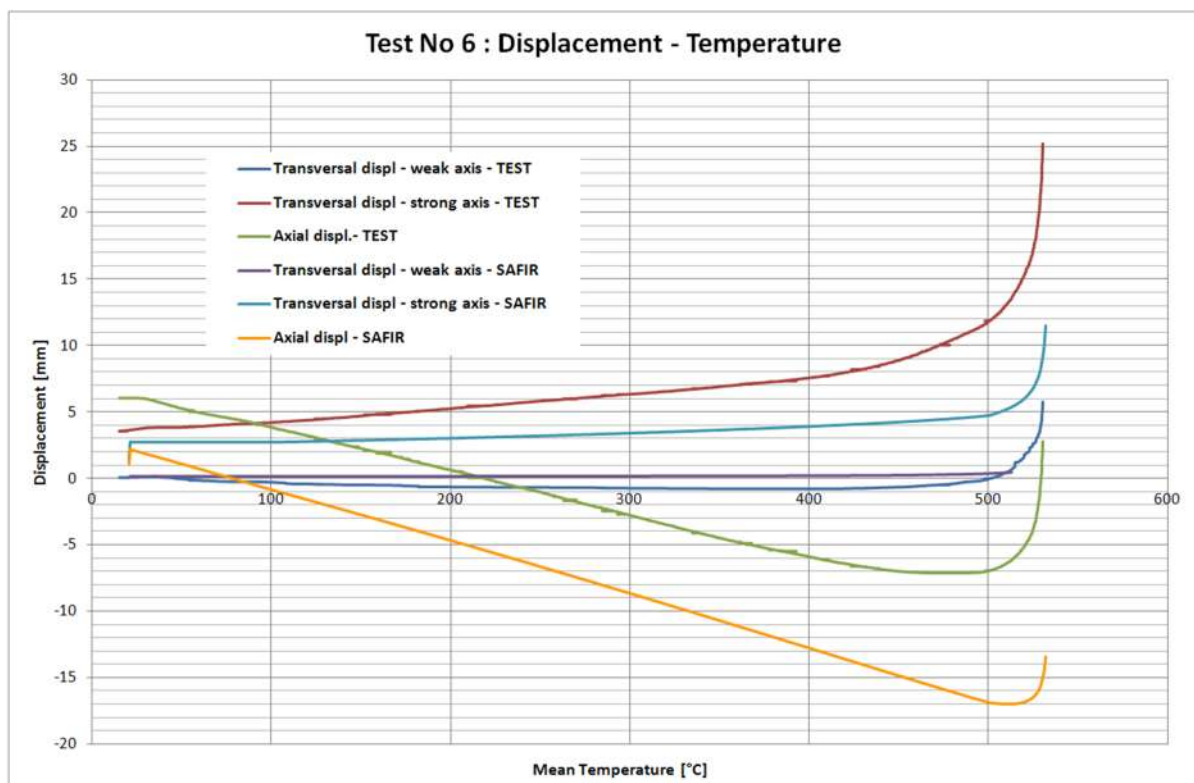


Figure 96: Displacements (mm) in function of temperature (°C) – SAFIR comparison

The following diagram illustrates the displacements of the column in function of the mean temperature for both experimental test and ANSYS simulation:

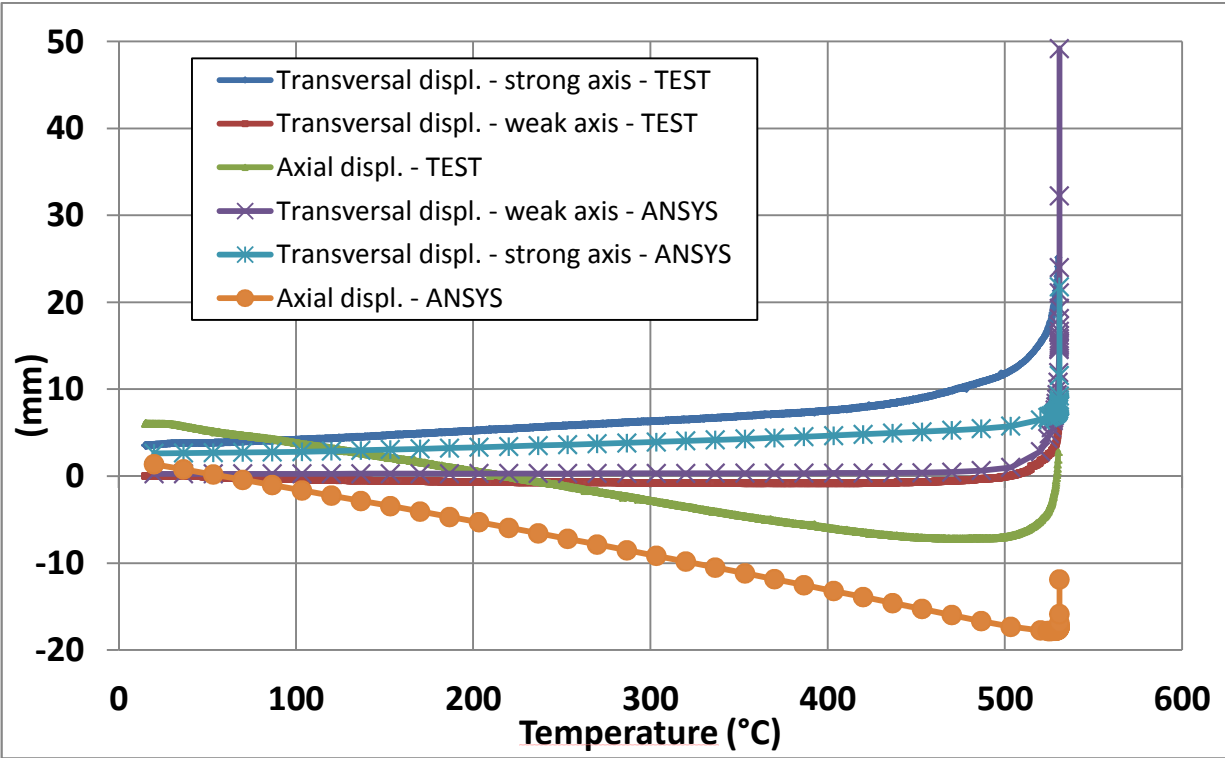


Figure 97: Displacements (mm) in function of temperature (°C) – ANSYS comparison

The failure mode obtained numerically is a global buckling along the weak axis with a local buckling of the flange at mid-height of the column:

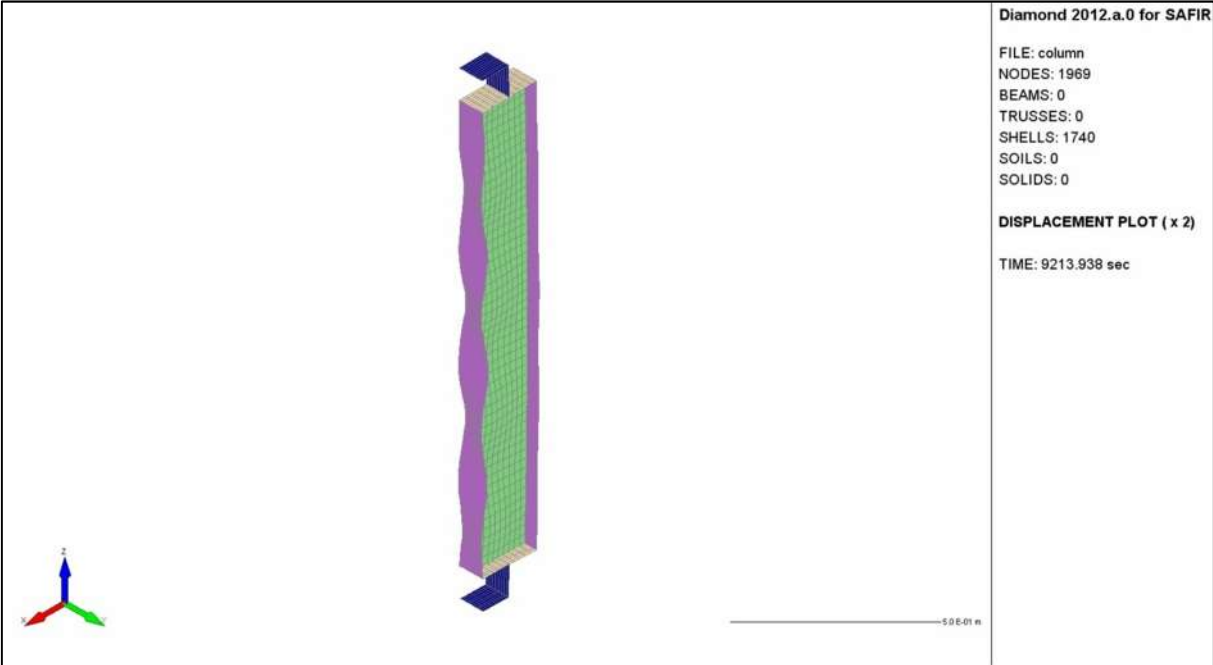


Figure 98: Numerical failure mode obtained with SAFIR

The failure mode obtained numerically with ANSYS is a global buckling along the weak axis as the experimental failure mode:

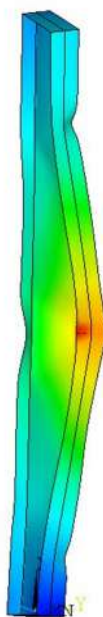


Figure 99: Numerical failure mode obtained with ANSYS

1.1.3.7 Test 7

The maximum steel grades of the flanges and of the web obtained by the material tests and used for the numerical simulations are given in the following table:

	f_y (MPa)
Web	585.5
Flanges	538

Table 50: Material properties for the numerical simulations

The global initial imperfections deduced from the manual measurement along the web and the flanges of the column are presented in Table 51. A global imperfection in the direction of the weak axis only, with a half sinusoidal shape, is set. The amplitude of this global imperfection is deduced from the profile of imperfection measured along the web. Around this global imperfection, some local imperfections are imposed to the web and to the flanges along the column. They have a sinusoidal shape in the direction perpendicular to the plane of the flange for the flanges and perpendicular to the web for the webs respectively.

Amplitude of the global imperfection in the direction of the weak axis (mm)	Amplitude of the local imperfection of the web (mm)	Amplitude of the local imperfection of the flange (mm)
1.5	0.5	0.6

Table 51: Amplitude of imperfections

The eccentricities between the axis of the pinned supports and the axis of the column were measured once the column was equipped and placed into the testing frame:

Eccentricity at the bottom basis (mm)	Eccentricity at the top basis (mm)
5	98

Table 52: Effective eccentricities

The modelled over-lengths of the column for bottom end and upper end are:

- Bottom end: $132.5 + 35 + 20/2 = 177.5$ mm
- Upper end: $132.5 + 32 + 35/2 = 185$ mm

The next table illustrates the results obtained in the fire test compared with the results obtained with both computer codes ANSYS and SAFIR:

Failure temperature (°C)					
Test	ANSYS	ϵ (%)	Test	SAFIR	ϵ (%)
622.8	634.3	1.8	622.8	631	1.3

Table 53: Failure temperature of simulations compared with experimental test

The following diagram illustrates the displacements of the column in function of the mean temperature for both experimental test and SAFIR simulation:

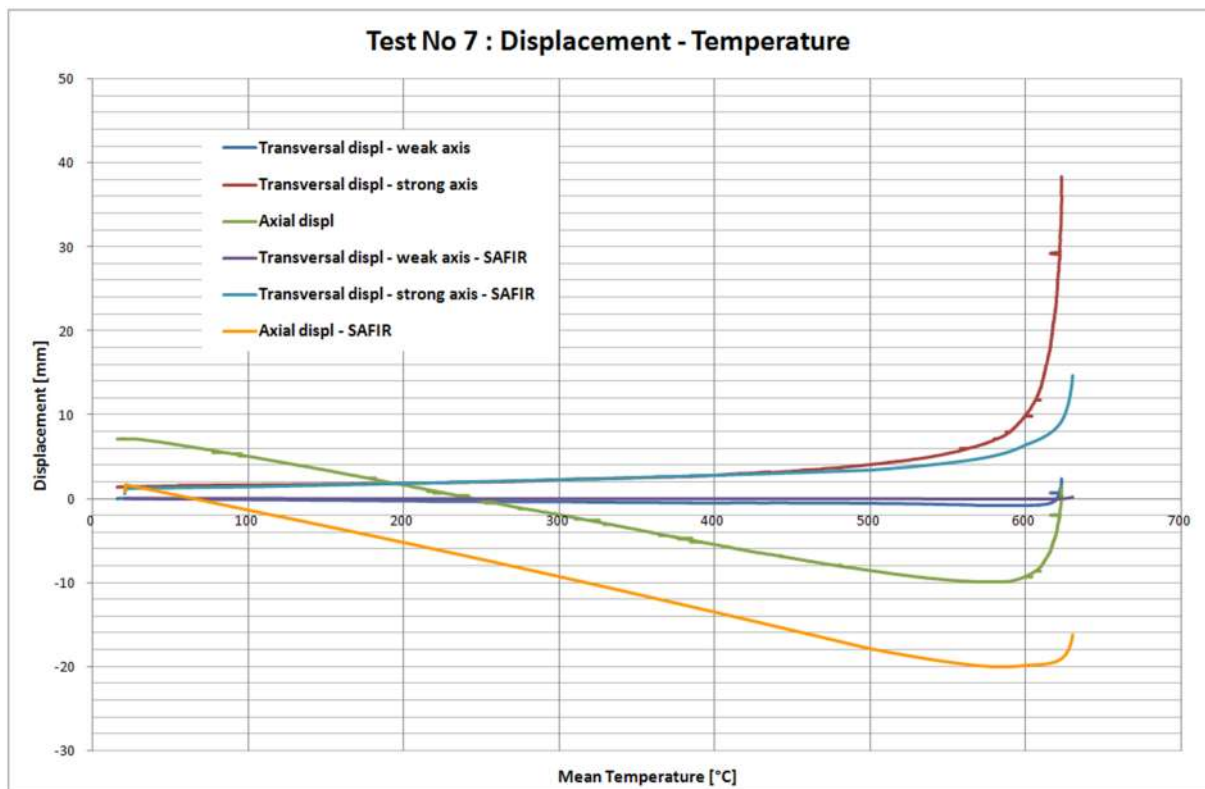


Figure 100: Displacements (mm) in function of temperature (°C) – SAFIR comparison

The following diagram illustrates the displacements of the column in function of the mean temperature for both experimental test and ANSYS simulation:

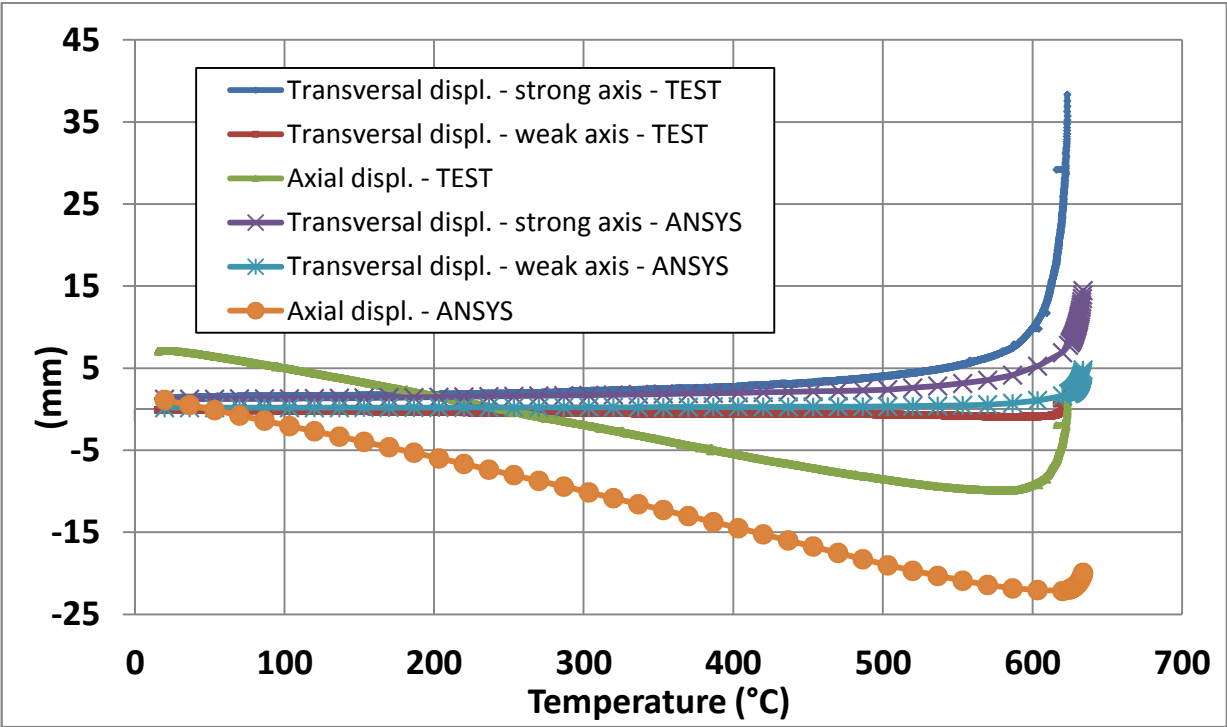


Figure 101: Displacements (mm) in function of temperature (°C) – ANSYS comparison

The failure mode obtained numerically is a global buckling along the weak axis with a local buckling of the flange at mid-height of the column:

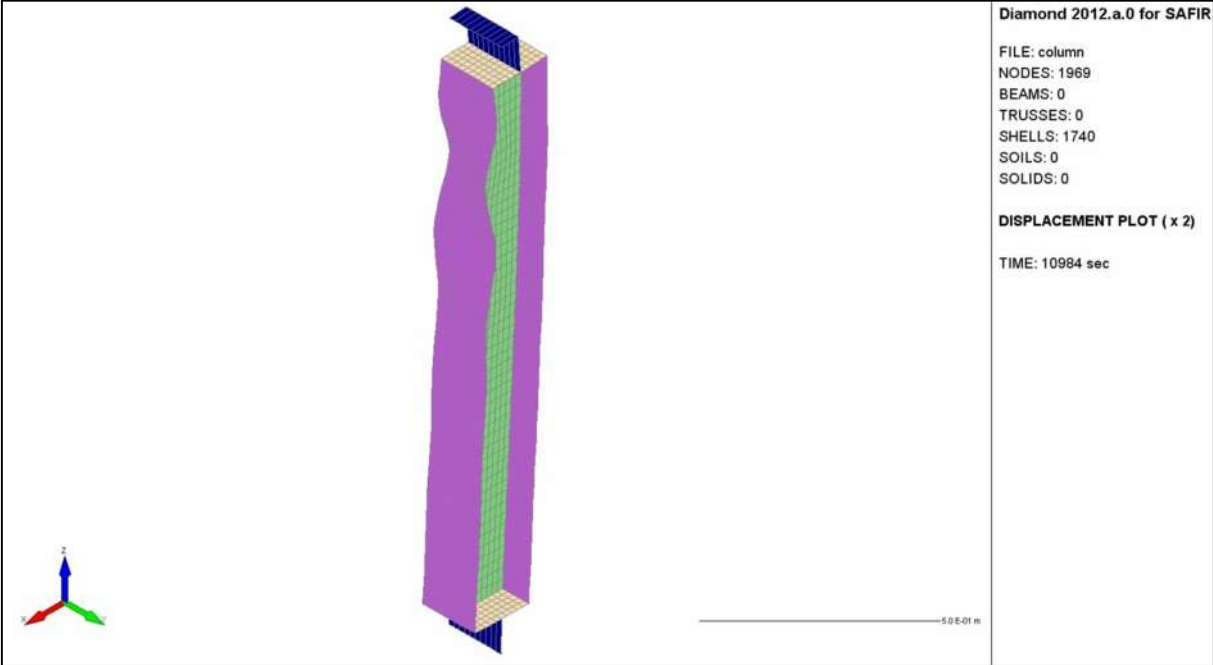


Figure 102: Numerical failure mode obtained with SAFIR

The failure mode obtained numerically with ANSYS is a global buckling along the weak axis as the experimental failure mode:

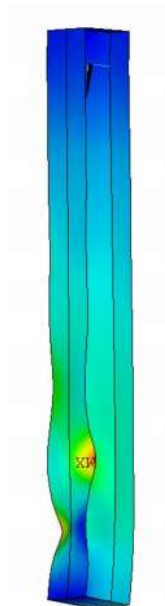


Figure 103: Numerical failure mode obtained with ANSYS

1.1.3.8 Test 8

The maximum steel grades of the flanges and of the web obtained by the material tests and used for the numerical simulations are given in the following table:

	f_y (MPa)
Web	482
Flanges	404

Table 54: Material properties for the numerical simulations

The global initial imperfections deduced from the manual measurement along the web and the flanges of the column are presented in Table 55. A global imperfection in the direction of the weak axis only, with a half sinusoidal shape, is set. The amplitude of this global imperfection is deduced from the profile of imperfection measured along the web. Around this global imperfection, some local imperfections are imposed to the web and to the flanges along the column. They have a sinusoidal shape in the direction perpendicular to the plane of the flange for the flanges and perpendicular to the web for the webs respectively.

Amplitude of the global imperfection in the direction of the weak axis (mm)	Amplitude of the local imperfection of the web (mm)	Amplitude of the local imperfection of the flange (mm)
1	2.8	1.5

Table 55: Amplitude of imperfections

The eccentricities between the axis of the pinned supports and the axis of the column were measured once the column was equipped and placed into the testing frame:

Eccentricity at the bottom basis (mm)	Eccentricity at the top basis (mm)
143.5	2.5

Table 56: Effective eccentricities

The modelled over-lengths of the column for bottom end and upper end are:

- Bottom end: $132.5 + 35 + 40/2 = 187.5$ mm
- Upper end: $132.5 + 32 + 20/2 = 177.5$ mm

The next table illustrates the results obtained in the fire test compared with the results obtained with both computer codes ANSYS and SAFIR:

Failure temperature (°C)					
Test	ANSYS	ϵ (%)	Test	SAFIR	ϵ (%)
504.5	536.8	6.0	504.5	537	6.1

Table 57: Failure temperature of simulations compared with experimental test

The following diagram illustrates the displacements of the column in function of the mean temperature for both experimental test and SAFIR simulation:

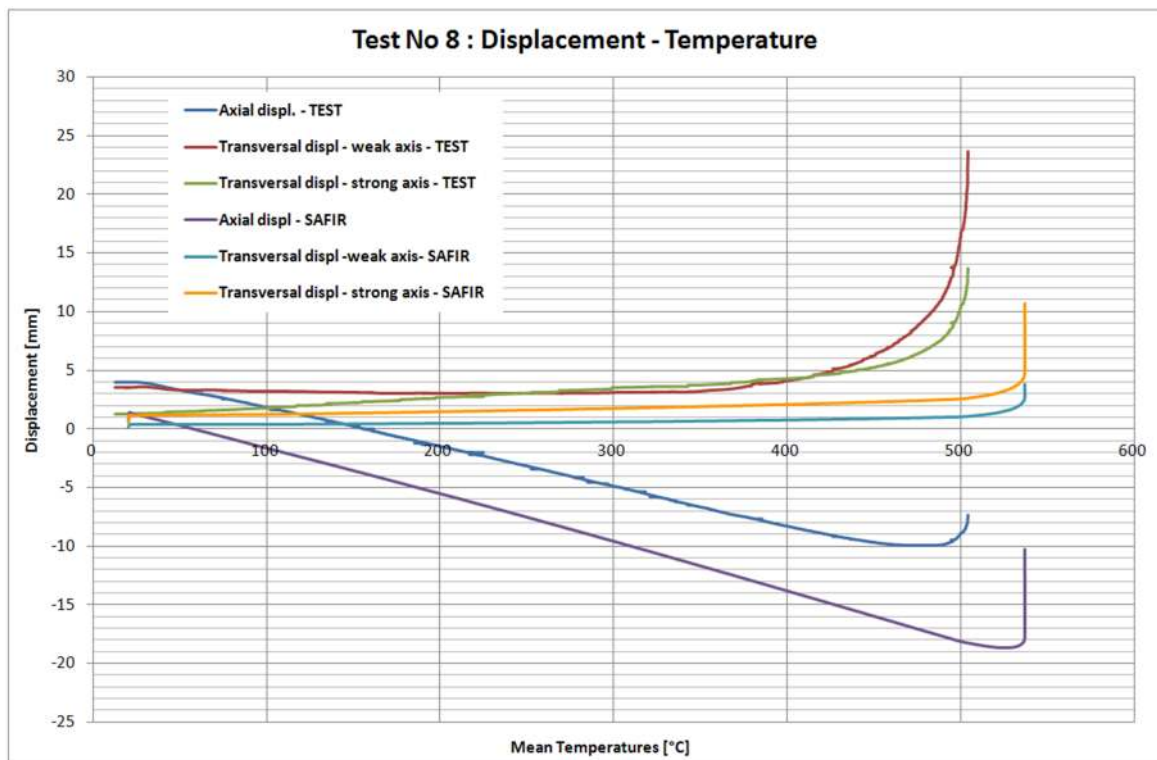


Figure 104: Displacements (mm) in function of temperature (°C) – SAFIR comparison

The following diagram illustrates the displacements of the column in function of the mean temperature for both experimental test and ANSYS simulation:

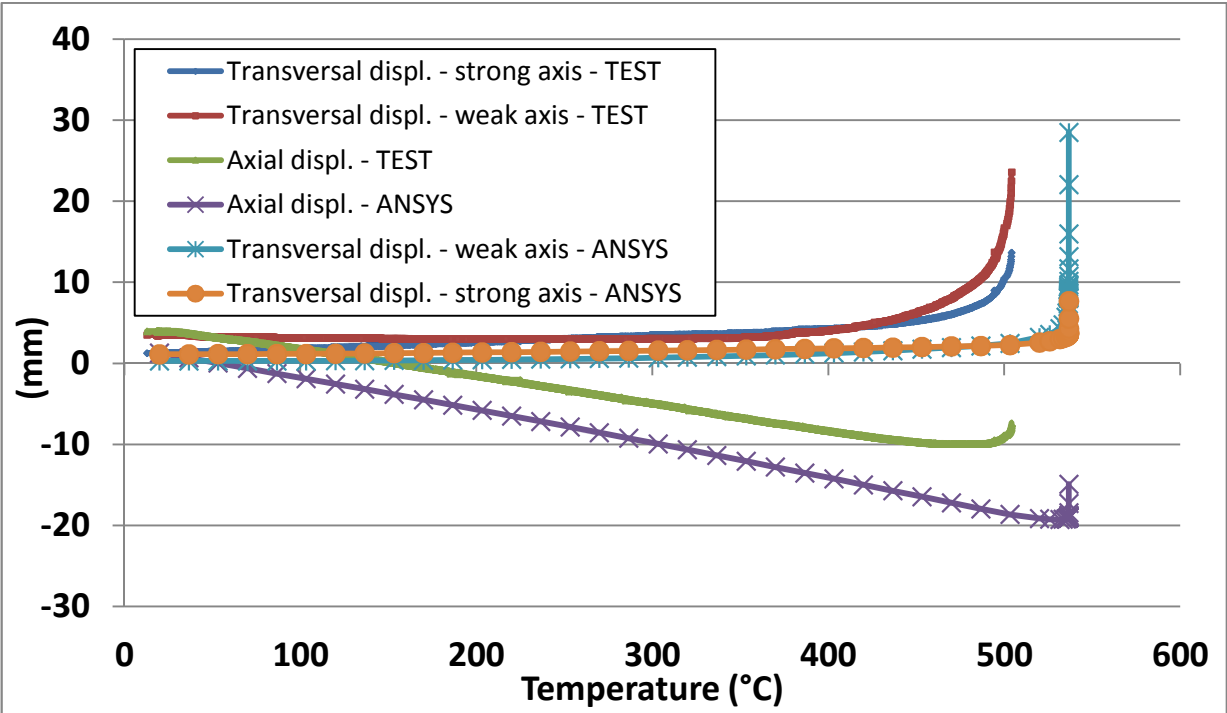


Figure 105: Displacements (mm) in function of temperature (°C) – ANSYS comparison

The failure mode obtained numerically is a global buckling along the weak axis with a local buckling of the flange at mid-height of the column:

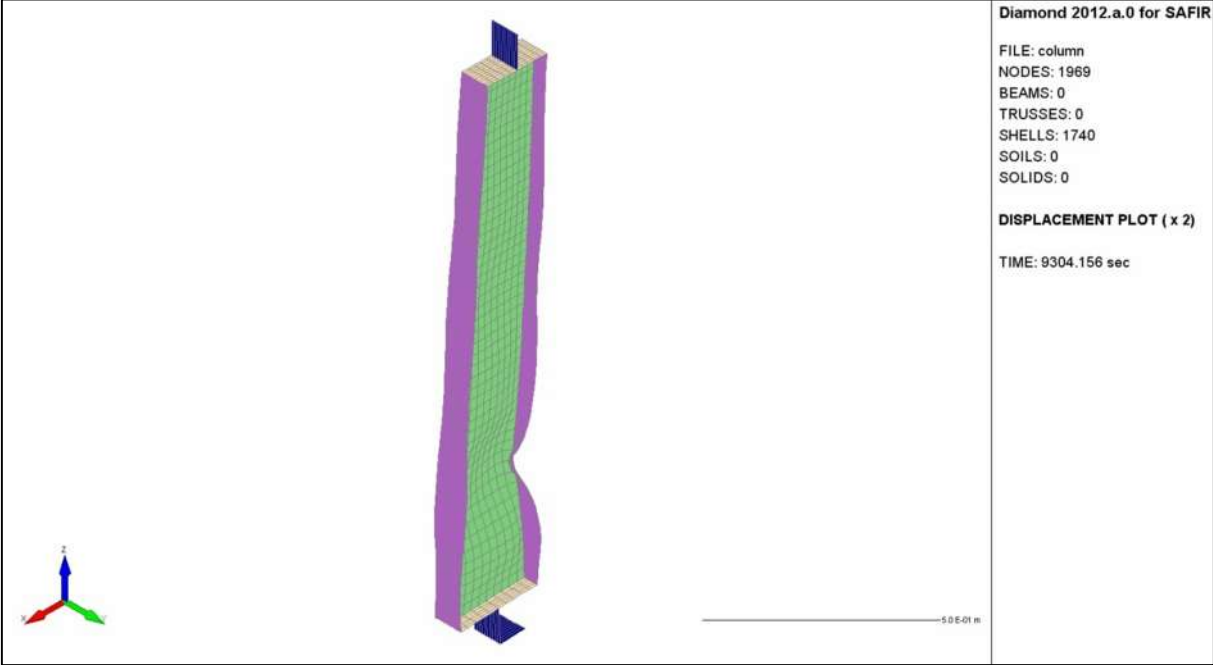


Figure 106: Numerical failure mode obtained with SAFIR

The failure mode obtained numerically with ANSYS is a global buckling along the weak axis as the experimental failure mode:

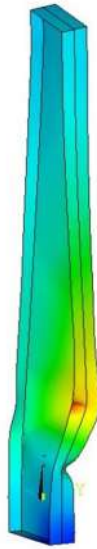


Figure 107: Numerical failure mode obtained with ANSYS

The comments on these results are given hereafter:

- Close results between softwares ANSYS and SAFIR in terms of failure mode and in terms of bearing load capacity of the columns
- Close values in terms of bearing load capacity between tests and simulations (maximum 6%)
- Failure modes are quite similar between experimental tests and simulations

2 Description of the parametric studies and comparisons with simple design rules

2.1 Numerical parametric study for class 4 columns subjected to axial compression

This parametric study is set up to have a consequent set of results regarding the resistance in axial compression of both welded and hot-rolled cross-sections. Within the context of this project it is necessary to study the influence of non-dimensional slenderness of columns in the final resistance.

2.1.1 Presentation of chosen parameters

As previously described, both welded and hot-rolled cross-sections are investigated. In the context of welded cross-sections, the following table illustrates the dimensions to take into account in the parametric study:

Combination	500x t_w +250x t_f				
t_w (mm)	4	6	8	10	12
t_f (mm)	6	8	10	12	14
Combination	450x t_w +250x t_f				
t_w (mm)	4	6	8	10	12
t_f (mm)	6	8	10	12	14

Table 58: Different possible dimensions for the welded columns

In the context of hot-rolled columns, twelve sections are investigated. They are taken from the catalogue of European I beams (IPE) and of European H beams (HE):

Hot-rolled sections		
IPE 200A	IPE 600A	HE 450AA
IPE 330	IPE 750 x173	HE 600AA
IPE 400A	HE 200AA	HE 700B
IPE 550	HE 340AA	HE 1000AA

Table 59: Studied hot-rolled sections

In the case of the welded sections, all the webs are class 4 in pure compression, whereas the flanges class varies from boundary class 3-4 to class 4 in pure compression. On the other hand, all the hot-rolled sections are class 3 or class 4 in pure compression.

Two steel grades are taken into account in the numerical simulations:

Steel grade
S355
S460

Table 60: List of steel grades

A total of five steady-state temperatures are investigated for this parametric study:

Temperature (°C)				
20	350	450	550	700

Table 61: Studied temperatures

Five lengths of column are calculated to check the effect of non-dimensional slenderness on resistance in axial compression:

Length (m)				
2	4	6	8	10

Table 62: Defined lengths of columns

Two types of failure are investigated:

- Weak axis failure
- Strong axis failure by putting some lateral restraints in the direction of the weak axis at the intersection between web and flange)

The load is an axial load without any eccentricity. The initial global imperfections are based upon the Eigen-modes obtained from a previous linear buckling analysis:

If the first mode is a global failure mode:

- Global imperfection : $L/750 \times 0.8$ with L is the column length
- Local imperfection based on the first local buckling mode: $a/100 \times 0.8 \times 0.7$ with a is the plate width (web or flange)

On the other hand, if the first buckling mode is a local one:

- Global imperfection : $L/750 \times 0.8 \times 0.7$ with L is the column length
- Local imperfection based on the first local buckling mode: $a/100 \times 0.8$ with a is the plate width (web or flange)

The columns are pinned-pinned: the vertical displacement is blocked at the bottom and free at the upper side, as illustrated in Figure 108 and in Figure 109:

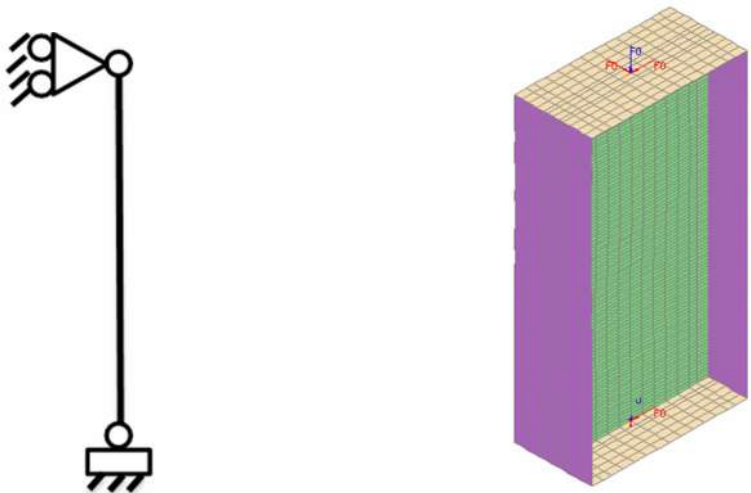


Figure 108: Static boundary conditions Figure 109: Boundary conditions of the numerical model

The finite element models are defined with the following assumptions:

- The finite elements are shells with four or eight nodes
- The load and the boundary conditions are applied at the central node of each end-plate
- The central node of the bottom end has its three translations fixed (U_x , U_y and U_z) and its R_z rotation blocked
- The central node of the upper end of the column has two fixed translations (U_x and U_y) and its R_z rotation blocked
- The axial load is applied on the central node of the top end of the column with an increasing intensity depend on time increments until mechanical failure
- The calculations remains in the static domain
- The modelling of the residual stresses determines the mesh of the cross-section according to the following proposed residual stress patterns:

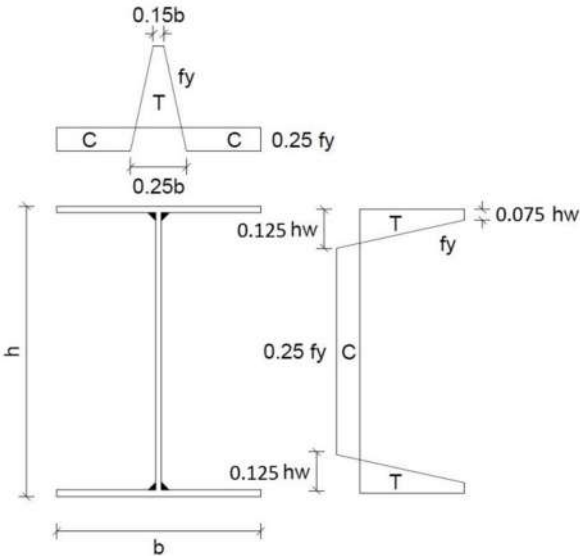


Figure 110: Residual stress pattern for welded cross-sections

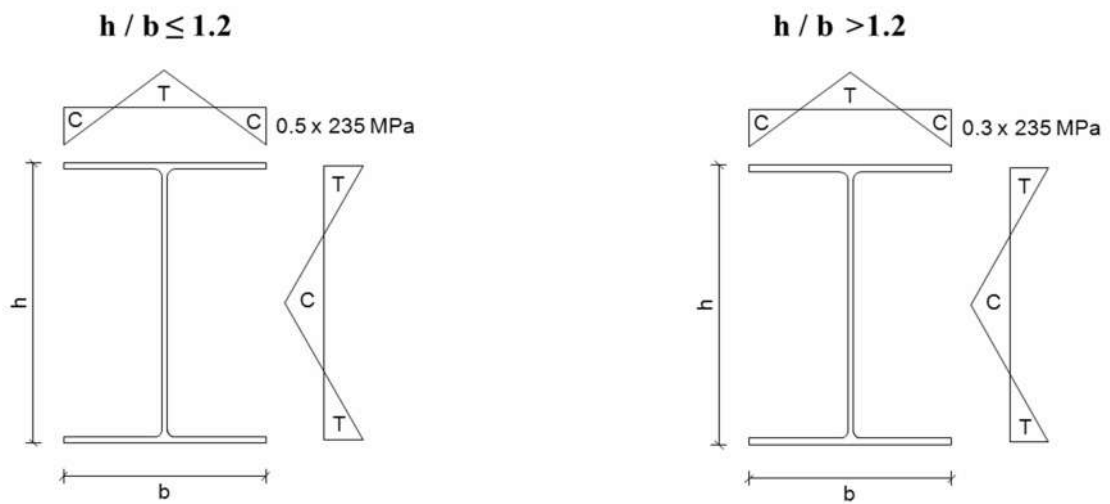


Figure 111: Residual stress pattern for hot-rolled cross-sections

The meshed areas are divided according to the previous residual stress pattern for welded cross-sections:

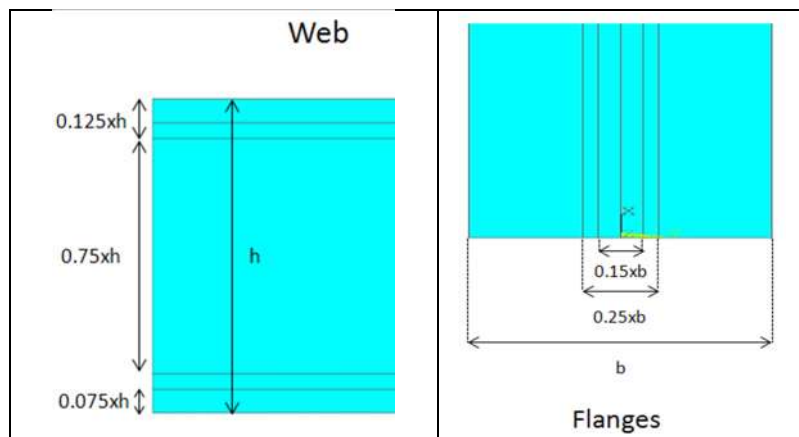


Figure 112: Discretization of meshed areas for welded cross-sections

This numerical parametric study represents a total of about 5500 simulations.

2.1.2 Detailed list of results of the parametric study and comparisons with simple design rules of EN 1993-1-2

As a first step in this part, the load bearing capacity of the columns is calculated with the simple design rules recommended by EN 1993-1-2. The formulae are presented hereafter. Both strong axis buckling and weak axis buckling are treated. The first step is the evaluation of the critical compressive load defined for strong axis buckling as:

$$N_{cr-strong} = \frac{\pi^2 E I}{(L_{strong})^2} \quad (1)$$

With I representing the inertia along the strong axis, E the Young modulus and L_{strong} is the buckling length along strong axis. For weak axis buckling the critical compressive load is defined as follows:

$$N_{cr-weak} = \frac{\pi^2 E I}{(L_{weak})^2} \quad (2)$$

With L_{weak} representing the buckling length along the weak axis of the column.

The following step is the evaluation of the non-dimensional slenderness of the column along strong axis:

$$\lambda_{strong} = \sqrt{A_{eff} f_y / N_{cr-strong}} \quad (3)$$

And weak axis:

$$\lambda_{weak} = \sqrt{A_{eff} f_y / N_{cr-weak}} \quad (4)$$

With A_{eff} representing the effective area of the class 4 cross-section in pure compression. f_y is the Yield strength of steel at room temperature.

The effective non-dimensional slenderness to take account for is defined as the maximum of non-dimensional slenderness:

$$\lambda = \max(\lambda_{strong}; \lambda_{weak}) \quad (5)$$

At high temperature the non-dimension slenderness becomes:

$$\bar{\lambda}_\theta = \lambda \sqrt{k_{0.2,\theta} / k_{E,\theta}} \quad (6)$$

The value of reduction factor is determined according to the following equations:

$$\chi_{fi} = \frac{1}{\varphi_{\theta} + \sqrt{\varphi_{\theta}^2 - \lambda_{\theta}^2}} \quad (7)$$

With

$$\varphi_{\theta} = 0.5 \times (1 + \alpha \times \lambda_{\theta} + \lambda_{\theta}^2) \quad (8)$$

And α is an imperfection factor corresponding to the cross-sections dimensions. The values are given from the following equation:

$$\alpha = 0.65 \times \sqrt{235/f_y} \quad (9)$$

The compressive buckling resistance in the fire design situation is finally obtained with the following formula:

$$N_{b,fi,Rd} = \chi_{fi} \times A_{eff} \times k_{0.2,\theta} \times f_y \quad (10)$$

The ratio between the failure load obtained through the numerical analysis and the failure load obtained with the simple design rules provided by EN 1993-1-2 is calculated for each column, and then, the mean, the standard deviation and the covariance are calculated for all of them, see following table:

	EN 1993-1-2/SAFIR (welded sections)	EN 1993-1-2/ABAQUS (hot rolled sections)
Mean	91.5% < 100%	83.3% < 100%
Standard deviation	6.1%	11.6%
Covariance	6.7%	13.9%
Unsafe cases	5.4% < 20%	3.5% < 20%
Ratio maximum	1.14 < 1.15	1,11. < 1.15

Table 63: Statistical data of comparison with EN 1993-1-2

The comparisons between the numerical simulations and the design points of EN 1993-1-2 for welded cross-sections are given in the following chart:

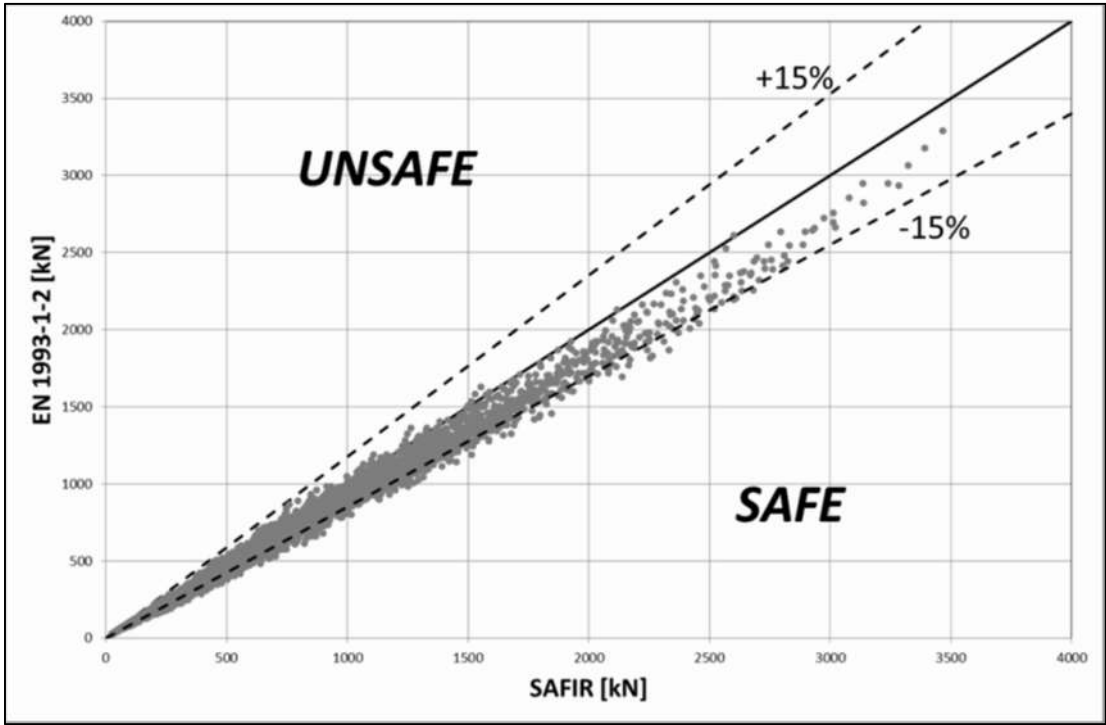


Figure 113: Comparison between EN 1993-1-2 design rules and numerical results for welded cross-sections

The comparisons between the numerical simulations and the design points of EN 1993-1-2 for hot-rolled cross-sections are given in the following chart:

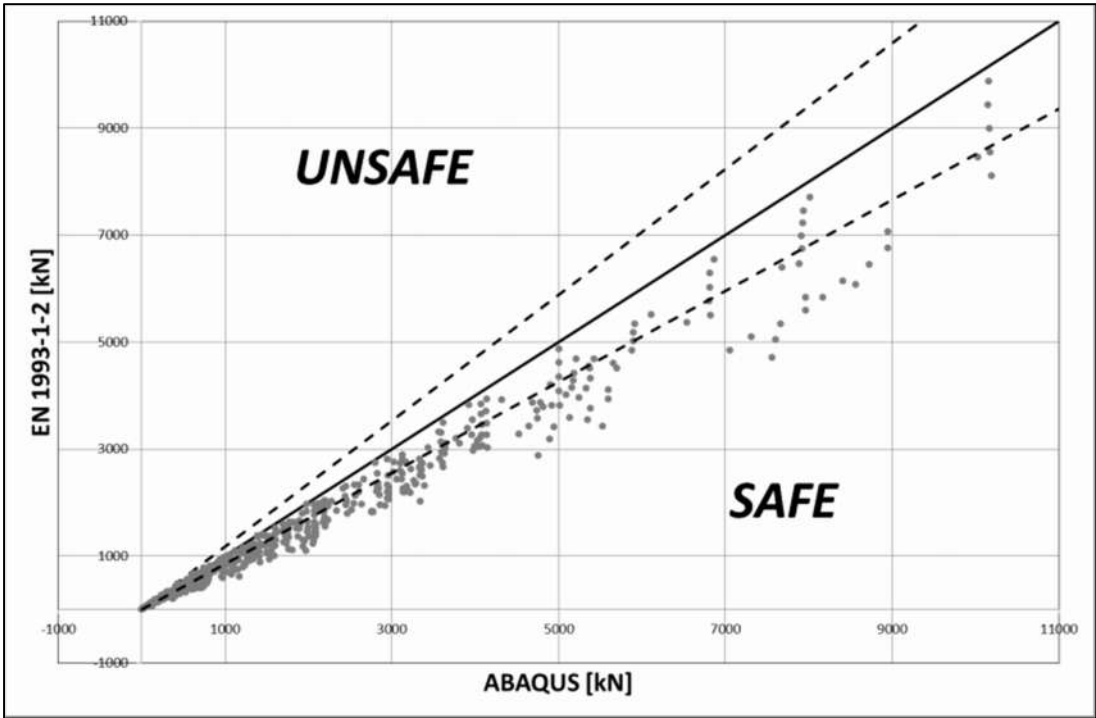


Figure 114: Comparison between EN 1993-1-2 design rules and numerical results for hot-rolled cross-sections

The values presented in Figure 113 and Figure 114 show that the current method recommended by EN 1993-1-2 is safe. This method is even too safe and un-economical in numerous cases, and the load bearing capacity calculated with formula from EN 1993-1-2 could be increased of almost 10% for welded sections, and of almost 20% for hot rolled sections. Therefore, new simple design rules are proposed with the objective to improve those results and the competitiveness of class 4 steel columns.

2.1.3 Detailed list of results of the parametric study and comparisons with new proposed simple design rules

The key point of this new proposed design rule is the use of the new effective cross-section calculation method defined for WP2 and described in the second deliverable. With this method, the effective area of the cross-section in compression is evaluated. Then, it is proposed to replace current $k_{0.2p,\theta}$ by $k_{y,\theta}$ as it was done for effective cross-section calculation too. The new method is described in the equations below:

$$N_{cr-strong} = \frac{\pi^2 E I}{(L_{strong})^2} \quad (11)$$

With I representing the inertia along the strong axis, E the Young modulus and L_{strong} is the buckling length along strong axis. For weak axis buckling the critical compressive load is defined as follow:

$$N_{cr-weak} = \frac{\pi^2 E I}{(L_{weak})^2} \quad (12)$$

With L_{weak} representing the buckling length along the weak axis of the column.

The following step is the evaluation of the non-dimensional slenderness of the column along strong axis:

$$\lambda_{strong} = \sqrt{A_{eff} f_y / N_{cr-strong}} \quad (13)$$

And weak axis:

$$\lambda_{weak} = \sqrt{A_{eff} f_y / N_{cr-weak}} \quad (14)$$

With A_{eff} representing the effective area of the class 4 cross-section in pure compression calculated with the new design method of FIDESC4 project. f_y is the Yield strength of steel at room temperature.

The effective non-dimensional slenderness to take account for is defined as the maximum of non-dimensional slenderness:

$$\lambda = \max(\lambda_{strong}; \lambda_{weak}) \quad (15)$$

At high temperature the non-dimension slenderness becomes:

$$\bar{\lambda}_\theta = \lambda \sqrt{k_{y,\theta} / k_{E,\theta}} \quad (16)$$

The value of reduction factor is determined according to the following equations:

$$\chi_{fi} = \frac{1}{\varphi_{\theta} + \sqrt{\varphi_{\theta}^2 - \lambda_{\theta}^2}} \quad (17)$$

With

$$\varphi_{\theta} = 0.5 \times (1 + \alpha \times \lambda_{\theta} + \lambda_{\theta}^2) \quad (18)$$

And α is an imperfection factor corresponding to the cross-sections dimensions. The values are given from the following equation:

$$\alpha = 0.65 \times \sqrt{235/f_y} \quad (19)$$

The compressive buckling resistance in the fire design situation is finally obtained with the following formula:

$$N_{b,fi,Rd} = \chi_{fi} \times A_{eff} \times k_{y,\theta} \times f_y \quad (20)$$

The ratio between the failure load obtained through the numerical analysis and the failure load obtained with new proposed simple design rules is calculated for each column, and then, the mean, the standard deviation and the covariance are calculated for all of them, see following table:

	New design rules/SAFIR (welded sections)	New design rules/ABAQUS (hot rolled sections)
Mean	93.0% < 100%	86.5% < 100%
Standard deviation	5.8%	12.6%
Covariance	6.2%	14.6%
Unsafe cases	11.9% < 20%	11.5% < 20%
Ratio maximum	1.109 < 1.15	1,112 < 1.150

Table 64: Statistical data of comparison with new design rule

The comparisons between the numerical simulations and the design points of the new proposed design rules for welded cross-sections are given in the following chart:

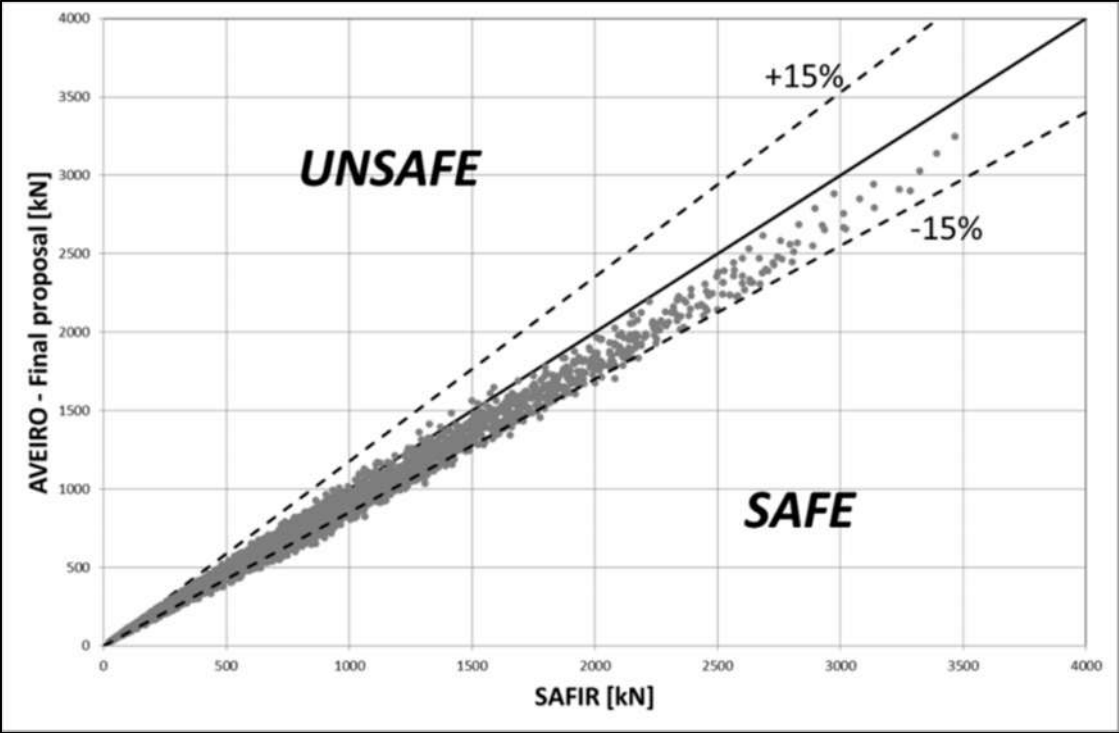


Figure 115: Comparison between new design rules and numerical results for welded cross-sections

The comparisons between the numerical simulations and the design points of the new proposed design rules for hot-rolled cross-sections are given in the following chart:

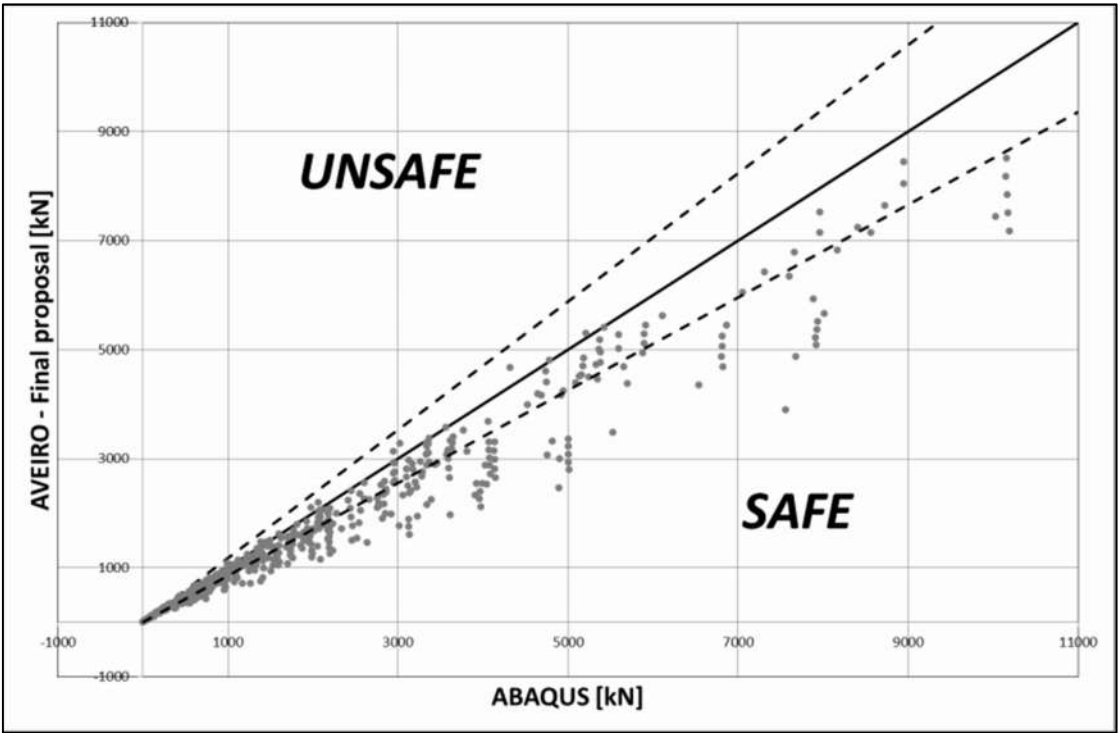


Figure 116: Comparison between new design rules and numerical results for hot-rolled cross-sections

The new proposed design rules rely on the new definition of the effective cross-section area calculation. The form of the rule remains very close to the current one of the EN 1993-1-2, except for the use of $k_{y,\theta}$ reduction factor instead of $k_{0,2p,\theta}$ factor, which is in accordance with previous defined design rules. These design rules remain safe enough and propose a more accurate comparison and also decrease the number of too safe cases which do not propose an economic design of class 4 steel columns.

2.2 Numerical parametric study for class 4 columns subjected to axial compression and bending

The aim of this parametric study is to have a consequent set of results regarding the resistance in combined compression and bending of both welded and hot-rolled beam-columns. The conducted simulations consider in-plane and out-of-plane buckling, several member lengths and cross-section dimensions and different temperatures. In addition to these parameters, different bending moment diagrams and load ratios are investigated.

2.2.1 Presentation of chosen parameters

Both welded and some hot-rolled cross-sections are investigated. In the context of welded cross-sections, the following table illustrates the dimensions to take into account in the parametric study:

450x4+150x5	Class 4 web and flanges
450x4+150x7	Class 4 web and boundary class 3-4 flanges
450x4+250x6	Class 4 web and flanges
450x4+250x12	Class 4 web and boundary class 3-4 flanges
1000x5+300x10	Class 4 web and flanges
1000x5+300x15	Class 4 web and boundary class 3-4 flanges
HE 340 AA	Boundary class 3-4 flanges
440-340x4+150x5	Class 4 flanges
1000-750x5+300x10	Class 4 flanges

Table 65: Different dimensions for investigated beam-columns

Two steel grades are taken into account in the numerical simulations:

Steel grade
S355
S460

Table 66: List of steel grades

A total of five steady-state temperatures are investigated for this parametric study:

Temperature (°C)				
20	350	450	550	700

Table 67: Studied temperatures

The different non-dimensional slenderness values taken into account are shown in the following table. The considered axis depends on which one is relevant:

$\bar{\lambda}_z, \bar{\lambda}_y$ or $\bar{\lambda}_{LT}$			
0.5	1.0	1.5	2.0

Table 68: Defined lengths of columns

Two compression plus bending situations are simulated:

- Bending on the strong axis with buckling on the weak axis
- Bending on the strong axis without any buckling restriction (LTB)

In addition to these parameters, different bending diagrams were defined as for lateral torsional buckling of beams investigation:

Uniform bending diagram ($\psi = 1$)	
Triangular bending diagram ($\psi = 0$)	
Bi-triangular bending diagram ($\psi = -1$)	
Parabolic bending diagram	

Table 69: Different bending diagrams

Concerning the loading combinations, it was proposed to calculate between three to five N/M interaction with cases with only bending moment and only axial compression. The details are given in the following equations:

	β				
N	0.2	0.4	0.6	0.8	M

Table 70: Load combinations

With β defined in the following equation:

$$\frac{N_{fi,Ed}}{M_{y,fi,Ed}} = \frac{1 - \beta}{\beta \times M_{y,fi,Rd}} \times N_{fi,Rd} \quad (21)$$

The other finite elements parameters are the same as those used for axial compression simulations (see 2.2.1).

2.2.2 Detailed list of results of the parametric study and comparisons with simple design rules of current EN 1993-1-2

According to EN 1993-1-2, the design buckling resistance $R_{fi,d}$ for a member without lateral restraints and with a Class 4 cross section subject to combined bending and axial compression in fire situation should be verified by satisfying the interaction curve defined by the two following equations for doubly symmetric cross-sections. These are the equations (4.21c) and (4.21d) respectively of Part 1.2 of EC3 adapted for Class 4, i.e., considering the effective cross-sectional properties:

$$\frac{N_{fi,Ed}}{\chi_{\min,fi} A_{eff} k_{0.2p,\theta} \frac{f_y}{\gamma_{M,fi}}} + \frac{k_y M_{y,fi,Ed}}{W_{eff,y,\min} k_{0.2p,\theta} \frac{f_y}{\gamma_{M,fi}}} + \frac{k_z M_{z,fi,Ed}}{W_{eff,z,\min} k_{0.2p,\theta} \frac{f_y}{\gamma_{M,fi}}} \leq 1 \quad (22)$$

$$\frac{N_{fi,Ed}}{\chi_{z,fi} A_{eff} k_{0.2p,\theta} \frac{f_y}{\gamma_{M,fi}}} + \frac{k_{LT} M_{y,fi,Ed}}{\chi_{LT,fi} W_{eff,y,\min} k_{0.2p,\theta} \frac{f_y}{\gamma_{M,fi}}} + \frac{k_z M_{z,fi,Ed}}{W_{eff,z,\min} k_{0.2p,\theta} \frac{f_y}{\gamma_{M,fi}}} \leq 1 \quad (23)$$

All symbols are those defined in Eurocode 3. k_y is defined with the following equation:

$$k_y = 1 - \frac{\mu_y N_{fi,Ed}}{\chi_{y,fi} A_{eff} k_{0.2p,\theta} \frac{f_y}{\gamma_{M,fi}}} \leq 3 \quad (24)$$

And:

$$\mu_y = (2 \beta_{M,y} - 5) \bar{\lambda}_{y,\theta} + 0.44 \beta_{M,y} + 0.29 \leq 0.8 \text{ but } \bar{\lambda}_{y,20^\circ\text{C}} \leq 1.1 \quad (25)$$

For equation (23), k_{LT} is defined with the following equation:

$$k_{LT} = 1 - \frac{\mu_{LT} N_{fi,Ed}}{\chi_{z,fi} A_{eff} k_{0.2p,\theta} \frac{f_y}{\gamma_{M,fi}}} \leq 1 \quad (26)$$

And:

$$\mu_{LT} = 0.15 \bar{\lambda}_{z,\theta} \beta_{M,LT} - 0.15 \leq 0.9 \quad (27)$$

The equivalent uniform moment factors $\beta_{M,LT}$ and $\beta_{M,y}$ are evaluated using the bending diagram corresponding to the major axis – $M_{y,fi,Ed}$. Only uniaxial bending (about the major axis) was considered in this numerical investigation. As a consequence, the terms related to the minor axis (z) are not to be taken into account.

The in-plane behaviour of the beam-columns is numerically investigated with the help of lateral restraints (preventing out-of-plane buckling) in the flanges as it is depicted in the following figure:

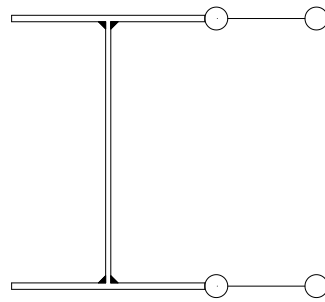


Figure 117: Additional restraints added to the model to prevent the out-of-plane displacements

Equation (22) was then employed considering the ultimate axial force and uniform bending moment given by numerical simulations as the design loads. Results are plotted in Figure 118 against the non-dimensional slenderness $\lambda_{y,\Theta}$ and in Figure 119 against the ratio between the applied bending moment and the cross-sectional bending resistance $M/M_{y,fi,Rd}$. In these figures, the line corresponding to the value 1 in the vertical axis defines the interaction curve. If the points, which represent the numerical results, are below the line, it means the stresses obtained numerically are below those predicted by equation (22) and therefore are unsafe and safe otherwise:

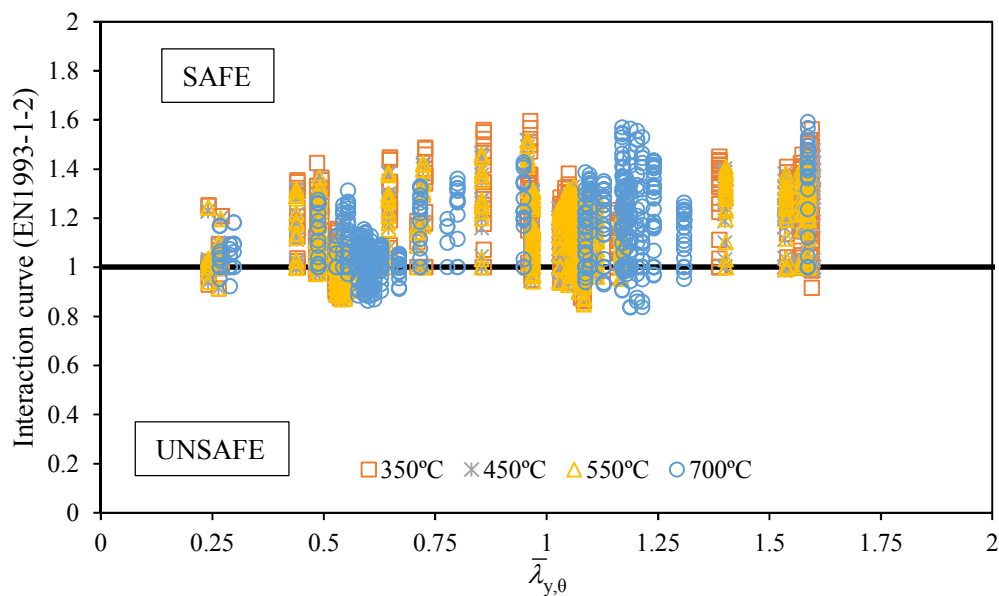


Figure 118: Comparison of the numerical analysis results with the EN 1993-1-2 interaction curve for various temperatures as a function of the beam-column slenderness

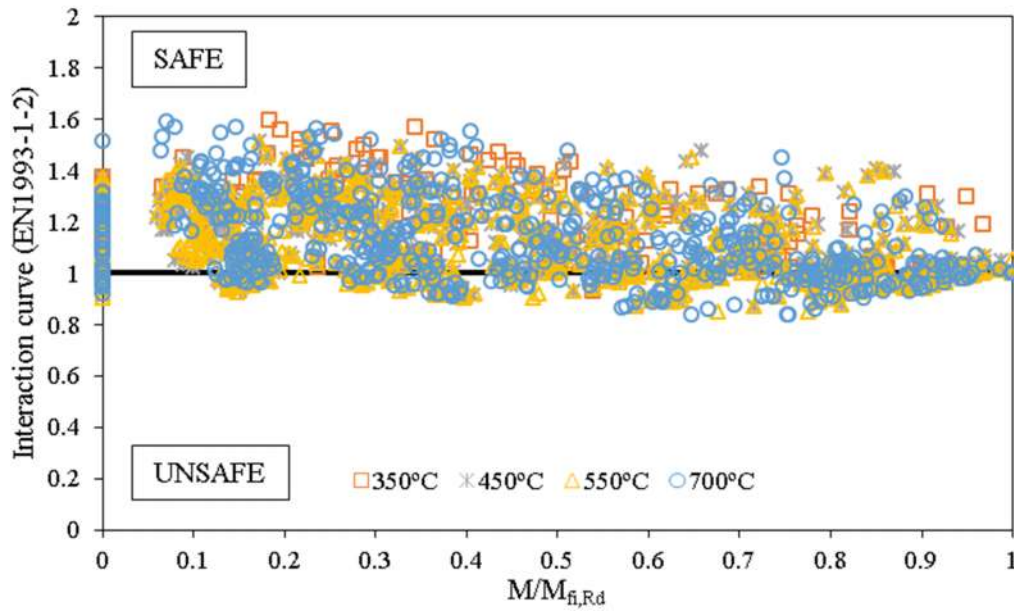


Figure 119: Comparison of the numerical analysis with the EN 1993-1-2 interaction curve for various temperatures as a function of the applied bending moment

The following table summarises the statistical data of the conducted simulations and comparisons:

Average ratio	0.90
Standard Deviation	14.73%
Most unsafe result point	1.20
Number of unsafe results	18.15%

Table 71: Statistical results (3074 simulations)

The out-of-plane behaviour of beam-columns was also investigated. Equation (23) was used considering ultimate axial load and bending moment (considered uniform along the member) given by the numerical simulations as the design loads. Results are plotted in Figure 120 against the non-dimensional slenderness $\lambda_{z,\theta}$ and in Figure 121 against the ratio between the applied bending moment and the cross-sectional bending resistance $M/M_{y,fi,Rd}$. In these figures, the horizontal line at the value 1 in the vertical axis defines the interaction curve. If the points that represent the numerical results are below the line it means the ultimate loads obtained numerically are below those predicted by equation (23) and therefore are unsafe or safe otherwise.

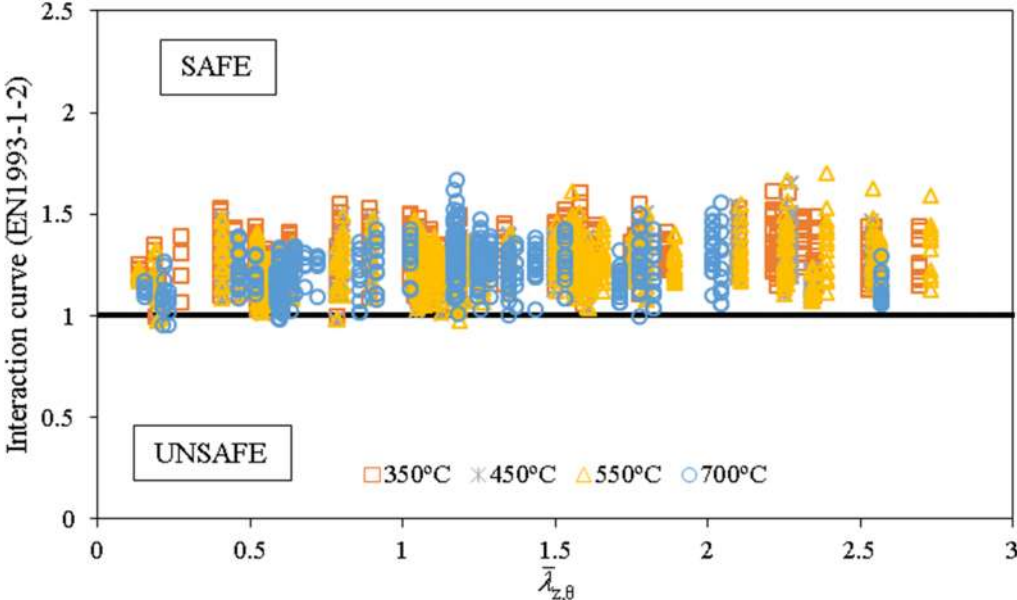


Figure 120: Comparison of interaction curve and the numerical cases studied for the out-of-plane behaviour in terms of non-dimensional slenderness

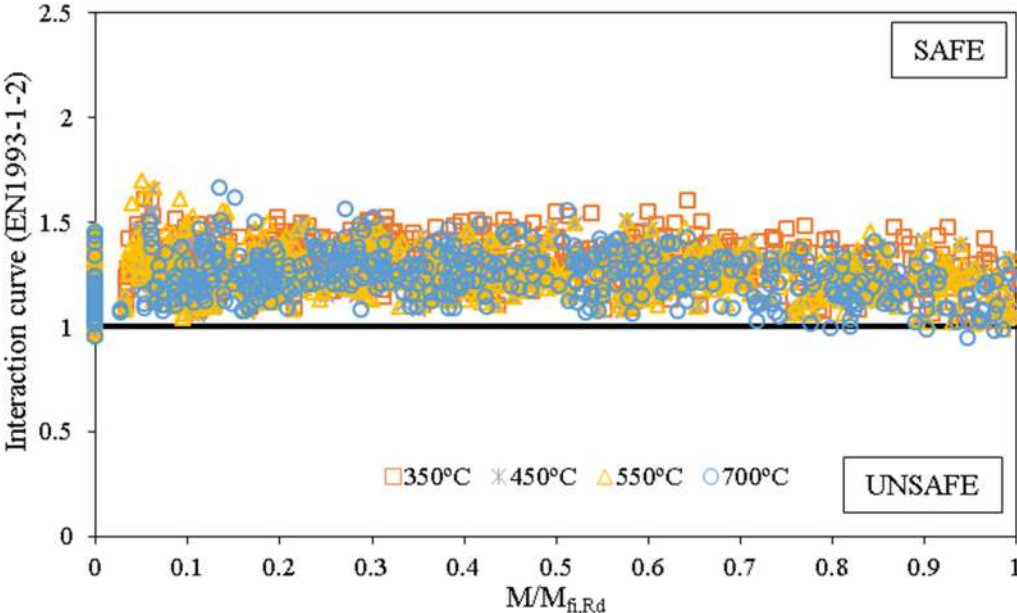


Figure 121: Comparison of interaction curve and the numerical cases studied for the out-of-plane behaviour in terms of the applied bending moment

The following table summarises the statistical data for out-of-plane cases of the conducted simulations and comparisons:

Average ratio	0.80
Standard Deviation	11.12%
Most unsafe result point	1.05
Number of unsafe results	0.74%

Table 72: Statistical results (2831 simulations)

It was admitted that the out-of-plane behaviour defined in the EN 1993-1-2 was safe enough when compared to the numerical simulations. This was not the case for the in-plane behaviour so that a calibration of the in-plane interaction factor was proposed. The details are shown hereafter.

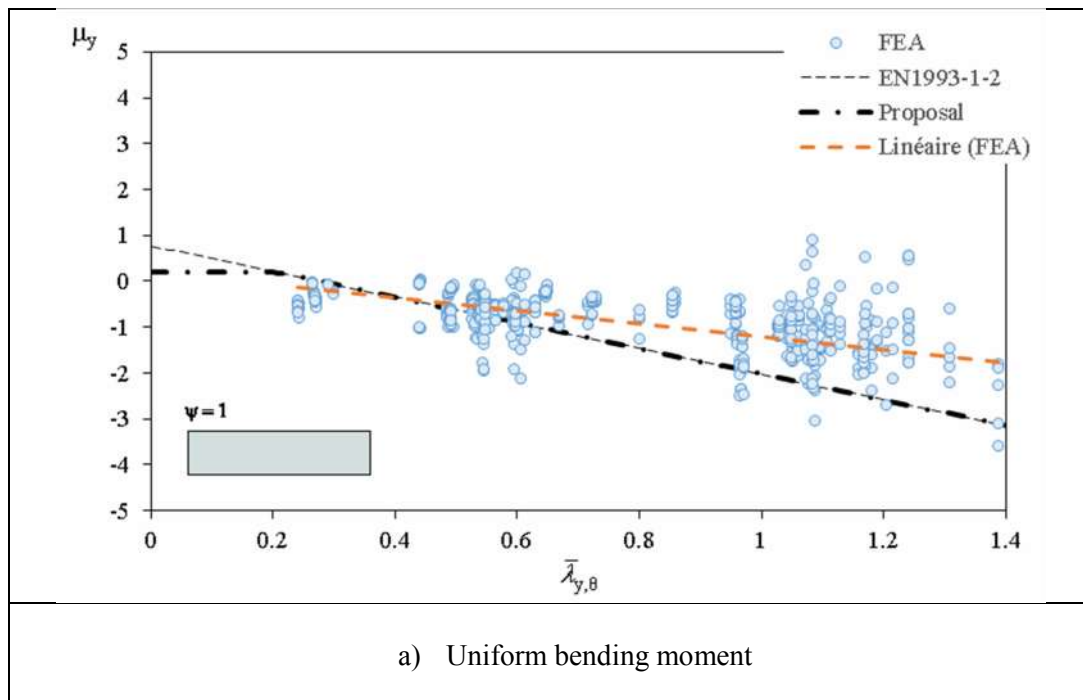
2.2.3 Calibration of in-plane interaction factor and update of reduction factors

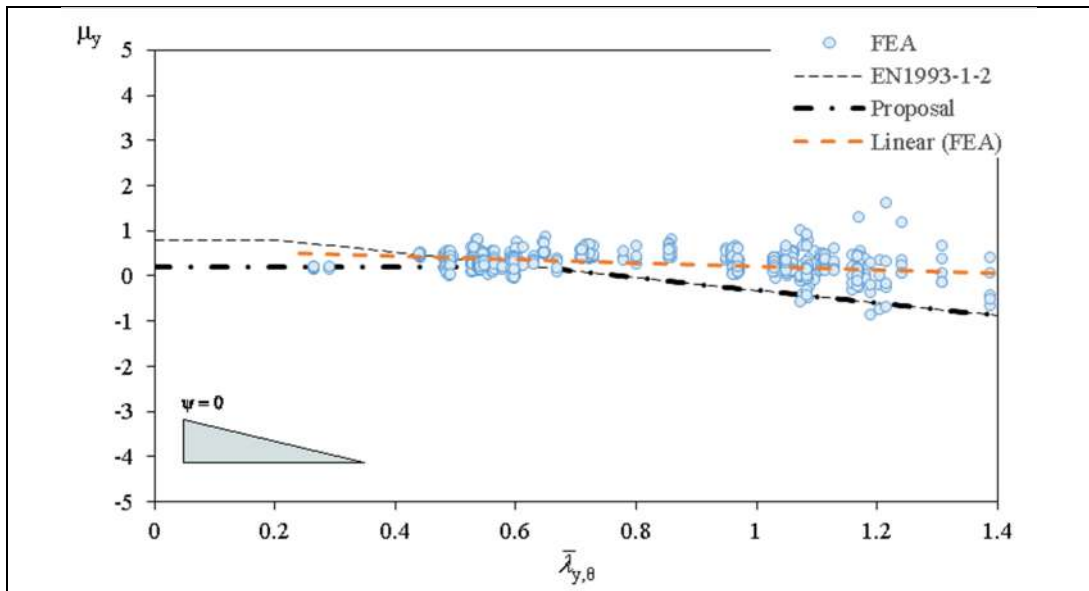
In order to reduce the number of unsafe results, see Table 71, the μ_y factor was calibrated following the same methodology adopted by Talamona in [3]. According to this procedure the following expression was used to extract from each numerical simulation the value of μ_y factor, which fulfils equation (22):

$$\mu_y = \frac{M_{y,fi,Rd,FEA,CS} \cdot N_{SAFIR} - \chi_{y,fi} \cdot N_{fi,Rd,FEA,CS} \cdot M_{y,fi,Rd,FEA,CS} + \chi_{y,fi} \cdot N_{fi,Rd,FEA,CS} \cdot M_{FEA}}{N_{FEA} \cdot M_{FEA}} \quad (28)$$

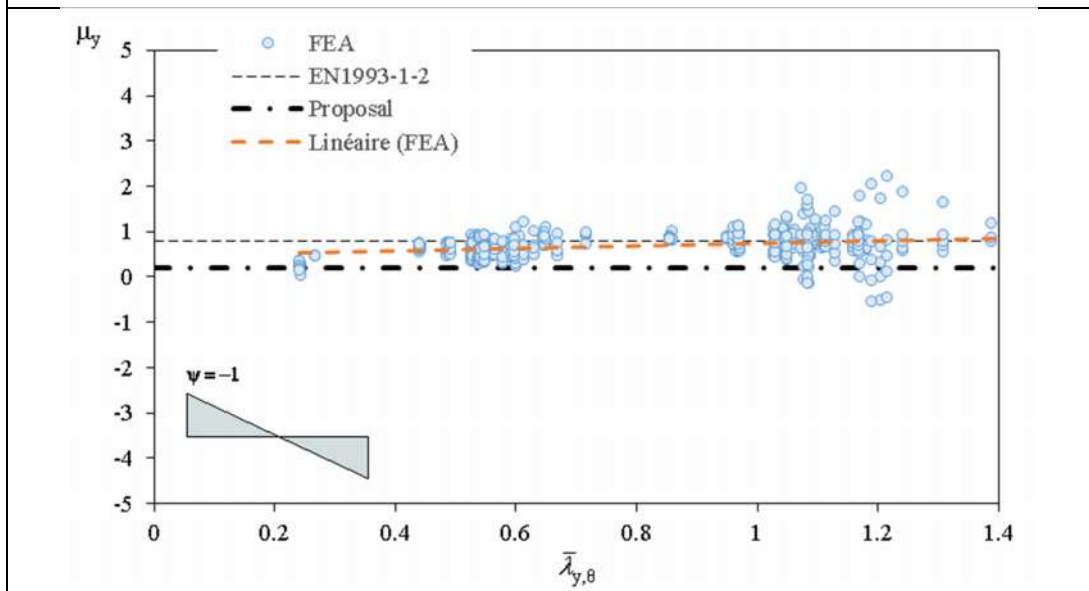
Where $N_{fi,Rd,FEA,CS}$ and $M_{y,fi,Rd,FEA,CS}$ are respectively the numerical axial and moment resistance obtained with finite elements analysis, using both ANSYS and SAFIR softwares, and N_{FEA} and M_{FEA} are the ultimate axial load and moment given by finite element analysis. The following charts show the evolution of μ_y factor as a function of the non-dimensional slenderness $\lambda_{y,\theta}$ with the proposed modification given by following equation (29), denoted as “proposal”. The “Linear (FEA)” term denotes the linear trend line of the numerical results:

$$\mu_y = (2\beta_{M,y} - 5)\bar{\lambda}_{y,\theta} + 0.44\beta_{M,y} + 0.29 \leq 0.2 \quad (29)$$





b) Triangular bending moment



c) Bi-triangular bending moment

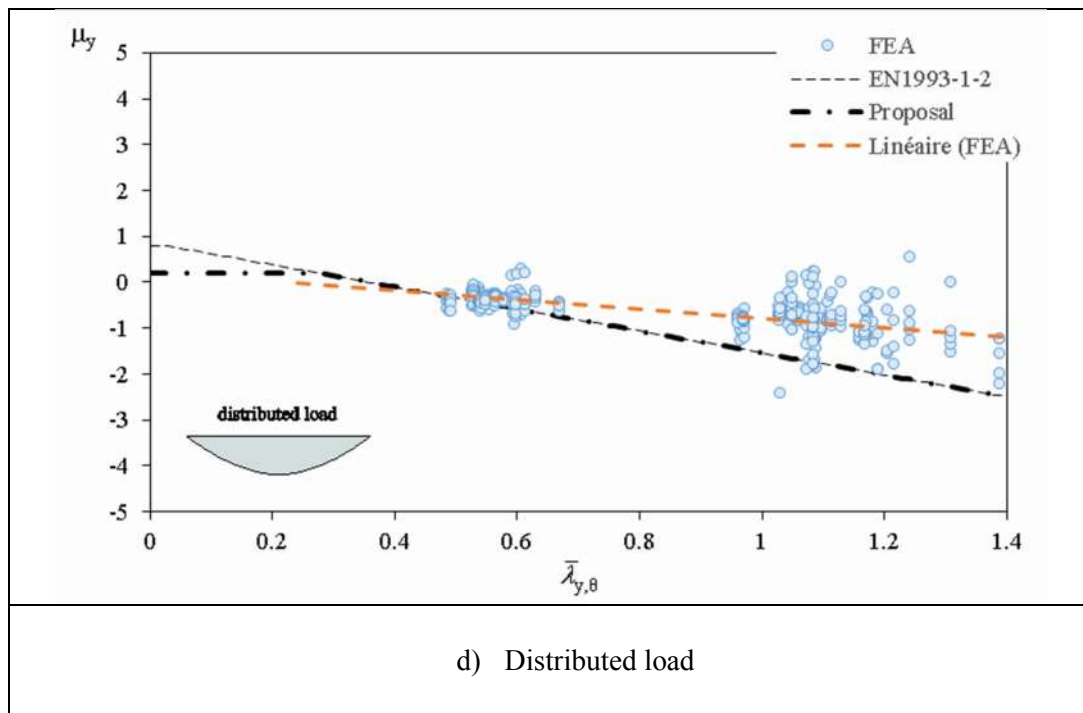


Figure 122: Calibration of factor μ_y for the in-plane behaviour of beam-columns considering different loading cases

By using equation (29) instead of equation (25), a limit value of 0.2 was introduced that changed the response obtained especially for the beam-columns subjected to bi-triangular bending moment ($\psi = -1$), see Figure 122 c). In this equation, the limit for the non-dimensional slenderness at normal temperature was also disregarded without losing accuracy and maintaining the same level of safety for the remaining cases as used in equation (25).

In the following figure, the results are plotted for a beam-column submitted to different moment distributions at a temperature of 550°C; the interaction curve with μ_y given in equation (29) is referred as “Proposed”:

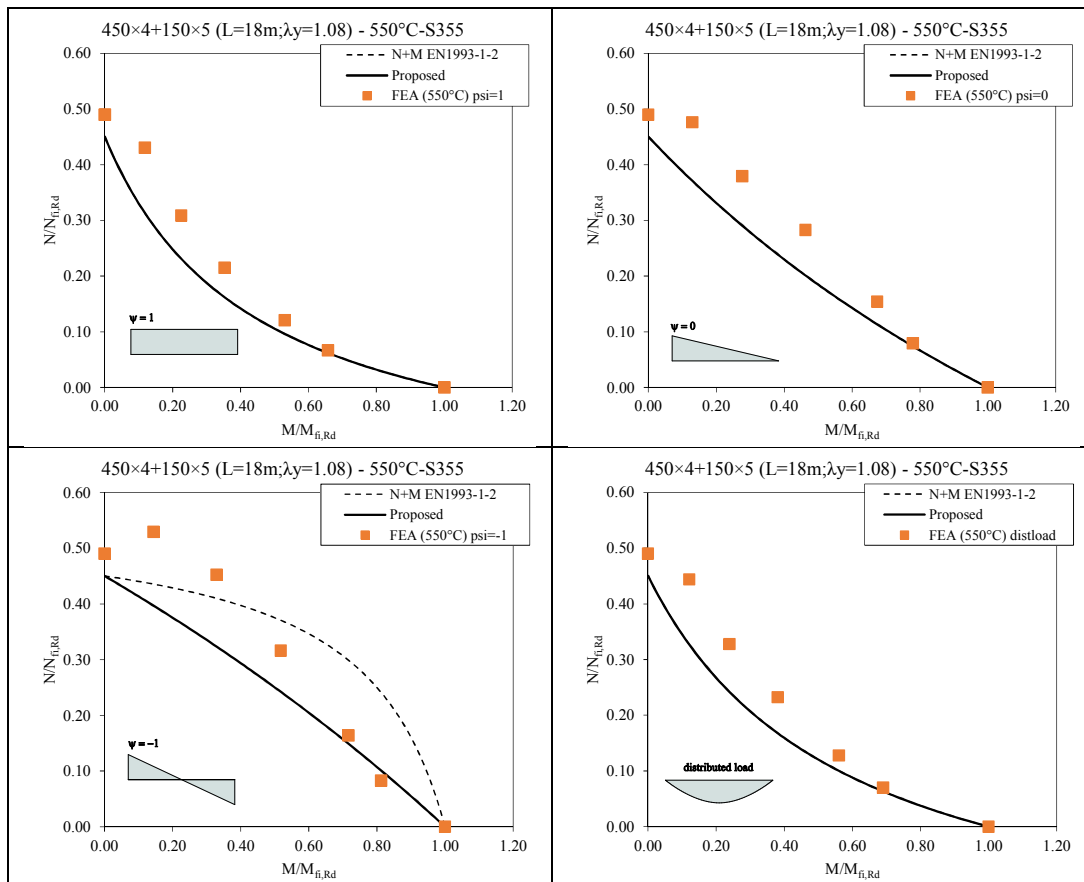


Figure 123: Interaction curves for a beam-column (length $L = 18$ m, $\lambda_{y,\Theta} = 1.0$) with a welded cross-section 450x4+150x5 submitted to different bending diagrams at 550°C

The improvements made with the proposed modification for the bi-triangular bending diagram ($\psi = -1$) are illustrated in the following figure:

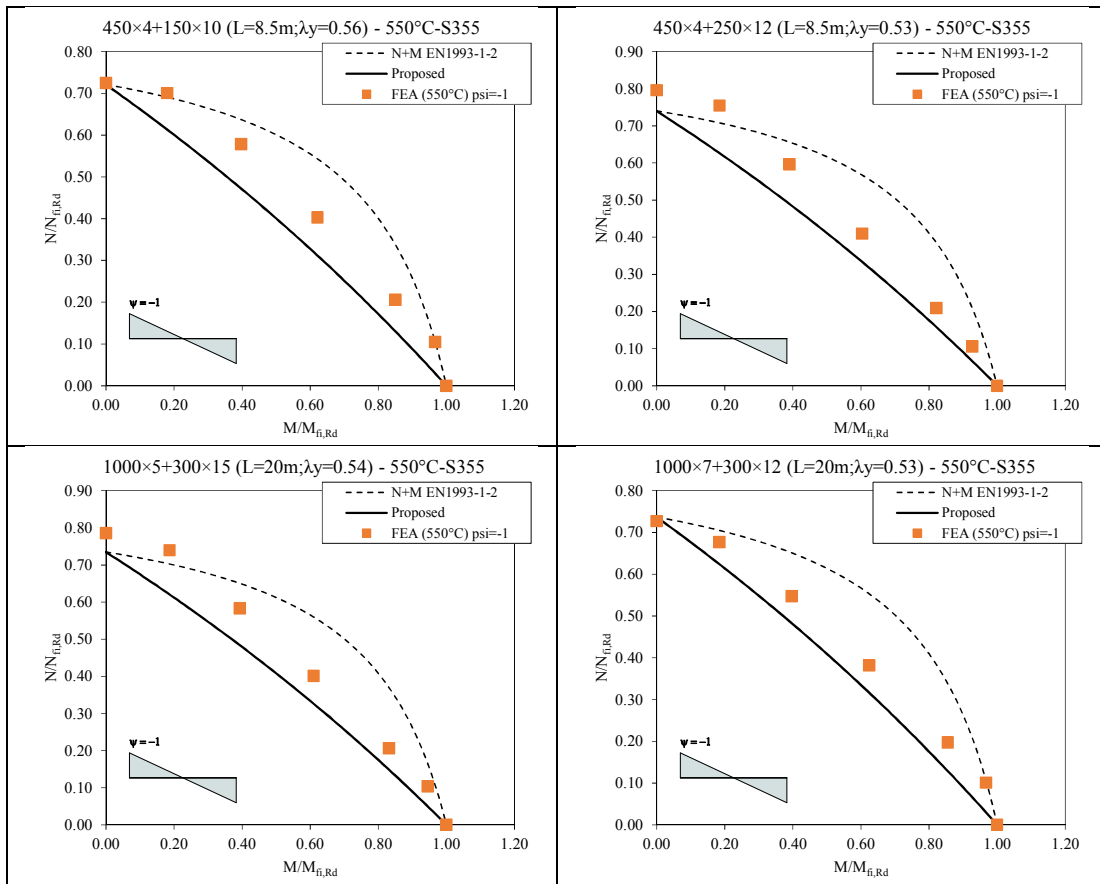


Figure 124: Improvement of the in-plane interaction curve for bi-triangular bending moment cases

In the following both figures, all the in-plane numerical results are plotted and confronted to equation (22) using μ_y from equation (29) as a function of the bending moment and the column slenderness respectively:

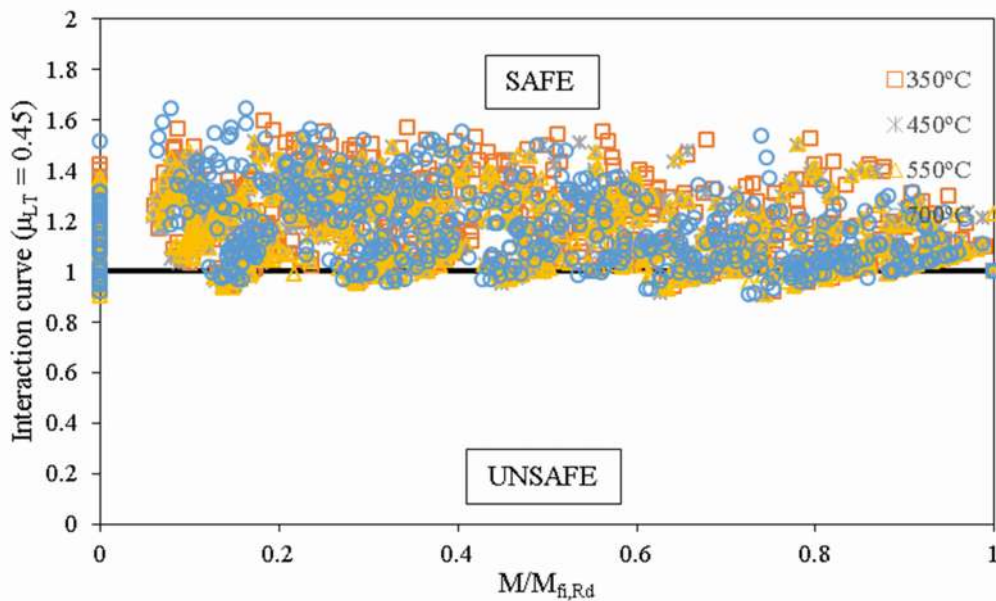


Figure 125: Comparison of interaction curves and numerical cases studied considering μ_y from equation (29) as a function of the applied bending moment

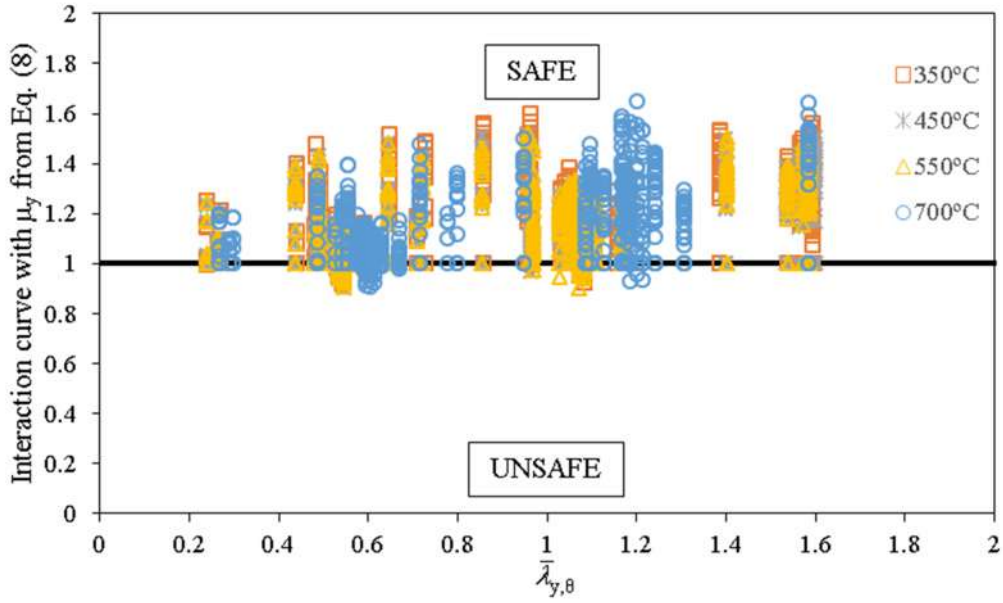


Figure 126: Comparison of interaction curves and numerical cases studied considering μ_y from equation (29) as a function of the column slenderness

The following table summarises the statistical data for in-plane cases of the conducted simulations and comparisons with calibrated equation:

Average ratio	0.87
Standard Deviation	14.79%
Most unsafe result point	1.11
Number of unsafe results	7.91%

Table 73: Statistical results (3074 simulations)

The calibrated design curves now allow a safer design of beam-column subjected to different types of loadings and at different temperatures.

To be consistent with the previous proposed design rules and with the fact that the calibration was done considering numerical values for resistance, it is proposed to update the reduction factor at high temperature for equations (22) and (23) which becomes:

$$\frac{N_{fi,Ed}}{\chi_{\min,fi} A_{eff} k_{y,\theta} \frac{f_y}{\gamma_{M,fi}}} + \frac{k_y M_{y,fi,Ed}}{W_{eff,y,\min} k_{y,\theta} \frac{f_y}{\gamma_{M,fi}}} + \frac{k_z M_{z,fi,Ed}}{W_{eff,z,\min} k_{y,\theta} \frac{f_y}{\gamma_{M,fi}}} \leq 1 \quad (30)$$

$$\frac{N_{fi,Ed}}{\chi_{z,fi} A_{eff} k_{y,\theta} \frac{f_y}{\gamma_{M,fi}}} + \frac{k_{LT} M_{y,fi,Ed}}{\chi_{LT,fi} W_{eff,y,\min} k_{y,\theta} \frac{f_y}{\gamma_{M,fi}}} + \frac{k_z M_{z,fi,Ed}}{W_{eff,z,\min} k_{y,\theta} \frac{f_y}{\gamma_{M,fi}}} \leq 1 \quad (31)$$

3 Application examples

3.1 Evaluation of the compression resistance of a class 4 axially loaded column

A column subjected to axial compression is considered heated up to 650°C. It is S460 steel grade with a Young modulus of 210000 MPa. The column is 10 m high and a lateral restraint is present at its mid-height. The aim of this example is to evaluate the buckling resistance in compression of this column with the new developed design rules described in 2.1.3. The dimensions of the cross-section are listed below:

$$h = 524 \text{ mm}$$

$$t_w = 10 \text{ mm}$$

$$b = 250 \text{ mm}$$

$$t_f = 12 \text{ mm}$$

Root fillet is assumed to be equal to zero

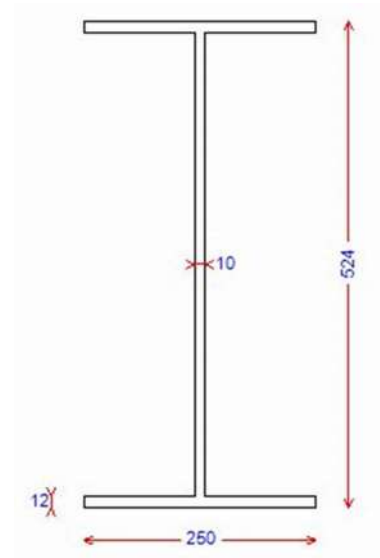


Figure 127: Dimensions of the cross-section

3.1.1 Classification of the cross-section

The following geometrical characteristics of the welded profile are relevant for the classification of the cross-section:

$$c_f = b/2 - t_w/2 = 120 \text{ mm (flange)}$$

$$c_w = h - 2t_f = 500 \text{ mm (web)}$$

As steel grade is S460:

$$\varepsilon_\theta = 0.85\varepsilon = 0.85 \sqrt{235/f_y} = 0.608 \text{ (the class of the section is evaluated in case of fire)}$$

The class of the web, which is the internal compression part of the column in axial compression, is evaluated. The details are shown in the following figure:

$$c_w/t_w = 500/10 = 50 > 42\varepsilon_\theta = 25.54 \rightarrow \text{Class 4 web}$$

Internal compression parts						
				Axis of bending		
				Axis of bending		
Class	Part subject to bending	Part subject to compression	Part subject to bending and compression			
1	$c/t \leq 72\epsilon$	$c/t \leq 33\epsilon$	when $\alpha > 0,5$: $c/t \leq \frac{396\epsilon}{13\alpha - 1}$ when $\alpha \leq 0,5$: $c/t \leq \frac{36\epsilon}{\alpha}$			
2	$c/t \leq 83\epsilon$	$c/t \leq 38\epsilon$	when $\alpha > 0,5$: $c/t \leq \frac{456\epsilon}{13\alpha - 1}$ when $\alpha \leq 0,5$: $c/t \leq \frac{41,5\epsilon}{\alpha}$			
3	$c/t \leq 124\epsilon$	$c/t \leq 42\epsilon$	when $\psi > -1$: $c/t \leq \frac{42\epsilon}{0,67 + 0,33\psi}$ when $\psi \leq -1$: $c/t \leq 62\epsilon(1 - \psi)\sqrt{(-\psi)}$			
$\epsilon = \sqrt{235/f_y}$	f_y	235	275	355	420	460
	ϵ	1,00	0,92	0,81	0,75	0,71

Figure 128: Classification ranges of internal compression part

The class of the compressive flange, which is the out-stand compression part of the column in compression, is evaluated. The details are shown in the following figure:

$$c_f/t_f = 120/12 = 10 > 14\epsilon_\theta = 8.51 \rightarrow \text{Class 4 flanges}$$

The cross-section of the welded profile is class 4 in pure compression.

3.1.2 Evaluation of the effective area in compression

The effective area of the cross-section in pure compression is obtained with the following equation. Thus, the normalised slenderness is given by:

$$\bar{\lambda}_p = \sqrt{\frac{f_y}{\sigma_{cr}}} = \frac{\bar{b}/t}{28.4 \times \epsilon \times \sqrt{k_\sigma}}$$

For the flange under consideration:

$$\bar{b} = c_f = 120 \text{ mm}$$

$$t = t_f = 12 \text{ mm}$$

$$\varepsilon = \sqrt{235/f_y} = 0.715$$

This factor is evaluated at room temperature when it comes to the calculation of the non-dimensional slenderness of the plates.

$$k_\sigma = 0.43$$

Stress distribution (compression positive)		Effective ^p width b_{eff}			
		$1 > \psi \geq 0:$ $b_{eff} = \rho c$			
		$\psi < 0:$ $b_{eff} = \rho b_c = \rho c / (1-\psi)$			
$\psi = \sigma_2/\sigma_1$	1	0	-1	$1 \geq \psi \geq -3$	
Buckling factor k_σ	0,43	0,57	0,85	$0,57 - 0,21\psi + 0,07\psi^2$	
		$1 > \psi \geq 0:$ $b_{eff} = \rho c$			
		$\psi < 0:$ $b_{eff} = \rho b_c = \rho c / (1-\psi)$			
$\psi = \sigma_2/\sigma_1$	1	$1 > \psi > 0$	0	$0 > \psi > -1$	-1
Buckling factor k_σ	0,43	$0,578 / (\psi + 0,34)$	1,70	$1,7 - 5\psi + 17,1\psi^2$	23,8

Figure 129: Buckling factor for outstand compression elements

Then:

$$\bar{\lambda}_p = \frac{120/12}{28.4 \times 0.715 \times \sqrt{0.43}} = 0.751$$

According to new design rules:

$$\rho = \frac{\left(\bar{\lambda}_p + 1.1 - \frac{0.52}{\varepsilon}\right)^{1.2} - 0.188}{\left(\bar{\lambda}_p + 1.1 - \frac{0.52}{\varepsilon}\right)^{2.4}} = 0.727$$

So that the effective width of the flange, b_{eff} , is:

$$b_{eff} = \rho c_f = 0.727 \times 120 = 87.27 \text{ mm}$$

Finally, the total effective width of flange to take account for is the following:

$$b_t = 2b_{eff} + t_w = 2 \times 87.27 + 10 = 184.55 \text{ mm}$$

The effective part of web in compression is evaluated with the following steps:

Stress distribution (compression positive)				Effective ^p width b_{eff}		
				$\psi = 1:$ $b_{eff} = \rho \bar{b}$ $b_{e1} = 0,5 b_{eff} \quad b_{e2} = 0,5 b_{eff}$		
				$1 > \psi \geq 0:$ $b_{eff} = \rho \bar{b}$ $b_{e1} = \frac{2}{5 - \psi} b_{eff} \quad b_{e2} = b_{eff} - b_{e1}$		
				$\psi < 0:$ $b_{eff} = \rho b_c = \rho \bar{b} / (1 - \psi)$ $b_{e1} = 0,4 b_{eff} \quad b_{e2} = 0,6 b_{eff}$		
$\psi = \sigma_2 / \sigma_1$	1	$1 > \psi > 0$	0	$0 > \psi > -1$	-1	$-1 > \psi > -3$
Buckling factor k_σ	4,0	$8,2 / (1,05 + \psi)$	7,81	$7,81 - 6,29\psi + 9,78\psi^2$	23,9	$5,98 (1 - \psi)^2$

Figure 130: Buckling factor for internal compression elements

In this case:

$$k_\sigma = 4$$

The web non-dimensional slenderness is:

$$\bar{\lambda}_p = \frac{500/10}{28,4 \times 0,715 \times \sqrt{4}} = 1,232$$

And

$$\rho = \frac{\left(\bar{\lambda}_p + 0,9 - \frac{0,26}{\varepsilon}\right)^{1,5} - 0,055 \times (3 + 1)}{\left(\bar{\lambda}_p + 0,9 - \frac{0,26}{\varepsilon}\right)^3} = 0,386$$

And the effective width of the web, b_{eff} , is:

$$b_{eff,w} = \rho \times c_w = 0,386 \times 500 = 192,81$$

Considering the effective area of the flange under compression, it is necessary to evaluate the new effective area of the cross-section:

$$A_{eff} = A - [(c_w - b_{eff,w}) \times t_w + (b - b_t) \times 2 \times t_f]$$

$$A_{eff} = 11000 - (500 - 192,81) \times 10 - (250 - 184,55) \times 2 \times 12$$

$$A_{eff} = 6357,21 \text{ mm}^2$$

3.1.3 Calculation of the compression resistance

The first step is to evaluate both slenderness along strong and weak axis in according to the respective I_{strong} , I_{weak} and the different buckling lengths.

Along the strong axis the inertia is defined as follows:

$$I_{strong} = \frac{1}{12} \times [b \times h^3 - (b - t_w) \times (h - 2 \times t_f)^3] = 497454666.67 \text{ mm}^4$$

The Euler critical compression load along strong axis is given with the following equation:

$$N_{cr,strong} = \frac{\pi^2 \times E \times I_{strong}}{L_{strong}} = 10310329.61 \text{ N}$$

With L_{strong} is equal to 10 m.

The non-dimensional slenderness along strong axis is given hereafter:

$$\lambda_{strong} = \sqrt{A_{eff} \times f_y / N_{cr,strong}} = 0.533$$

Along the weak axis the inertia is defined as follows:

$$I_{weak} = \frac{1}{12} \times [2 \times t_f \times b^3 + (h - 2 \times t_f) \times t_w^3] = 31291666.67 \text{ mm}^4$$

The Euler critical compression load along weak axis is given with the following equation:

$$N_{cr,weak} = \frac{\pi^2 \times E \times I_{weak}}{L_{weak}} = 2594225.52 \text{ N}$$

With L_{weak} equal to 5 m as a lateral restraint is present at mid-height of the column.

The non-dimensional slenderness along weak axis is given hereafter:

$$\lambda_{weak} = \sqrt{A_{eff} \times f_y / N_{cr,weak}} = 1.062$$

The maximum non-dimensional slenderness is for the weak axis so the slenderness at high temperature is evaluated as follow for $T = 650^\circ\text{C}$ (reduction factor for high temperature design are available in Table 3.1 of EN 1993-1-2:

$$\lambda_\theta = \lambda_{weak} \times \sqrt{k_{y,\theta} / k_{E,\theta}} = 1.062 \times \sqrt{0.35 / 0.22} = 1.339$$

Then

$$\varphi_\theta = 0.5 \times (1 + \alpha \times \lambda_\theta + \lambda_\theta^2) = 0.5 \times \left(1 + 0.65 \times \sqrt{\frac{235}{460}} \times 1.339 + 1.339^2 \right) = 1.708$$

Finally

$$\chi_{fi} = \frac{1}{\varphi_\theta + \sqrt{\varphi_\theta^2 - \lambda_\theta^2}} = \frac{1}{1.708 + \sqrt{1.708^2 - 1.339^2}} = 0.361$$

The compressive resistance of the column at 650°C is defined with the following equation:

$$N_{b,fi,Rd} = \chi_{fi} \times A_{eff} \times k_{y,\theta} \times f_y = 0.361 \times 6357.21 \times 0.35 \times 460 = 369918.53 \text{ N}$$

As a conclusion:

$$N_{b,fi,Rd} = 369.92 \text{ kN}$$

3.2 Resistance of a beam-column subjected to combined axial compression and bending

This example describes the analytical solution of the beam-column checked with FIDESC4 software (deliverable n°6: software). All analytical steps are described in the following parts.

Consider a 2.7 m high built up beam-column in steel grade S355, as shown in Figure 131.

$h = 460 \text{ mm}$ (total depth of the section)

$b = 150 \text{ mm}$

$t_w = 4 \text{ mm}$

$t_f = 5 \text{ mm}$

$a = 5 \text{ mm}$ (effective throat thickness of the fillet weld)

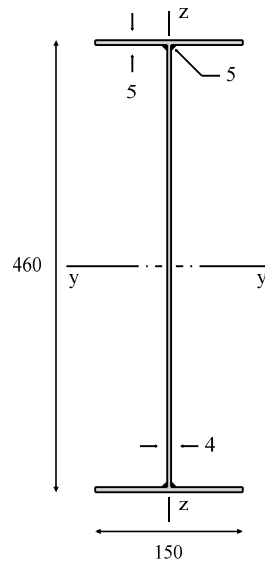


Figure 131: Dimensions of the built-up cross-section

Assuming that the beam-column is subjected to a uniform bending moment diagram which design value in fire situation is $M_{y,fi,Ed} = 20 \text{ kNm}$ about major axis and to an axial compression force in fire situation of $N_{fi,Ed} = 20 \text{ kN}$. The lateral torsional buckling of the beam-column is prevented. Evaluate:

- the critical temperature of the beam-column considering both the cross-sectional resistance (Eq. (6.44) from EN 1993-1-1 adapted to fire) and the beam-column resistance using Eq. (4.21c) from EN 1993-1-2;
- the fire resistance of the beam-column at a temperature of $500 \text{ }^\circ\text{C}$.

3.2.1 Formulae used

To solve the worked example the following formulae will be used:

- For the fire resistance of the cross-section, Eq. (6.44) from EN 1993-1-1 adapted to fire with the new procedure to evaluate the effective properties:

$$\frac{N_{fi,Ed}}{A_{eff} k_{y,\theta} \frac{f_y}{\gamma_{M,fi}}} + \frac{M_{y,fi,Ed}}{W_{eff,y,min} k_{y,\theta} \frac{f_y}{\gamma_{M,fi}}} \leq 1 \quad (32)$$

- For the fire resistance of the beam-column, Eq. (4.21c) from EN 1993-1-2, adapted to profiles with class 4 cross-sections, with the new proposal for effective properties:

$$\frac{N_{fi,Ed}}{\chi_{\min,fi} A_{eff} k_{y,\theta} \frac{f_y}{\gamma_{M,fi}}} + \frac{k_y M_{y,fi,Ed}}{W_{eff,y} k_{y,\theta} \frac{f_y}{\gamma_{M,fi}}} \leq 1 \quad (33)$$

3.2.2 Classification of the cross-section

3.2.2.1 General

The following geometrical characteristics of the welded profile are relevant for the classification of the cross section (see Figure 132).

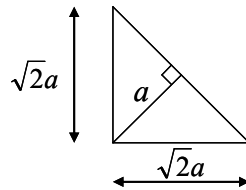


Figure 132: Weld dimensions

$$c_f = b/2 - t_w/2 - \sqrt{2} \cdot 5 = 65.93 \text{ mm (flange)}$$

$$c_w = h - 2t_f - 2\sqrt{2} \cdot 5 = 435.86 \text{ mm (web)}$$

As the steel grade is S355:

$$\varepsilon = \sqrt{235/f_y} = 0.814$$

$$\varepsilon_\theta = 0.85 \times \varepsilon = 0.85 \sqrt{235/f_y} = 0.692$$

3.2.2.2 Combined bending about y-y (major axis) and compression

The class of the flange in compression (Figure 133) is:

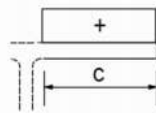


Figure 133: Flange in compression.

The following ratio lets have the class of the flange in compression:

$$c_f/t_f = 65.93/5 = 13.16 \text{ mm} > 14\varepsilon \Rightarrow \text{Class 4}$$

The class of the web in combined bending about y-y (major axis) and compression (Figure 134) is:

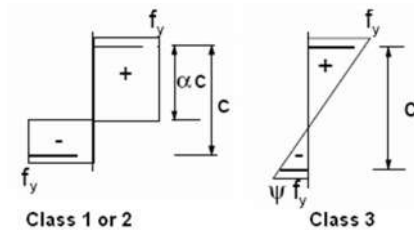


Figure 134: Web in combined bending about y-y and compression.

Class 1 or 2:

$$\alpha = \frac{1}{2} + \frac{N_{Ed}}{2ct_w f_y} = \frac{1}{2} + \frac{20 \times 10^3}{2 \times 435.86 \times 4 \times 355} = 0.516$$

As $\alpha > 0.5$ and

$$c_w/t_w = 435.86/4 = 108.96 > \frac{496\varepsilon}{13\alpha - 1} = 60.13$$

The web is not Class 1 or 2.

Class 3:

$$\psi = \frac{2N_{Ed}}{Af_y} - 1 = \frac{2 \times 20 \times 10^3}{3300 \times 355} - 1 = -0.966$$

$$c_w/t_w = 435.86/4 = 108.96 > 42\varepsilon / (0.67 + 0.33\psi) = 82.8 \Rightarrow \text{Class 4}$$

The cross section of the welded profile is Class 4 in combined bending about y-y (major axis) and compression.

3.2.3 Evaluation of the effective area and effective section modulus

3.2.3.1 Effective area in compression

The effective area of the cross section in pure compression is obtained using EN 1993-1-5 and the new approach developed in the framework of the project FIDESC4.

The normalized slenderness is given by:

$$\bar{\lambda}_p = \sqrt{\frac{f_y}{\sigma_{cr}}} = \frac{\bar{b}/t}{28.4\varepsilon\sqrt{k_\sigma}}$$

For the flanges under compression:

$$\bar{b} = c_f = 65.93 \text{ mm}$$

$$t = t_f = 5 \text{ mm}$$

$$\varepsilon = \sqrt{235/f_y} = 0.814 \text{ (Note: this factor is evaluated at normal temperature)}$$

$$k_{\sigma} = 0.43$$

Giving

$$\bar{\lambda}_p = \frac{65.93/5}{28.4 \times 0.814 \sqrt{0.43}} = 0.87 > 0.748$$

And

$$\rho = \frac{\left(\bar{\lambda}_p + 1.1 - \frac{0.52}{\varepsilon}\right)^{1.2} - 0.188}{\left(\bar{\lambda}_p + 1.1 - \frac{0.52}{\varepsilon}\right)^{2.4}} = \frac{\left(0.87 + 1.1 - \frac{0.52}{0.814}\right)^{1.2} - 0.188}{\left(0.87 + 1.1 - \frac{0.52}{0.814}\right)^{2.4}} = 0.615$$

And the effective width of the flange, b_{eff} , is:

$$b_{eff} = \rho \bar{b} = 0.615 \times 65.93 = 40.54 \text{ mm}$$

$$b = 2b_{eff} + t_w + 2\sqrt{2} \times 5 = 2 \times 40.54 + 4 + 2\sqrt{2} \times 5 = 99.22 \text{ mm}$$

For the web under bending and compression:

$$\bar{b} = c_w = 435.86 \text{ mm}$$

$$t = t_w = 4 \text{ mm}$$

$$\varepsilon = \sqrt{235/f_y} = 0.814 \text{ (note this factor is evaluated at normal temperature)}$$

$$k_{\sigma} = 4$$

Giving

$$\bar{\lambda}_p = \frac{435.86/4}{28.4 \times 0.814 \sqrt{4}} = 2.358 > 0.673$$

And

$$\rho = \frac{\left(\bar{\lambda}_p + 0.9 - \frac{0.26}{\varepsilon}\right)^{1.5} - 0.055(3 + \psi)}{\left(\bar{\lambda}_p + 0.9 - \frac{0.26}{\varepsilon}\right)^3} \leq 1.0$$

Where $\psi = 1$, giving

$$\rho = \frac{\left(2.358 + 0.9 - \frac{0.26}{0.814}\right)^{1.5} - 0.055(3+1)}{\left(2.358 + 0.9 - \frac{0.26}{0.814}\right)^3} = 0.190$$

And the effective width of the web, b_{eff} , is:

$$b_{eff} = \rho \bar{b} = 0.190 \times 435.86 = 82.76 \text{ mm}$$

$$b_{e1} = 0.5b_{eff} = 0.5 \times 82.76 = 41.38 \text{ mm}$$

$$b_{e2} = 0.5b_{eff} = 0.5 \times 82.76 = 41.38 \text{ mm}$$

The effective area of the cross section is shown in Figure 135.

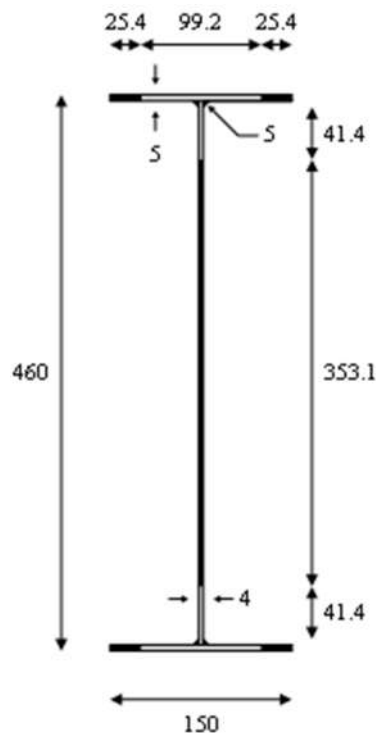


Figure 135: Effective area of the cross-section under compression.

$$A_{eff} = A - (353.1 \times 4 + 4 \times 25.4 \times 5) = 1379.75 \text{ mm}^2$$

3.2.3.2 Effective area and section modulus in bending about y-y (major axis)

The effective section modulus of the cross section in bending about y-y (major axis) is obtained using clause 4.4(3) of EN 1993-1-5: “For flange elements of I-sections and box girders the stress ratio ψ used in Table 4.1 and Table 4.2 should be based on the properties of the gross cross-sectional area, due allowance being made for shear lag in the flanges if relevant. For web elements the stress ratio ψ used in Table 4.1 should be obtained using a stress distribution based on the effective area of the compression flange and the gross area of the web”.

The normalized slenderness for the flange under compression:

$$\bar{b} = c_f = 65.93 \text{ mm}$$

$$t = t_f = 5 \text{ mm}$$

$$\varepsilon = \sqrt{235/f_y} = 0.814 \text{ (Note: this factor is evaluated at normal temperature)}$$

$$k_\sigma = 0.43$$

Giving

$$\bar{\lambda}_p = \frac{65.93/5}{28.4 \times 0.814 \sqrt{0.43}} = 0.87 > 0.748$$

And

$$\rho = \frac{\left(\bar{\lambda}_p + 1.1 - \frac{0.52}{\varepsilon}\right)^{1.2} - 0.188}{\left(\bar{\lambda}_p + 1.1 - \frac{0.52}{\varepsilon}\right)^{2.4}} = \frac{\left(0.87 + 1.1 - \frac{0.52}{0.814}\right)^{1.2} - 0.188}{\left(0.87 + 1.1 - \frac{0.52}{0.814}\right)^{2.4}} = 0.615$$

And the effective width of the flange, b_{eff} , is:

$$b_{eff} = \rho \bar{b} = 0.615 \times 65.93 = 40.54 \text{ mm}$$

$$b = 2b_{eff} + t_w + 2\sqrt{2} \times 5 = 2 \times 40.54 + 4 + 2\sqrt{2} \times 5 = 99.22 \text{ mm}$$

Evaluation of the new position of the centre of gravity, considering the effective area of the compression flange and the gross area of the web:

$$A' = A - [(150 - 99.22) \times 5] = 3046.08 \text{ mm}^2$$

$$z'_G = \frac{\left(A \times \frac{460}{2}\right) - \left[\left((150 - 99.22) \times 5\right) \times \left(460 - \frac{5}{2}\right)\right]}{A'} = 211.04 \text{ mm}$$

Evaluation of the stress ratio ψ :

$$\psi = \frac{\sigma_2}{\sigma_1} = -\frac{b_t}{b_c}$$

Where b_c and b_t are defined in Figure 136:

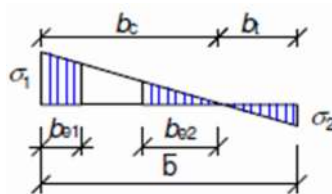


Figure 136: Evaluation of web stress ratio.

$$\psi = -\frac{b_t}{b_c} = -\frac{211.04 - 5 - \sqrt{2} \times 5}{460 - \sqrt{2} \times 5 - 211.04 - 5} = -\frac{198.96}{236.89} = -0.8399$$

$$k_\sigma = 7.81 - 6.29\psi + 9.78\psi^2 = 19.99$$

Giving

$$\bar{\lambda}_p = \frac{435.86/4}{28.4 \times 0.814 \sqrt{19.99}} = 1.055 > 0.5 + \sqrt{0.085 - 0.055\psi} = 0.862$$

And

$$\rho = \frac{\left(1.055 + 0.9 - \frac{0.26}{0.814}\right)^{1.5} - 0.055(3 + (-0.8399))}{\left(1.055 + 0.9 - \frac{0.26}{0.814}\right)^3} = 0.451$$

And the effective width of the web, b_{eff} , is:

$$b_{eff} = \rho b_c = \rho c_w / (1 - \psi) = 0.451 \times 435.86 / (1 - (-0.8399)) = 106.86 \text{ mm}$$

$$b_{e1} = 0.4b_{eff} = 0.4 \times 106.86 = 42.74 \text{ mm}$$

$$b_{e2} = 0.6b_{eff} = 0.6 \times 106.86 = 64.12 \text{ mm}$$

The length of the non-effective area of the web is:

$$b = b_c - b_{e1} - b_{e2} = 236.89 - 42.74 - 64.12 = 130.03 \text{ mm}$$

The new position of the centre of gravity should be evaluated:

$$A'' = A - (150 - 92.22) \times 5 - 130.03 \times 4 = 2525.95 \text{ mm}^2$$

$$z''_G = \frac{\left(A \times \frac{460}{2}\right) - \left[(150 - 92.22) \times 5 \times \left(460 - \frac{5}{2}\right)\right]}{A''} - \frac{\left[130.03 \times 4 \times \left(460 - 5 - \sqrt{2} \times 5 - 42.74 - \frac{130.03}{2}\right)\right]}{A''}$$

$$= 184.45 \text{ mm}$$

The effective area of the cross section under bending about the major axis is:

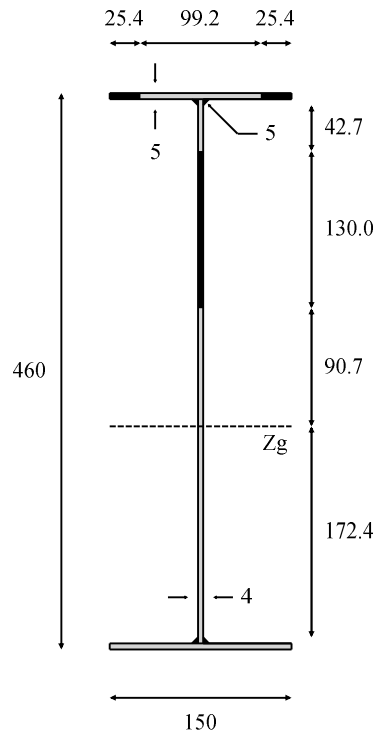


Figure 137: Effective area of the cross-section under bending about the major axis.

The second moment of area of the effective cross section takes the value:

$$I_{y,eff} = 82582234 \text{ mm}^4$$

And the effective section modulus is

$$W_{y,eff,min} = \min \left[\frac{I_{y,eff}}{z''_G}, \frac{I_{y,eff}}{h - z''_G} \right] = 299694 \text{ mm}^3$$

It must be emphasized that it was necessary to calculate three times the position of the centre of gravity before evaluating the effective section modulus. This example showed that the evaluation of the effective properties of a Class 4 cross section is a laborious task and that the software developed in the scope of the project will be of great interest for the daily design work of engineers with such type of steel members.

3.2.4 Evaluation of the critical temperature

As the bending moment diagram along the member is uniform, the cross sectional capacity is not more critical than the overall stability of the member. Although it is not necessary, in this case, to check the resistance of the cross section, this verification will be done here as an example.

3.2.4.1 Cross-section verification

According to Eq. (32), the collapse occurs when

$$\frac{N_{fi,Ed}}{A_{eff} k_{y,\theta} \frac{f_y}{\gamma_{M,fi}}} + \frac{M_{y,fi,Ed}}{W_{eff,y,min} k_{y,\theta} \frac{f_y}{\gamma_{M,fi}}} = 1$$

From where it is possible to obtain the value of the reduction factor for the 2% proof strength of steel, $k_{y,\theta}$ at collapse.

$$k_{y,\theta} = \frac{N_{fi,Ed}}{A_{eff} \frac{f_y}{\gamma_{M,fi}}} + \frac{M_{y,fi,Ed}}{W_{eff,y,min} \frac{f_y}{\gamma_{M,fi}}}$$

Substituting values in this equation, comes

$$k_{y,\theta} = \frac{N_{fi,Ed}}{A_{eff} \frac{f_y}{\gamma_{M,fi}}} + \frac{M_{y,fi,Ed}}{W_{eff,y,min} \frac{f_y}{\gamma_{M,fi}}} = \frac{20}{489.81} + \frac{20}{106.39} = 0.229$$

By interpolation on the Table 3.1 of EN1993-1-2 for the proof strength at 2% plastic strain, the following intermediate critical temperature is obtained:

$$\theta_{a,cr} = 700.9^\circ$$

3.2.4.2 Buckling resistance of the beam-column

The buckling length is:

$$l_{fi} = L = 2700 \text{ mm}$$

The non-dimensional slenderness at elevated temperature is given by:

$$\bar{\lambda}_\theta = \bar{\lambda} \cdot \sqrt{\frac{k_{y,\theta}}{k_{E,\theta}}}$$

And depends on the temperature and an iterative procedure is needed to calculate the critical temperature. Starting with a temperature of 20°C at which:

$$\bar{\lambda}_{20^\circ\text{C}} = \bar{\lambda} = \sqrt{\frac{A_{eff} f_y}{N_{cr}}}$$

Where the Euler critical load:

- about the major axis: $N_{cr} = \frac{\pi^2 EI_y}{l_{fi}^2} = \frac{\pi^2 \times 210 \times 108012500}{2700^2} = 30709 \text{ kN}$
- about the minor axis: $N_{cr} = \frac{\pi^2 EI_z}{l_{fi}^2} = \frac{\pi^2 \times 210 \times 2814900}{2700^2} = 800 \text{ kN}$

Giving

- about the major axis: $\bar{\lambda}_{y,20^\circ\text{C}} = \bar{\lambda}_y = \sqrt{\frac{A_{eff} f_y}{N_{cr}}} = 0.126$

- about the minor axis: $\bar{\lambda}_{z,20^\circ C} = \bar{\lambda}_z = \sqrt{\frac{A_{eff} f_y}{N_{cr}}} = 0.782$

The reduction factor for the flexural buckling χ_{fi} is evaluated using:

$$\alpha = 0.65 \cdot \sqrt{235/f_y} = 0.65 \cdot \sqrt{235/355} = 0.529$$

The reduction factors for flexural buckling χ_{fi} at normal temperature are:

- about the major axis:

$$\phi_{y,20^\circ C} = \frac{1}{2} \left[1 + \alpha \bar{\lambda}_{y,20^\circ C} + \bar{\lambda}_{y,20^\circ C}^2 \right] = \frac{1}{2} \times \left[1 + 0.529 \times 0.126 + 0.126^2 \right] = 0.541$$

and

$$\chi_{y,20^\circ C} = \frac{1}{\phi_{y,20^\circ C} + \sqrt{\phi_{y,20^\circ C}^2 - \bar{\lambda}_{y,20^\circ C}^2}} = \frac{1}{0.541 + \sqrt{0.541^2 - 0.126^2}} = 0.937$$

- about the minor axis:

$$\phi_{z,20^\circ C} = \frac{1}{2} \left[1 + \alpha \bar{\lambda}_{z,20^\circ C} + \bar{\lambda}_{z,20^\circ C}^2 \right] = \frac{1}{2} \times \left[1 + 0.529 \times 0.782 + 0.782^2 \right] = 1.013$$

And

$$\chi_{z,20^\circ C} = \frac{1}{\phi_{z,20^\circ C} + \sqrt{\phi_{z,20^\circ C}^2 - \bar{\lambda}_{z,20^\circ C}^2}} = \frac{1}{1.013 + \sqrt{1.013^2 - 0.782^2}} = 0.604$$

The collapse occurs when the reduction factor for the 2% proof strength of steel, $k_{y,\theta}$ takes the value (Eq. 33):

$$k_{y,\theta} = \frac{N_{fi,Ed}}{\chi_{min,fi} A_{eff} f_y} + \frac{k_y M_{y,fi,Ed}}{W_{eff,y} f_y}$$

Where

$$k_y = 1 - \frac{\mu_y N_{fi,Ed}}{\chi_{y,fi} A_{eff} k_{y,\theta} \frac{f_y}{\gamma_{M,fi}}} \leq 3$$

With

$$\mu_y = (2\beta_{M,y} - 5)\bar{\lambda}_{y,\theta} + 0.44\beta_{M,y} + 0.29 \leq 0.2 \quad \text{with } \bar{\lambda}_{y,20^\circ C} \leq 1.1$$

For a uniform bending diagram $\beta_{M,y}$ takes the value, with $\psi = 1$

$$\beta_{M,y} = 1.8 - 0.7\psi = 1.8 - 0.7 \times 1.0 = 1.1$$

And so

$$\mu_y = (2 \times 1.1 - 5) \times 0.126 + 0.44 \times 1.1 + 0.29 = 0.420 > 0.2 \text{ so } \mu_y = 0.2$$

And

$$k_y = 1 - \frac{\mu_y N_{fi,Ed}}{\chi_{y,fi} A_{eff} k_{y,\theta} \frac{f_y}{\gamma_{M,fi}}} = 0.991$$

From which the degree of utilization is:

$$k_{y,\theta} = \frac{N_{fi,Ed}}{\chi_{min,fi} A_{eff} f_y} + \frac{k_y M_{y,fi,Ed}}{W_{eff,y} f_y} = 0.254$$

By interpolation on the Table 3.1 of EN1993-1-2 for the proof strength at 2% plastic strain, the following intermediate critical temperature is obtained

$$\theta_{cr} = 690.01^\circ C$$

The non-dimensional slenderness at elevated temperature is a function of the temperature and the iterative procedure shown in Table 74 is needed:

θ [°C]	$\sqrt{\frac{k_{y,\theta}}{k_{E,\theta}}}$	$\bar{\lambda}_{y,\theta} = \bar{\lambda}_y \cdot \sqrt{\frac{k_{y,\theta}}{k_{E,\theta}}}$	$\bar{\lambda}_{z,\theta} = \bar{\lambda}_z \cdot \sqrt{\frac{k_{y,\theta}}{k_{E,\theta}}}$	$\chi_{min,fi}$	k_y	$k_{y,\theta}$	θ_{cr} [°C]
20	1,000	0.126	0.782	0.604	0.991	0.254	690.01
690.01	1.310	0.165	1.024	0.479	0.965	0.267	684.70
684.70	1.301	0.164	1.018	0.482	0.967	0.266	684.81
684.81	1.301	0.164	1.018	0.482	0.967	0.266	684.81

Table 74: Iterative procedure for evaluation of the critical temperature

After iterations, a critical temperature of $\theta_{a,cr} = 684.8^\circ C$ is obtained.

3.2.5 Fire resistance

At 500°C the reduction factor for the 2% proof strength of steel, $k_{y,\theta}$ takes the value:

$$k_{y,\theta} = 0.780$$

3.2.5.1 Cross-section verification

Replacing the value of $k_{y,\theta}$ in Eq. 30:

$$\frac{N_{fi,Ed}}{A_{eff} k_{y,\theta} \frac{f_y}{\gamma_{M,fi}}} + \frac{M_{y,fi,Ed}}{W_{eff,y,min} k_{y,\theta} \frac{f_y}{\gamma_{M,fi}}} \leq 1$$

It comes:

$$0.293 \leq 1$$

This means that the cross-section of the beam-column resists to a temperature of 500°C.

3.2.5.2 *Buckling verification of the beam-column*

Replacing the value of $k_{y,\theta}$ in Eq. 31:

$$\frac{N_{fi,Ed}}{\chi_{min,fi} A_{eff} k_{y,\theta} \frac{f_y}{\gamma_{M,fi}}} + \frac{k_y M_{y,fi,Ed}}{W_{eff,y} k_{y,\theta} \frac{f_y}{\gamma_{M,fi}}} \leq 1$$

It comes:

$$0.334 \leq 1$$

This means the beam-column resists to a temperature of 500°C.

4 List of references

- [1] EN 1993-1-2, Eurocode 3, Design of Steel Structures – Part 1-2: General rules Structural fire design, 2005
- [2] EN 1993-1-5, Eurocode 3, Design of Steel Structures – Part 1-5: Plated structural elements, 2006
- [3] Talamona D.; *Flambement de poteaux métalliques sous charges excentrées à haute température*, 1995